

[Supporting Information]

Greener Photocatalytic Route to Hetero-Selective Glaser Coupling Reaction: Role of Hole/Oxygen in Air

Subhendu Sekhar Bag,^{*,1,2} Sayantan Sinha,² Siddharth Singh¹ and Animes K Golder²

¹Chemical Biology/Genomics Laboratory, Department of Chemistry, and ²Centre for the Environment, Indian Institute of Technology Guwahati, North Guwahati-781039, Assam, India. Fax: +91-361-258-2349; Tel:+91-361-258-2324. E-mail: ssbag75@iitg.ac.in

Research Topics	Page Numbers
1. Experimental Section	S2-S3
2. UV-visible Spectroscopy and Calculation of Bandgap	S4
3. Analysis of XRD spectra	S4-S6
4. X-Ray Photoelectron Spectroscopy	S6
5. FE-TEM and HR-TEM images and Lattice d-spacing from FE-TEM	S6-S7
6. Optimization of Photocatalytic Glaser Coupling Reaction	S8
7. Role of Donor/Acceptor Functional groups In Controlling The Yield of The Desired Hetero-Glaser Product	S8-S10
8. Study of Reaction Kinetics of Hetero-Glaser, Homo-Glaser Reactions: Study of Role of Hole and Air as Oxidants of Cu(I) to Cu(II) in the Catalytic Cycle	S11-S20
9. Substrate Scope of the Photocatalytic Glaser Reaction	S20-S21
10. Recyclability and Stability of The Photocatalyst	S21-S22
11. Procedures for Atomic Absorption Spectroscopic Measurement to Test the Leached out Concentration of Cu²⁺	S23
12. Characterization of Synthesized Glaser Products	S24-S30
13. NMR ¹H and ¹³C of Glaser Derivatives Synthesized Through Photocatalytic Route	S31-S77

1. EXPERIMENTAL SECTION

1.1. General Experimental (Materials and Methods)

All the chemicals unless specified were procured from Sigma Aldrich and used without further purification. Copper chloride ($\text{CuCl}_2 \cdot 2\text{H}_2\text{O}$), titanium isopropoxide and tertiary butanol were procured from Merck and Spectrochem. Synthesis of photocatalyst was successfully carried out at our laboratory. Organic extracts were dried over anhydrous sodium sulfate. Solvents were removed in a rotary evaporator under reduced pressure. Silica gel (60–120 mesh size) was used for the column chromatography. Reactions were monitored by TLC on silica gel 60 F254 (0.25 mm). ^1H NMR spectra were recorded either at Bruker make 400 or 600 MHz NMR instrument (mentioned accordingly). ^{13}C NMR spectra were recorded at 150 MHz. Coupling constants (J value) were reported in hertz (Hz). The chemical shifts were shown in ppm downfield from tetramethylsilane, using residual chloroform ($\delta = 7.26$ in ^1H NMR and $\delta = 77.23$ in ^{13}C NMR), DMSO- d_6 ($\delta = 2.5$ in ^1H NMR and $\delta = 39.5$ in ^{13}C NMR), as internal standards. Masses of the synthesized organic molecules were recorded with HR mass spectrometer and data analyzed by using in-built software. IR spectra were recorded in KBr on a FT-IR spectrophotometer. Samples for FTIR analysis were dissolved in methanol. Water was taken from a Milli-Q purification system.

1.2. Synthesis of Photocatalyst ($\text{Cu}^{2+}@\text{TiO}_2$)

We adapted a simple sol-gel technique for synthesis of Cu(II)-doped TiO_2 . To synthesize $\text{Cu}^{\text{II}}@\text{TiO}_2$ nanocomposite, 10 ml solution of titanium (IV) isopropoxide was mixed with 100 ml of $\text{CuCl}_2 \cdot 2\text{H}_2\text{O}$ (0.01M) in distilled water and was stirred at 4°C for 1 h.²⁴ The solution was acidified with nitric acid and the precipitated material produced was kept under the stirring condition to form a homogenized sol which was aged till 28 h and dried at 90°C . The powder obtained was washed, dried and annealed at 500°C for 1 h to afford $\text{Cu}^{\text{II}}@\text{TiO}_2$ nanocomposite with a doping level of 2.5% w/w.

The exact procedure is as followed: in a typical experiment $\text{CuCl}_2 \cdot 2\text{H}_2\text{O}$ (0.01M) was added to 100 ml of distilled water with temperature maintained at 4°C and kept under continuous stirring. To the solution 10 ml of Titanium (IV) isopropoxide was further added drop wise and left for hydrolyzation for 1 h. The solution was acidified with nitric acid and the precipitated material produced was kept under stirring condition to form a homogenized sol. Aging of the sol was done till 28 h and then dried at 90°C . The powder obtained was bluish -white in color washed several times with water to remove impurities and was again subjected to further drying. The powder was annealed at 500°C for 1 h. A bluish-white/grey powder was obtained. The structural morphology of the prepared nanocomposite (NC) was studied by obtaining HRTEM images, XRD, XPS and solid phase UV-visible data.

1.3. Characterization of Synthesized Photocatalyst ($\text{Cu}^{2+}@\text{TiO}_2$)

1.3.1. Study of UV-Visible spectra

UV-visible study was carried out for powder samples of $\text{Cu}^{2+}@\text{TiO}_2$ and TiO_2 in a Perkin Elmer make L750 model using Tungsten-halogen and Deuterium interface and a cell of path length 1cm. Data analysis was done using the in-built UV WinLab software version 6.0.3.0730.

1.3.2. Analysis of XRD spectra

Crystallinity and phase of the synthesized photocatalyst was studied through X-ray Diffraction analysis on a Rigaku make Micromax-007HF diffractometer, using Cu K α (1.54 Å) radiation. An R-Axis IV++ x-ray detector is used to detect the diffracted x-rays. The scanning velocity was fixed at 2°/min and diffraction pattern was recorded in the angular 2 θ range 5-80°. The average particle size was found to be 42.85 nm as measured using Scherrer's equation (1). Calculation of FWHM of XRD peaks was performed through mathematical simulation using Gaussian function.

$$B = \frac{K\lambda}{L\cos\theta} \rightarrow (1)$$

1.3.3. X-Ray Photoelectron Spectroscopy

X-ray Photoelectron Spectra of the catalyst was obtained using a ESCALAB Xi+ X-Ray Photoelectron Spectroscopy, Thermo Fisher Scientific. The instrument is operated on twin anode facility. Dual anode Mg K α /Al K α Micro focused monochromated Al K α X-ray sources and dual anode Al/Mg K α source. Double focusing, 180 degree hemispherical analyzer is provided for magnetic and multi-elemental electrostatic input lenses for spectroscopic study.

1.3.4. Study of FE-TEM images

Morphology of Cu²⁺@TiO₂ was investigated by FE-TEM. The sample for the same was prepared by suspending the nanocomposite (NC) powder in acetone and then casting it on to the TEM grid (300 mesh), following this the grid was allowed to dry overnight at 40 °C. Imaging was carried out in JEOL, 2100F Field Emission Transmission Electron Microscope. Electron microscopy parameters were set at a resolution of 1.4 Å (lattice) and 1.94 Å (point to point). All images and analysis were obtained at 200 kV accelerating voltage. In the process three magnification modes (at 200 kV) were maintained at: Standard magnification mode: 2,000 \times to 1,500,000 \times ; Selected area magnification mode: 2,000 \times to 1,500,000 \times ; Low magnification mode (LOW MAG): 50 \times to 1,000 \times . SAED camera length was controlled at 8 to 20 cm. The HR-TEM images were obtained through selection of ultra-high resolution (URH) pole piece in the objective lens. The objective aperture sizes are 20, 40, 60 and 120 μ m in diameter. SAD aperture sizes are 10, 20, 50 and 100 μ m in diameter. In Low-Mag mode, the objective lens is turned off and the objective mini-lens is made active.

2. UV-Visible Spectroscopy and Calculation of Bandgap

The UV-visible spectra of TiO_2 in $\text{Cu}^{\text{II}}@ \text{TiO}_2$ nanocomposite exhibited a blue shift of 53 nm for the surface Plasmon resonance band wavelength cutoff region compared to the virgin TiO_2 ($\lambda > 400$ nm) which might be due to the formation of the TiO_2 shell on Cu^{2+} surface. The optical shift can be related to the inter-electron transfer between the core and shell (**Figure S1**). A change in the UV-visible absorption indicates an increased concentration of charge carrier filling the Fermi level in the conduction band. However, the band gap of the material synthesised is calculated to be 3.29 eV (calculated from Tauc's Plot, **Figure S1c**) reflecting Cu^{2+} doped rutile TiO_2 structure.

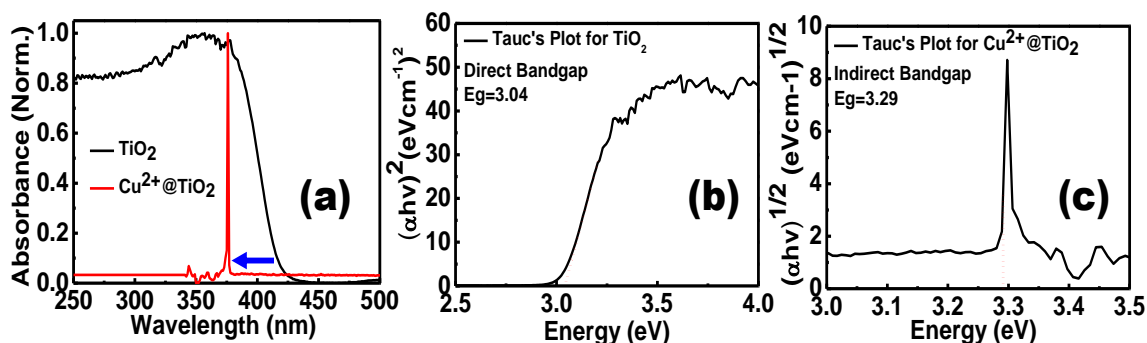


Figure S1. (a) UV-visible spectra (solid phase) of $\text{Cu}^{2+}@ \text{TiO}_2$ and Virgin TiO_2 showing the blueshift of the wavelength cutoff region for $\text{Cu}^{2+}@ \text{TiO}_2$. Bandgap determination form Tauc's Plot for (b) Virgin TiO_2 (c) $\text{Cu}^{2+}@ \text{TiO}_2$.

3. Analysis of XRD spectra

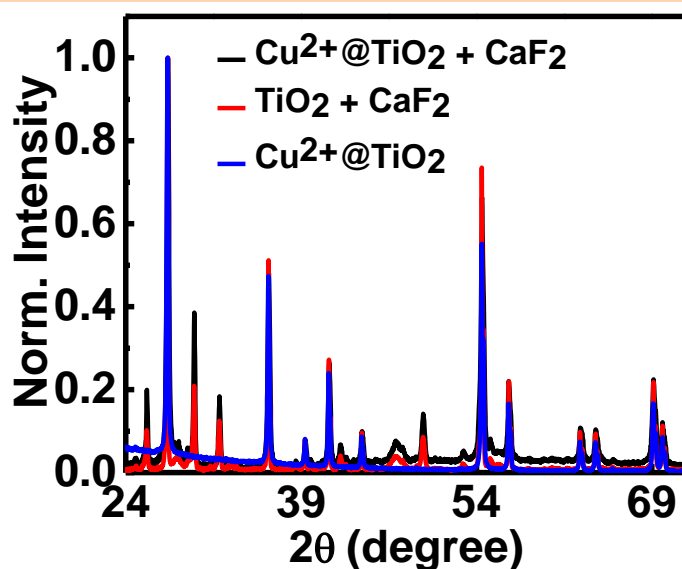
We clearly delineate the positioning of major peaks at 27.44° (110), 36.08° (101), 41.24° (111), 54.33° (211), 56.63° (220) which corresponds well with the TiO_2 rutile crystalline phase (JCPDS 01-087-0710). Correlating the diffraction peak positions between virgin TiO_2 and $\text{Cu}^{2+}@ \text{TiO}_2$ we could easily infer that alteration in the crystalline structure of TiO_2 has taken place due to doping of Cu^{2+} . A shift of 0.1° in the 2θ value was observed.

Table S1: XRD Study

FWHM calculation from Gaussian Fit of XRD data of $\text{Cu}^{2+}@\text{TiO}_2$

Peak (2-Theta)	FWHM	Crystallite Size (nm)
27.57646	0.19549	39.46677837
36.21685	0.60789	12.42134051
40.23648	0.93065	8.015437209
42.12835	0.54278	13.65827641
44.50313	0.99282	7.405853115
54.47789	0.75585	9.344857863
66.72945	2.57338	2.578307076
69.16591	0.80773	8.097476801
Average		12.62

Crystal Refinement study with CaF_2



The Digital Photograph of $\text{Cu}^{2+}@TiO_2$



The crystallinity and phase of the synthesised photocatalyst were studied through X-ray diffraction analysis revealing the average particle size as 43 nm fitted with the TiO_2 rutile

crystalline phase (JCPDS 01-087-0710). The doping with Cu^{2+} -ion afforded TiO_2 sample with a greenish colour. The Cu^{2+} ion dopant is most likely located in interstitial positions of the lattice rather than directly in Ti^{4+} sites because of the relatively large size of the dopant ion (Cu^{2+} , 0.87 Å) compared to Ti^{4+} (0.745 Å). Interestingly, we did not observe any diffraction peak corresponding to oxides of Cu (Cu_xO_y).

4. X-Ray Photoelectron Spectroscopy

Analysis of X-ray photoelectron spectroscopy (XPS) revealed the presence of Cu^{2+} ion as indicated by the binding energies of 933.7 and 953.5 eV corresponding to Cu 2p_{3/2} and Cu 2p_{1/2} spin-orbit splitting components (**Figure 2b**). The sharp, broad and singlet shake-up peaks in the XPS spectrum at 942.9 eV and 962.1 eV indicated 2p/3d satellite peak of Cu^{2+} ion which is different from the oxides or hydroxides. Moreover, we found the intensity ratio of the satellite peak to the 2p_{3/2} peak as 0.8 indicating the possible presence of pure Cu^{2+} ion coordinated through the lattice oxygen of TiO_2 which is again supported from the binding energy of 528.6 eV corresponding to O 1s component (**Figure S2**).

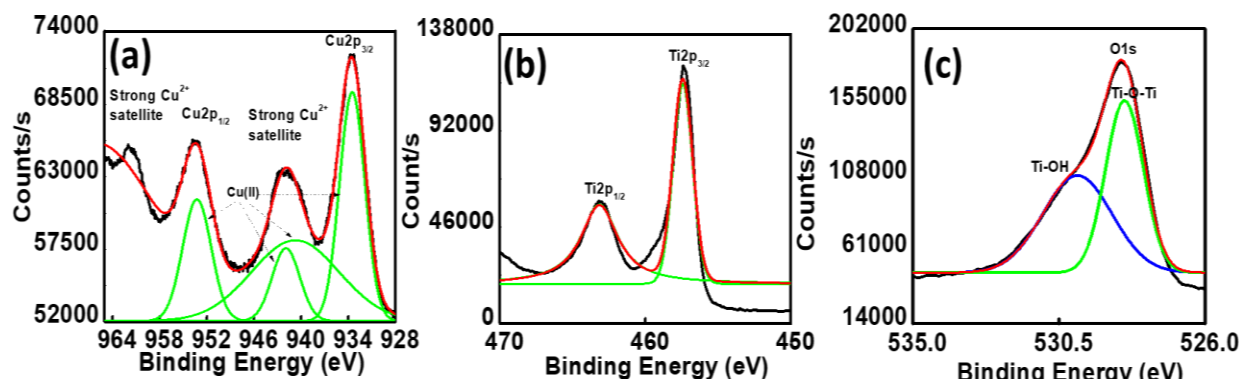


Figure S2. (a) XPS spectra of Cu^{2+} @ TiO_2 nanocatalyst showing strong satellite peaks of Cu^{2+} ; (b) XPS spectra of Ti 2p peaks of synthesized Cu^{2+} @ TiO_2 ; (c) XPS spectra of O 1s peaks of synthesized Cu^{2+} @ TiO_2 .

5. FE-TEM and HR-TEM images and Lattice d-spacing from FE-TEM

The FE-TEM and HR-TEM images (**Figure S3**) clearly showed that the Cu^{2+} @ TiO_2 is well dispersed and near-circular featuring the outer shell TiO_2 encapsulating multiple Cu cores supporting the observed SP band shift in the UV-vis spectra. The size of the nanoparticle obtained from TEM is also well matched with the value obtained from Scherrer's equation. Inter lattice spacing of the Cu^{2+} - TiO_2 interface was calculated and found to be 0.34, indicating that the Cu^{2+} metal ions are possibly well incorporated into TiO_2 lattice, in the interstitial position of TiO_2 near the surface of the particles (**Figure S4**). These Cu^{2+} species would efficiently uptake one photogenerated electron from the TiO_2 conduction band leading to Cu^{1+} . Thus, a rapid reduction of Cu^{2+} to Cu^{1+} would probably take place once TiO_2 is photoexcited.

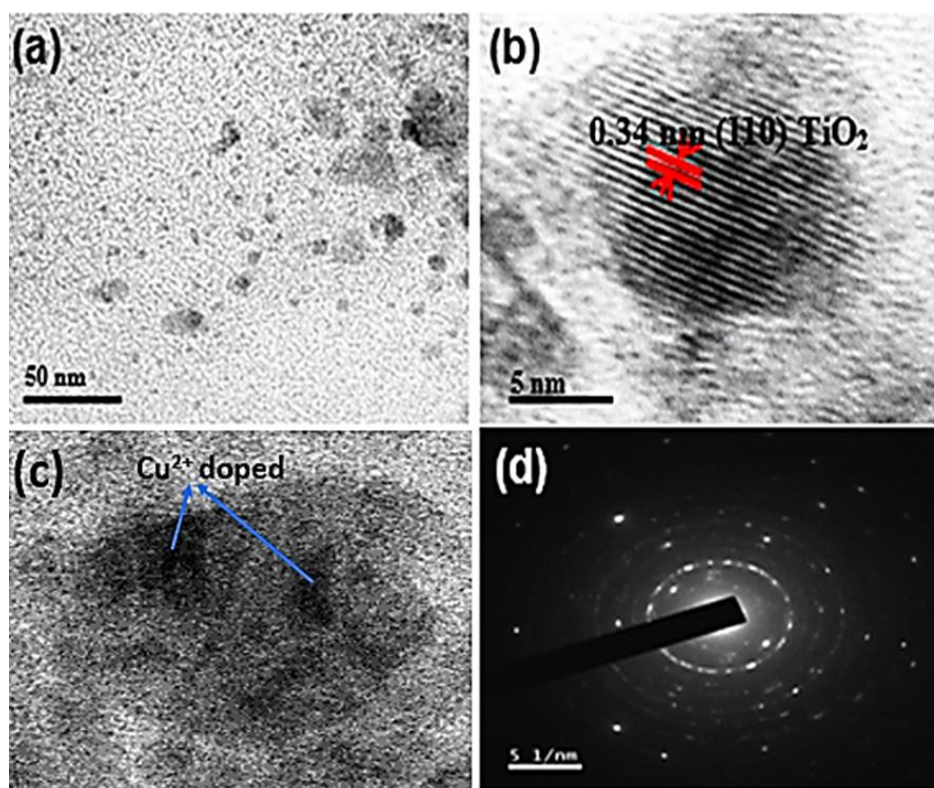


Figure S3. (a) FE-TEM image of $\text{Cu}^{2+}@\text{TiO}_2$; (b)HR-TEM image confirming TiO_2 in $\text{Cu}^{2+}@\text{TiO}_2$ from the Inter lattice d-spacing of the core-shell interface(c) HR-TEM image showing successful doping of Cu^{2+} in $\text{Cu}^{2+}@\text{TiO}_2$; (d) SAED pattern of $\text{Cu}^{2+}@\text{TiO}_2$.

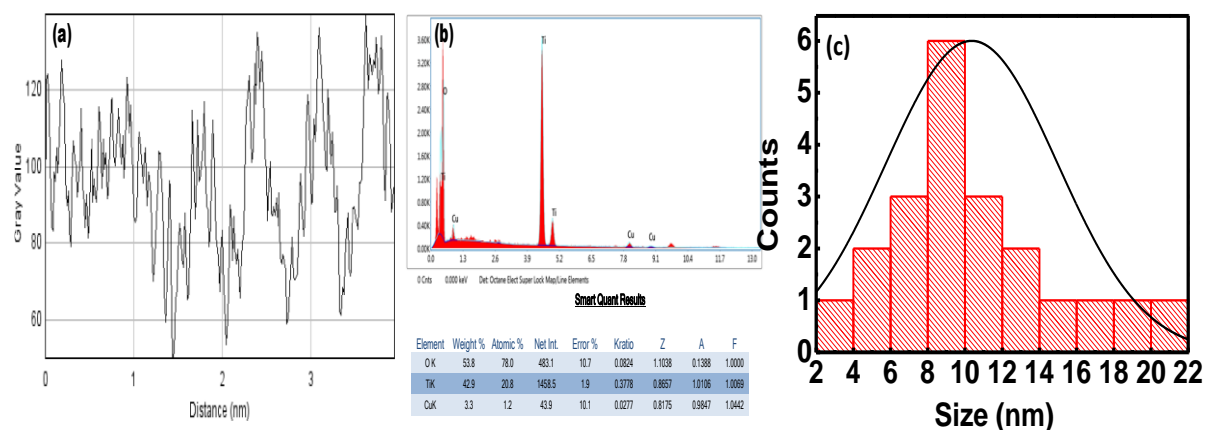


Figure S4. (a) Inter Lattice d-spacing calculation of $\text{Cu}^{2+}@\text{TiO}_2$ interface in synthesized $\text{Cu}^{2+}@\text{TiO}_2$ nanocomposite using FFT (Fourier Transform algorithm) (b) Quantitative Elemental Analysis of $\text{Cu}^{2+}@\text{TiO}_2$ using electron dispersive spectroscopy (EDS) (c) Size Distribution of $\text{Cu}^{2+}@\text{TiO}_2$ from TEM.

6. Optimization of Photocatalytic Glaser Coupling Reaction

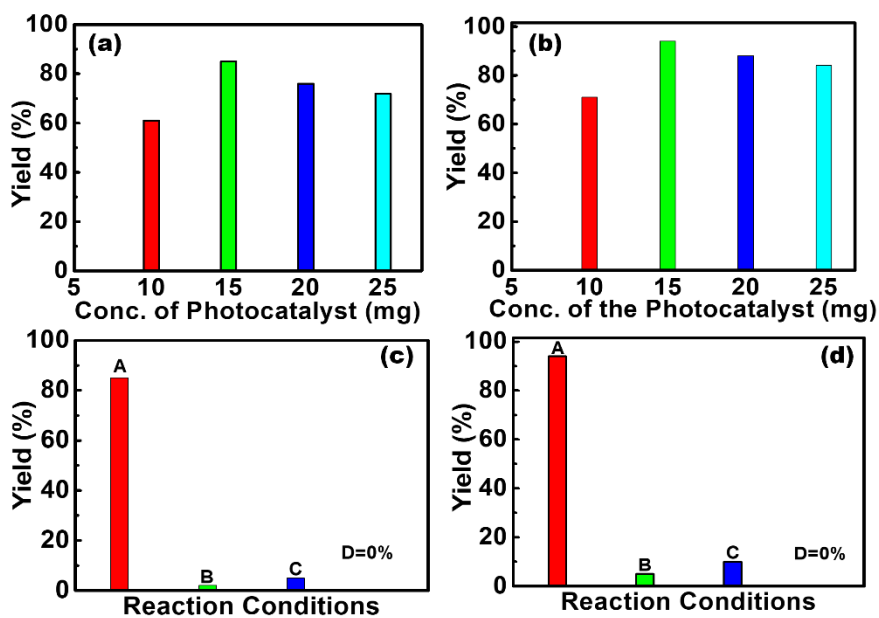
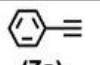
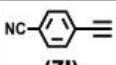
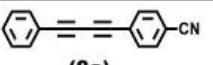
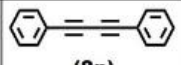
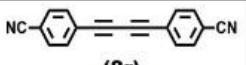
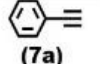
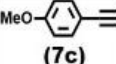
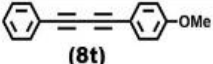
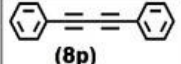
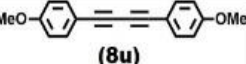
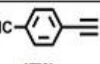
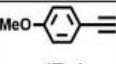
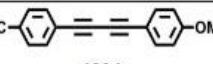
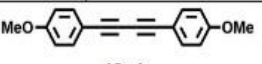
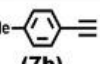
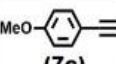
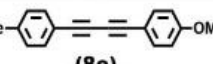
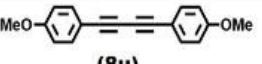


Figure S5. Optimization of the photocatalyst load for the (a) Hetero-Glaser (synthesis of **8a**) and (b) Homo-Glaser coupling (synthesis of **8p**), respectively. Yields obtained after 1 h reaction under different experimental conditions for (c) Hetero-Glaser and (d) Homo-Glaser; **A**: light irradiated photocatalytic reaction; **B**: Reaction under dark condition without photocatalyst; **C**: Reaction under the dark condition with photocatalyst; **D**: Reaction in presence of only light (without photocatalyst).

7. Role of Donor/Acceptor Functional groups In Controlling The Yield of The Desired Hetero-Glaser Product

The, unsubstituted aromatic alkyne **7a** and acceptor functional group containing aromatic-alkyne **7l** (henceforth we will describe as acceptor-alkyne) were utilized as starting materials with varying the mole ratio of one alkyne (1 to 1.5) keeping other alkyne fixed. Thus, the reaction between alkyne **7a** and acceptor-alkyne **7l** was carried out in three different equivalence of mole ratios. When the alkyne **7a** was taken in 1.5 or 1.0 equivalent with respect to the other alkyne **7l**, we obtained the maximum yield of 90 % for the desired hetero-Glaser product **8a**. In both the cases, the homo-Glaser product **8p** was also formed as by-product in negligible amount (5-12 %). However, when the acceptor-alkyne **7l** was taken in 1.5 equivalent with respect to unsubstituted alkyne **7a**, we observed 3 products (spots from the TLC). The homo-Glaser by-products **8p** (from alkyne **7a**) and **8r** (from acceptor-alkyne **7l**) were also obtained with negligible yield of 4% and 20%, respectively (**Table S2**).

Table S2. Hetero-Glaser selectivity of donor/acceptor substituted alkynes.

SI. No.	Reactant Alkynes		Hetero-Glaser Products		
1.					
	Mole ratios		Yield		
	1.5	1.0	85%	6%	-----
	1.0	1.0	90%	5%	-----
	1.0	1.5	65%	4%	20%
2.					
	Mole ratios		Yield		
	1.5	1.0	82%	6%	-----
	1.0	1.0	56%	25%	-----
	1.0	1.5	60%	5%	15%
3.					
	Mole ratios		Yield		
	1.5	1.0	80%	2%	
	1.0	1.0	86%	4%	
	1.0	1.5	80%	13%	
4.					
	Mole ratios		Yield		
	1.5	1.0	72%	20%	
	1.0	1.0	73%	10%	
	1.0	1.5	70%	15%	

Next, to understand the hetero-Glaser selectivity of donor/acceptor substituted alkynes, we performed reaction between unsubstituted alkyne **7a** and donor group substituted alkyne **7c** (henceforth we will describe as donor-alkyne) in their various mole ratio. Thus, 1.5:1 mole ratio of alkyne **7a** and donor-alkyne **7c** afforded the hetero-Glaser product **8t** as a major (82% yield) and a negligible amount (6%) of the by-product **8p** (homo-Glaser of **7a**). On the other hand, when alkyne **7a** and donor-alkyne **7c** was taken in 1:1 mole ratio, we obtained hetero-selective Glaser product **8t** in 50% yield along with 25% of the homo-Glaser by-product **8p**. On the contrary, three products were obtained when we took 1.5: 1 mole ratio of donor-alkyne **7c** and **7a**. Again the hetero-selective Glaser product **8t** was obtained as major (60% yield) product along with small amount of homo-Glaser side products **8p** and **8u** (homo-Glaser of donor-alkyne **7c**) with 5% and 15% yields, respectively (**Table S2**).

Next, we tested the hetero-selective Glaser coupling among a donor-substituted alkyne (**7c**) and an acceptor-substituted alkyne (**7l**) with their various mole ratios. Thus, the reactions between **7l** and **7c** in 1.5:1 and 1: 1 mole ratios resulted in two products in 2h out of which the hetero-selective Glaser product **8h** was obtained as the major product with 80-86% yield along with a negligible amount (2-4%) of homo-Glaser product **8u** (from donor-alkyne **7c**). On the other hand, when the donor-alkyne **7c** was

taken 1.5 times the acceptor-alkyne **7l**, slight increase in yield (13%) of the homo-Glaser product **8u** (from donor-alkyne **7c**) was obtained; though the reaction maintain its hetero-Glaser selectivity to yield 80% hetero-product **8h** as major one in 2h (**Table S2**). The final sets of reactions were performed between **7b** and **7c**, both of which contains a donor functional group. When **7b** containing *-p-Me* as donor, was used in 1.5 and 1.0 equivalence with respect to **7c** containing a *-p-OMe* as donor functional group, the hetero-Glaser product **2e** was obtained as a major product with yield of 72-73%. We also observed the formation of homo-Glaser side product **8u**, arising from the reactant alkyne having stronger donor group (**7c**), as minor product with an isolated yield of only 20-10%. On the other hand, when **7c** was taken 1.5 equivalent with respect to **7b**, again we observed the hetero-Glaser product **8e** as the major product with yield of 70% along with the same homo-Glaser side product **8u** with yield of 15%. Interestingly, none of the cases could afford any trace of homo-Glaser side product arising from the reactant alkyne having relatively weaker donor group (**7b**).

Thus, from all the above experimental results depicted in **Table S2**, we can conclude that all the reactions underwent smoothly with high hetero-Glaser selectivity over the possible homo-Glaser coupling irrespective of the mole ratios of the two reactive hetero-alkyne partners. The yields of selective hetero-Glaser products are very good in all the cases of donor-acceptor alkyne partners. The yields of hetero-Glaser products also vary depending on the electronics (donor-acceptor substituents) of the alkyne partners. The donor alkyne partner always afforded a negligible amount (6-20%) of homo-Glaser side product irrespective of its mole ratio with respect to the acceptor alkyne partner. Interestingly, slight excess (1.5 equivalent) of the acceptor alkyne afforded minimum amount of the homo-Glaser side product (2%) and maximized yield of 80% of the hetero-Glaser product with the donor-alkyne partner. However, optimum yield of the hetero-Glaser product was also obtained when we took donor-alkyne in slight excess wherein we observed 10-20% of the homo-Glaser side product from the donor-alkyne. Thus, to test substrate scope of the hetero-selective Glaser coupling protocol with optimum yield using our smart photocatalyst, we carried out all the reactions by taking either of the acceptor- or the donor-alkyne in slight excess.

8. Study of Reaction Kinetics of Hetero-Glaser, and Homo-Glaser: Study of Role of Hole and Air as Oxidants of Cu(I) to Cu(II) in the Catalytic Cycle

8.1. Photocatalytic Reaction Set-up under Air/Nitrogen Condition

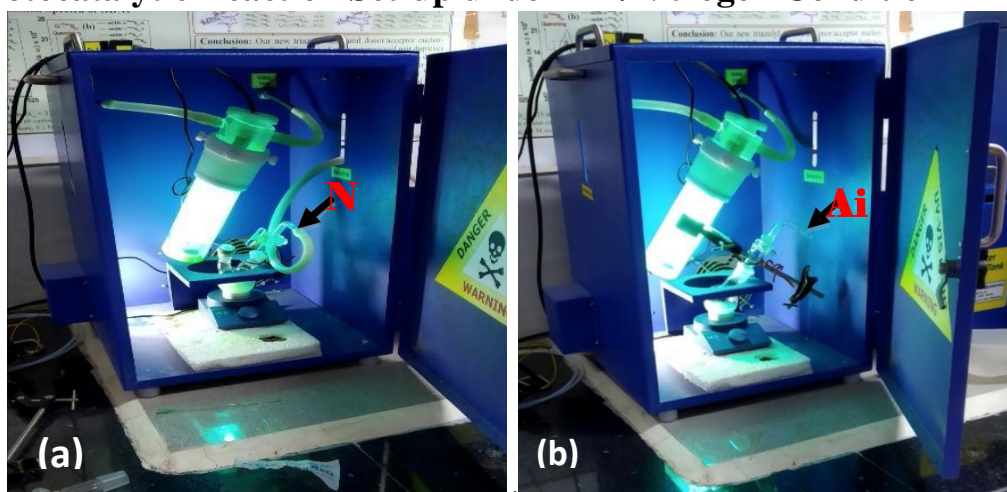


Figure S6. (a) Photocatalytic Reaction set-up under Nitrogen condition; (b) Photocatalytic Reaction set-up under aerobic condition.

8.2. General Kinetics of Hetero-/Homo-Glaser:

The reactions between different alkynes for hetero-Glaser coupling and same alkynes for homo-Glaser coupling reactions were performed under different solvent systems and reaction conditions (t-BuOH/H₂O/Air, t-BuOH/H₂O/N₂, THF/Air, THF/N₂) in the photocatalytic reactor. 5 mL of aliquot was directly collected from the reaction mixture at particular time intervals. The aliquots collected were immediately quenched with methanol and then subjected to general work-up in Ethyl Acetate, NH₄Cl, and Brine. After work up the reaction mixture obtained was directly prepared for NMR without purification. The comparative yield was calculated using the sp C-H proton signal of one of the starting alkynes. The relative reduction of the sp C-H proton signal with time can be correlated with the signal from sp C-H proton from the alkynes at 0 min.

8.3. Study of Kinetics of Hetero-Glaser Reactions Under Various Solvent and Atmospheric Conditions

8.3.1. In Water/^tBuOH and Air (Under Aerobic Condition): Photocatalytic Synthesis of Compound 8a (hetero-Glaser)

The hetero-Glaser reaction was carried out between phenylacetylene (**7a**, 1.5 equiv.) and 4-ethynylbenzotrile (**7l**, 1 equiv.), in two different solvent systems (H₂O/^tBuOH and THF) under both aerobic as well as anaerobic conditions. The reactions in all the four cases of the hetero-Glaser reaction was continued till the complete consumption of both the starting materials monitored at regular time intervals with TLC. In the first case, reaction was carried out in H₂O/^tBuOH/air system which offered a good and steady reaction progression. Aliquots from the reaction were collected at intervals of 0, 15, 30, 45, 60, 75 and 90 min. After a short workup and drying, ¹H NMR spectra were recorded for each aliquote

The detailed observations of the reaction monitored by TLC is as follows. We obtained a steady and good progress in reaction between phenyl acetylene (1.5 eq.) and 4-ethynylbenzotrile (1 eq.) over time. Two spots were seen from TLC constantly till 90 minutes of reaction. In 0 min 1st spot (upper spot; R_f = 0.95; Hex = 100%) corresponding to phenyl acetylene and 2nd spot (lower spot; R_f = 0.15; Hex = 100%) corresponding to 4-ethynylbenzotrile was observed and confirmed from NMR. However, when the sample collected at 15 min was subjected to TLC, both the spots showed reduction in the intensity. However, the spots maintained similar R_f as compared to 0 min TLC. In 30 min as checked from TLC the lower spot intensity increased as compared to 15 min TLC while the upper spot intensity decreased. From the NMR study of crude reaction mixture it was found out that the corresponding peak of proton (alkyne) for 4-ethynylbenzotrile has almost vanished. This justifies that the desired hetero coupled product has formed. TLC of reaction mixture at 45 min showed that the intensity of the lower spot has increased while the upper spot intensity has decreased significantly. A similar observation was seen from the NMR study. It was found that 4-ethynylbenzotrile was completely used up and compound (**8a**)

has been completely formed. However, from NMR studies it is also reflected that a very minute amount (3%) of homocoupled product of phenyl acetylene has been formed in 30 min and 45 min. While as 1.5 eq. of phenyl acetylene was used therefore the corresponding proton (alkyne) peak for excess phenyl acetylene could be detected. The reaction was allowed to continue to understand the fate of the excess phenyl acetylene. At 60 min not much change was observed from the TLC when compared with 45 min TLC. The lower spot intensity remained unaltered while the upper spot intensity was very faint with a faint spot arising just below the upper spot was observed. From NMR it was observed that the intensity of proton peak corresponding to phenyl acetylene decreased significantly. At 75 min significant changes in the TLC was observed with respect to the upper spot. A new spot at $R_f = 0.9$ was observed and no spot corresponding to phenyl acetylene at $R_f = 0.95$ was found. A similar observation was detected from the NMR study. At 60 min no corresponding proton peaks of terminal alkynes were recorded. Hence these observations suggest that homocoupling of the excess phenyl acetylene has taken place. The reaction was further continued till saturation. At 90 min the TLC showed no change as compared to 75 min TLC. The NMR study was also in accordance with the TLC observation.

As calculated from NMR the relative yield of compound **8a** was calculated 0%, 74.38%, 76.5%, 85% at time interval of 0 min, 15 min, 30 min, and 45 min (100% conversion). Similarly, the relative yield for homo-coupled product **8p** was calculated to be 0% (0 min), 0.99% (15 min), 3% (30 and 45 min), 5.4% (60 min), 11.8% (75 min) and 12% (90 min; 100% conversion). As we know that ^tBuOH is a good hole scavenger therefore we can infer that O₂ has played an important role in maintaining catalytic activity. The stack plot of NMR spectra of samples collected at particular time interval is shown in **Figure S7** along with a plot of % relative yield vs. Time.

In summary, with time we observed significant changes. Complete consumption of alkyne **7l** was observed in 60 min while alkyne **7a** was exhausted in 75 min. The relative yield of desired hetero-Glaser product **8a** and homo-Glaser side product **8p** was calculated from the NMR stack plot and found as 85% and 12%, respectively (**Figure S7**).

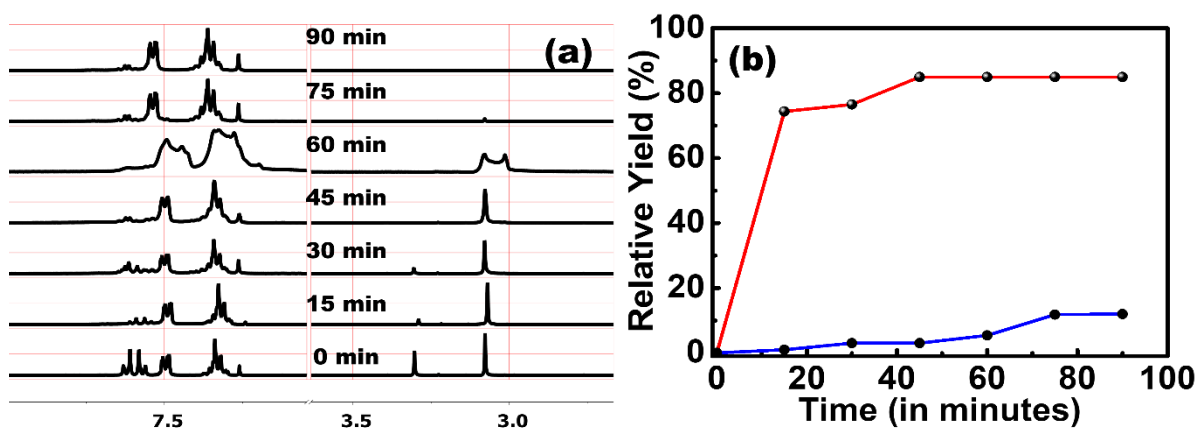


Figure S7. (a) ¹H NMR stack plot of time dependent kinetic study for photocatalytic synthesis of compound **8a** in water/^tBuOH and air system. (b) Relative Yield (%) of **8a** and **8p** is calculated from NMR stack plot.

8.3.2. In Water/^tBuOH and N₂ (Under Anaerobic Condition): Photocatalytic Synthesis of Compound 8a

The reactions in second case was carried out in H₂O/^tBuOH solvent system under inert N₂ atmosphere. The reaction progress was monitored by TLC and ¹H NMR spectra of the aliquots were recorded following the same protocol as stated above. The time dependent observation from TLC discussed as follows.

We observed that when performing the reaction between phenyl acetylene (1.5 eq.) and 4-ethynylbenzonitrile (1 eq.) under anaerobic condition keeping all other conditions, catalyst and solvent system same, we did not get promising yield of compound **8a**. Two spots were seen from TLC constantly till 90 minutes of reaction. In 0 min 1st spot (upper spot; R_f=0.95; Hex=100%) corresponding to phenyl acetylene and 2nd spot (lower spot; R_f=0.15; Hex=100%) corresponding to 4-ethynylbenzonitrile was observed and confirmed from NMR. However, when the sample collected at 15 min was subjected to TLC, both the spots showed reduction in the intensity as compared to 0 min TLC. However, the spots maintained similar R_f as compared to 0 min TLC. This observation remained constant till 60 min. The particular finding is significant as promising conversion is not reported as was the case when the reaction was done in presence of air/oxygen. This suggests that areal oxygen has an important role to play in maintaining the catalytic cycle by oxidizing Cu(I) to Cu(II). NMR study of reaction mixture from 15 min to 60 min also supported the TLC observation. TLC of reaction mixture at 75 min showed another 5%-10% decrease in intensity of the lower spot as compared to TLC at 60 min. NMR study also supported our observation. A similar TLC was observed at 90 min, however a very faint spot with minimal intensity was observed at R_f=0.9. However, from NMR study no significant relative yield could be calculated for the compound **8p**.

As calculated from NMR the relative yield of compound **8a** was calculated 0%, 24.31% and 36.38% at time interval of 0 min, 15 min to 60 min, and 75 min to 90 min respectively. However, no significant relative yield could be calculated for **8p**. Under anaerobic reaction condition we did not obtain a promising yield of desired compound **8a**. The underlying reason correlates to the disruption in the catalytic cycle. Under anaerobic condition Oxygen is not present to convert Cu(I) to Cu(II) and therefore complete photocatalytic conversion has not taken place. The stack plot of NMR spectra of samples collected at particular time interval is shown in **Figure S8** along with a plot of % relative yield vs. time.

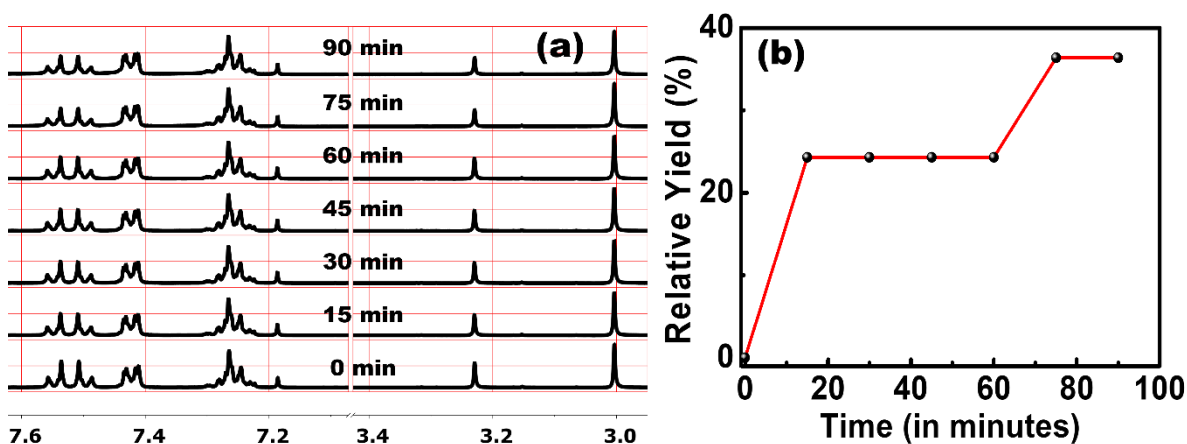


Figure S8. ¹H NMR stack plot of time dependent kinetic study for photocatalytic synthesis of compound 8a in water/^tBuOH and N₂ system. (b) Relative Yield (%) of 8a (side product 8p could not be detected) is calculated from NMR stack plot.

In summary, full conversion was not observed and both the starting materials **7i** and **7a** remained partially unreacted even after 90 minutes. The maximum relative yield of **8a** was calculated to be 36.38% while no significant relative yield could be observed for **8p**.

8.3.3. In THF and Air (Under Aerobic Condition): Photocatalytic Synthesis of Compound 8a

Aerobic condition and THF solvent system was utilised to carry out the reactions of the third case of first set. Reaction progression was smooth and steady as indicated from total conversion of starting material **7i** within 30-45 minutes resulting in formation of desired hetero-Glaser compound **8a**. The observation was reflected from the TLC of 30 min and 45 min. The detailed TLC observation and reaction progression status is discussed as follows.

We obtained a steady and good progress in reaction between phenyl acetylene (1.5 eq.) and 4-ethynylbenzotrile (1 eq.) over time when reaction was performed in THF solvent under air. Two spots were seen from TLC constantly till 90 minutes of reaction. In 0 min 1st spot (upper spot; R_f = 0.95; Hex = 100%) corresponding to phenyl acetylene and 2nd spot (lower spot; R_f = 0.15; Hex = 100%) corresponding to 4-ethynylbenzotrile was observed and confirmed from NMR. However, when the sample collected at 15 min was subjected to TLC, the upper spot and lower spots showed 50% reduction in the intensity. However, the spots maintained similar R_f as compared to 0 min TLC. A similar observation from NMR study confirms formation of desired compound. In 30 min as checked from TLC the lower spot intensity increased as compared to 15 min TLC while the upper spot intensity slightly reduced. From the NMR study of crude reaction mixture, it was found out that the corresponding peak of proton (alkyne) for 4-ethynylbenzotrile has almost vanished. Also the corresponding proton peak for phenyl acetylene also showed reduced signal intensity as compared to 0 min and 15 min NMR. This justifies that the desired hetero coupled product has formed along with a very minute homo coupled product of phenyl acetylene. TLC of reaction mixture at 45 min showed that the intensity of the lower spot has increased while the upper spot intensity has decreased significantly. A similar observation was seen from the NMR study. It was found that 4-ethynylbenzotrile was completely used up and compound **8a** has been completely formed. While as 1.5 eq. of phenyl acetylene was used therefore the corresponding proton (alkyne) peak for excess phenyl acetylene could be detected. However, at the same time very minimal homo-coupled product of phenyl acetylene has also started forming as suggested from NMR kinetics. The reaction was allowed to continue to understand the fate of the excess phenyl acetylene. At 60 min significant change was observed from the TLC when compared with 45 min TLC. The lower spot intensity remained unaltered while along with a faint upper spot (R_f=0.95) another spot just below the upper spot corresponding to the spot for **8p** was observed. From NMR it was observed that the intensity of proton peak corresponding to phenyl acetylene decreased significantly rather almost vanished. At 75 min significant changes in the TLC was observed with respect to the upper spot. A new spot at R_f=0.9 was observed and no spot corresponding to phenyl acetylene at R_f=0.95 was found. A similar observation was detected from the NMR study. Hence these observations suggest that homocoupling of the excess phenyl acetylene has taken place. The reaction was further continued till saturation. At 90 min the TLC showed

no change as compared to 75 min TLC. The NMR study was also in accordance with the TLC observation.

As calculated from NMR the relative yield of compound **8a** was calculated 0%, 56.10%, 65.45%, 85% at time interval of 0 min, 15 min, 30 min, and 45 min (100% conversion). Similarly, the relative yield for homo-coupled product **8p** was calculated to be 0% (0 min), 0.92% (15 min), 3.6% (30 and 45 min), 11.04% (60 min and 75 min), and 12% (90 min; 100% conversion). As we know that THF is not a hole scavenger therefore we can infer that O₂ as well as the hole have played their respective roles in maintaining catalytic activity. The stack plot of NMR spectra of samples collected at particular time interval is shown in **Figure S9**. The observation from TLC was correlated with the NMR kinetics study as shown in **Figure S9**.

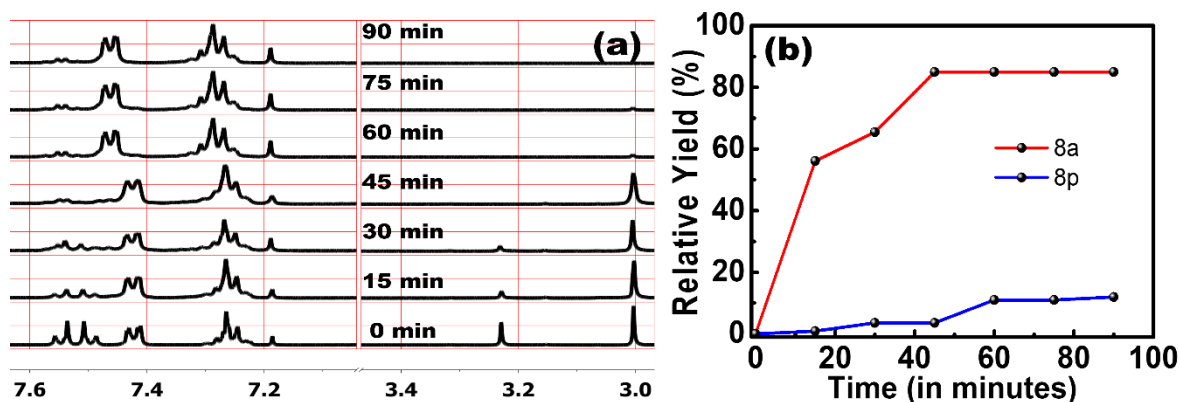


Figure S9. ¹H NMR stack plot of time dependent kinetic study for photocatalytic synthesis of Compound **8a** in THF and Air. (b) Relative Yield (%) of **8a** and **8p** is calculated from NMR stack plot.

8.3.4. In THF and N₂ (Under Anaerobic Condition): Photocatalytic Synthesis of Compound **8a**

To understand the role of hole the reactions in the fourth case of first set was carried out under anaerobic condition (N₂) and THF solvent system. The detailed TLC observation and reaction progression status is discussed as follows.

Reaction between phenyl acetylene (1.5 eq.) and 4-ethynylbenzotrile (1.0 eq.) was carried out in THF solvent system under anaerobic condition. 0 min TLC showed two spots. 1st spot (upper spot; R_f = 0.95; Hex = 100%) corresponding to phenyl acetylene and 2nd spot (lower spot; R_f = 0.15; Hex = 100%) corresponding to 4-ethynylbenzotrile was observed and confirmed from NMR. In the 15 min TLC both the spot intensities decreased. As found from NMR study formation of desired compound was seen. Following these TLC at 30 min showed increase in intensity of lower spot while the upper spot intensity reduced. Similar type of observations were obtained from TLC at 45 min and 60 min. From NMR study at 60 minutes no proton peak corresponding to 4-ethynylbenzotrile was obtained hence complete conversion to **8a** has been achieved. However very minute yield of **8p** can be

inferred from NMR study during the 45 min and 60 min. The 75 min and 90 min TLC showed significant change in observation. The lower spot remained same however a new spot corresponding to **8p** at $R_f = 0.9$ was observed. The upper spot corresponding to phenyl acetylene vanished.

As calculated from NMR the relative yield of compound **8a** was calculated 0%, 14.45%, 56.10%, 70.81% and 85% (100% conversion) at time interval of 0 min, 15 min, 30 min, 45 min and 60 min (100% conversion). Similarly, the relative yield for homo-coupled product **8p** was calculated to be 0% (0 min-30 min), 4.28% (45 min and 60 min), 11.14% (75 min), and 12% (90 min; 100% conversion). The reaction was performed under anaerobic condition hence oxygen do not have a role in maintaining the catalytic cycle. However, from kinetics study we can understand that complete conversion has taken place hence the catalytic cycle has been well maintained. Hence as THF is not a hole scavenger therefore role of hole in maintaining the catalytic cycle has been hence proved. The stack plot of NMR spectra of samples collected at particular time interval is shown in **Figure S10**.

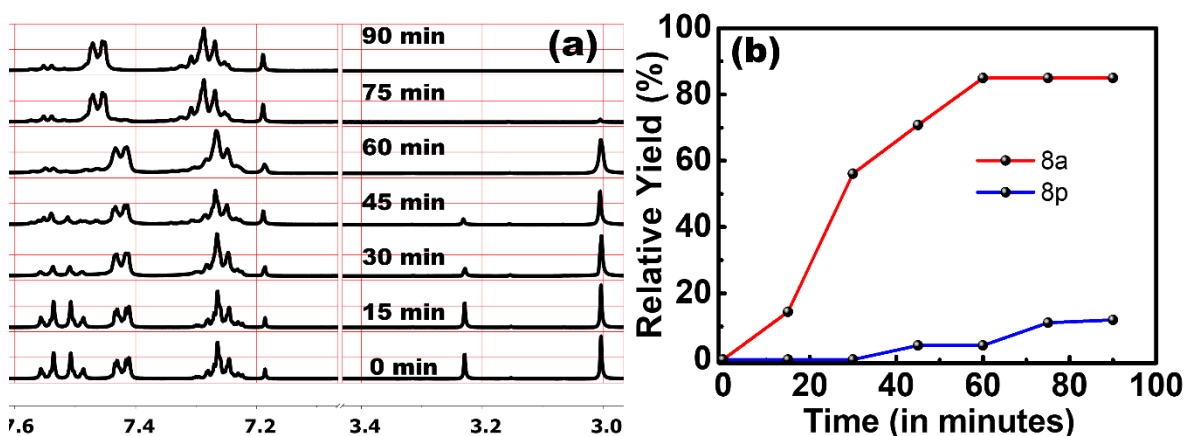


Figure S10. (a) ^1H NMR stack plot of time dependent kinetic study for photocatalytic synthesis of compound **8a** in THF under anaerobic condition. (b) Relative Yield (%) of **8a** and **8p** is calculated from NMR stack plot.

As observed from the NMR study of reaction kinetics shown in **Figure S10** and continuous monitoring of the reaction progress with TLC, we can say that the reaction proceeded smoothly with good relative yield (85%) of desired hetero-Glaser compound **8a** and trace amount of homo-Glaser side product **8p** (12%). From the TLC as well as NMR study it was confirmed that total consumption of one of the starting alkyne **7l** was reported within 45 minutes showing full conversion to **8a**. On continuing the reaction, **7a** was completely used up within 75 minutes.

8.3.5. Conclusion on the Kinetics of Hetero-Glaser Under various Conditions

Based on the experimental observations and NMR studies from different classes of reactions in the first set we need to establish a understanding about the role of hole/oxygen in the catalytic process. We, thus, observed a complete conversion of the starting materials offered the desired hetero-Glaser product **8a** with 85% relative yield along with a minute amount of homo-Glaser side product, **8p** with maximum 12% relative yield when the reaction was carried under the condition of either $\text{H}_2\text{O}/t\text{BuOH}/\text{air}$, or THF/air or THF/N_2 (**Scheme 1**).

However, when the reaction was performed under N₂ using H₂O/^tBuOH as a solvent system, we obtained a maximum relative yield of 36% for the desired hetero-Glaser product **8a**, and the formation of undesired side product **8p** was not detected. As we know, ^tBuOH is a good hole scavenger, so when the reaction was performed in H₂O/^tBuOH/Air, the catalytic cycle was maintained in the presence of oxygen present in the air. Therefore, we thought to replace ^tBuOH and select a solvent that is not a hole quencher so that we can find out the role of oxygen in the air and the hole very clearly. Thus, a reaction was performed in THF under air and N₂, separately. We found out that the reaction progresses smoothly, and good yield of the desired hetero-Glaser product (**8a**) was obtained in both the cases. Therefore, we can conclude that both the hole and oxygen play an important role in maintaining the catalytic cycle.²³ From the study, we can infer that the synthesized photocatalyst is smart, self-sustainable and can work under any reaction condition. **Figure 4** shows the comparative relative yield of compounds **8a** and **8p** under various reaction conditions.

8.4. Study of Kinetics of Homo-Glaser Reactions Under Various Solvent and Atmospheric Conditions

The homo-Glaser reactions were carried out with phenylacetylene (**7a**) to obtain the final product **8p**. Reaction in H₂O/^tBuOH and air resulted in production of desired product **8p**. Reaction was carried on till complete consumption of starting alkyne **7a**. From TLC we found out that the starting alkyne **7a** was completely consumed within 40 min (**Figure S11**).

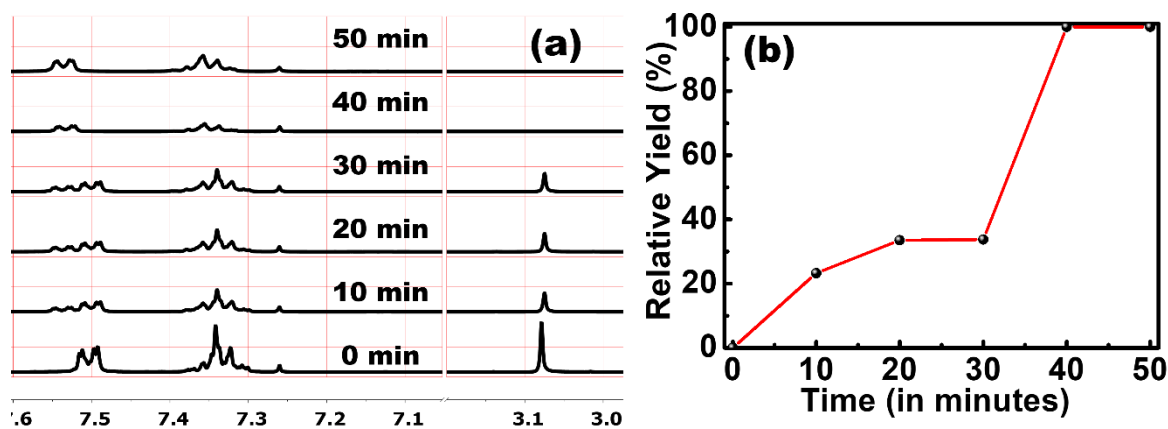


Figure S11. (a) ¹H NMR stack plot of time dependent kinetic study for photocatalytic synthesis of compound **8p** in water/^tBuOH and air system. (b) Relative Yield (%) of **8p** calculated from NMR stack plot.

Similarly, when the reaction was performed in the same solvent system in absence of air, the rate of production of desired compound **8p** became sluggish. When monitored from TLC we found out that **7a** was not totally consumed and from 40 minutes onwards no change in the TLC could be observed (**Figure S12**).

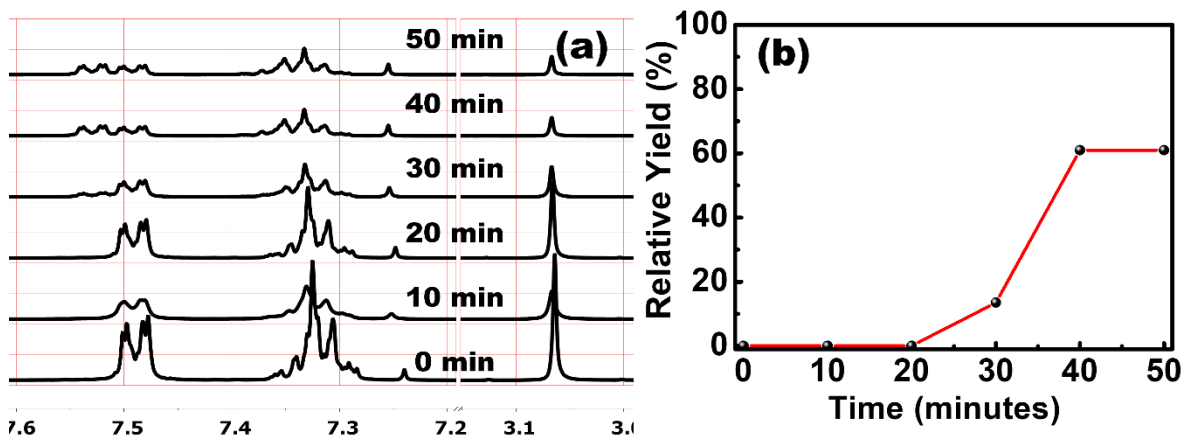


Figure S12. (a) ^1H NMR stack plot of time dependent kinetic study for photocatalytic synthesis of compound **8p** in water/ $t\text{BuOH}$ and N_2 system. Relative Yield (%) of **8p** calculated from NMR stack plot. (b) Relative Yield (%) of **8p** calculated from NMR stack plot.

In case of reactions performed in THF, under both the aerobic (**Figure S13**) and anaerobic (**Figure S14**) conditions we observed total consumption of **7a** within 20-30 min, as monitored by TLC. Our observations were in accordance to the NMR study.

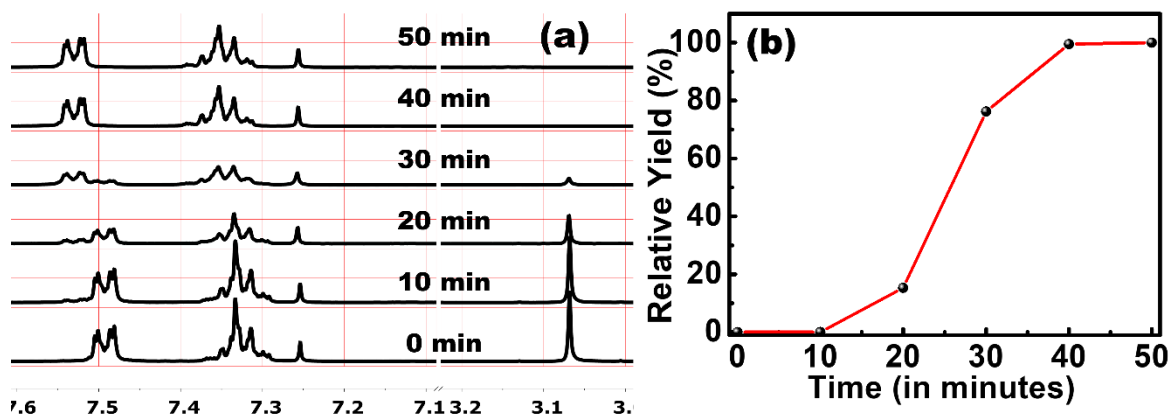


Figure S13. (a) ^1H NMR stack plot of time dependent kinetic study for photocatalytic synthesis of compound **8p** in THF and Air. Relative Yield (%) of **8p** calculated from NMR stack plot.

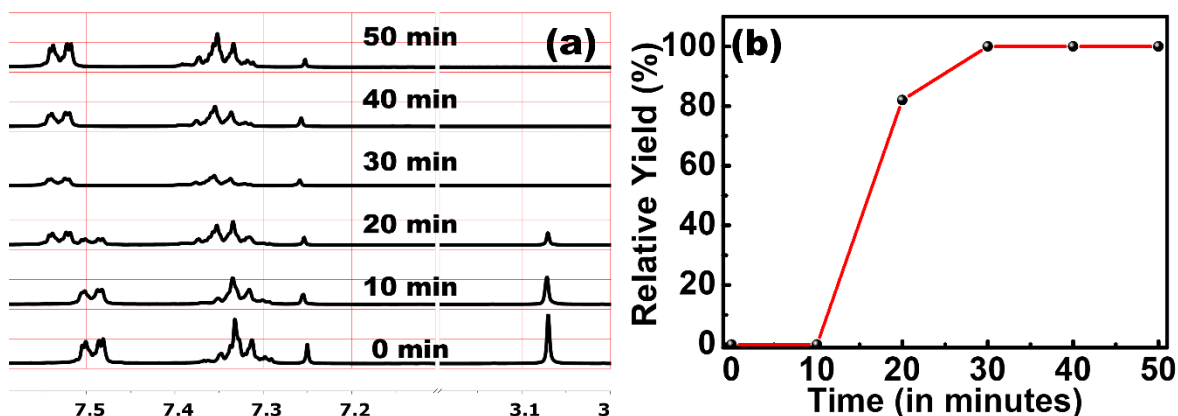


Figure S14. ^1H NMR stack plot of time dependent kinetic study for photocatalytic synthesis of compound **8p** in THF under anaerobic condition. (b) Relative Yield (%) of **8p** calculated from NMR stack plot.

Conclusion on the Kinetics of Homo-Glaser Under various Conditions: Analysis of the experimental findings and NMR study we found out that when the photocatalytic homo-Glaser reaction was performed in $^t\text{BuOH}/\text{H}_2\text{O}$ under the aerobic condition we obtained steady and good progress of the reaction over time. At 0 minute time, we did not observe the formation of the desired product (**8p**). However, yield of 23, 33, 34, 100 and 100% was obtained, respectively, at a time interval of 10, 20, 30, 40 and 50 minutes, respectively. In this case O_2 has played an important role in maintaining catalytic activity as $^t\text{BuOH}$ solvent is a good hole scavenger.²³ Similarly, when the reaction was performed using same solvent system under anaerobic (N_2) condition we observed that complete conversion of starting material to product **8p** did not take place. However, product was obtained, but the yield was moderate. Initially, at 20 minutes no product was identified. However, at 30 minutes, we observed a relative yield of only 13%, which ultimately reached a maximum yield of 61% after 50 minutes. Interestingly, in this condition the initiation of the reaction was found to be slow which resulted in a sluggish rate. The sluggish reaction rate is the possible outcome of occupied hole and absence of atmospheric O_2 hampering the catalytic cycle.²³ Following this we replaced the solvent system with THF, and the reaction was carried under both aerobic and anaerobic conditions. It was found out that initiation of reaction was slower as compared to $\text{H}_2\text{O}/^t\text{BuOH}$ system. It took 20 min for the reaction to start. At 20 min the yield was calculated to be only 15%. Afterwards, the yield shot up to almost 76%, which is much higher when compared to the yield obtained at 30 min for reaction in $\text{H}_2\text{O}/^t\text{BuOH}$ system. We further extended our understanding of the catalytic cycle behaviour by performing another reaction in THF under anaerobic condition to justify the role of hole. We found out that the initiation of the reaction started at 20 minute in THF/ N_2 condition it took 20 min for the reaction to initiate but surprisingly the yield was 82%. The kinetics study for standardization of homo-Glaser coupling to afford **8p** is shown in **Figure S15**.

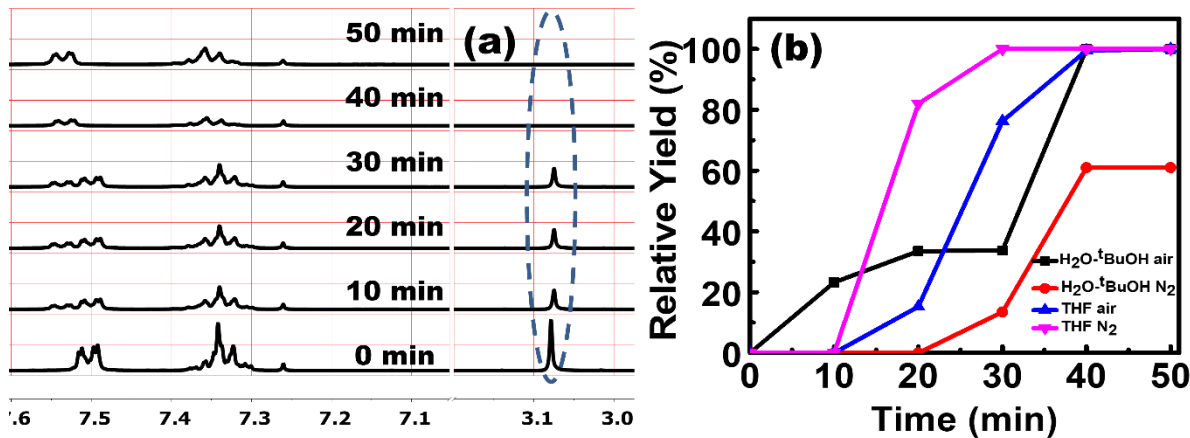


Figure S15. (a) ¹H NMR stack plot of time dependent kinetic study for photocatalytic synthesis of homo-Glaser compound **8p** in water/^tBuOH and air system. (b) Comparative relative yield from NMR kinetics study of homo-Glaser reaction for the synthesis of **8p** under different conditions and solvent systems.

9. Substrate Scope of the Photocatalytic Glaser Reaction

9.1. General Procedure for Photocatalytic Glaser Coupling

For hetero-Glaser coupling, the first alkyne **7i** (0.3 mmol, 1 equiv.) was taken in 20 ml of MQ H₂O and ^tBuOH (1:1) and stirred till solubility, following which the second alkyne **7a** (0.45 mmol, 1.5 equiv.) was added. Similarly, in-case of homocoupling, initially in the same solvent was dissolved the corresponding amount of terminal alkyne **7a** (0.3 mmol, 1 equiv.). In both the cases, the reaction mixture was stirred until the alkynes are entirely solubilised. To the reaction mixture was added the environmentally benign base, K₂CO₃ (0.45 mmol, 1.5 equiv.) and left to stir for 5 min. After that, 15 mg (0.1 mmol, 0.3 equiv.) of Cu²⁺@TiO₂ was added and again stirred for 5 min. After a stipulated time, the reaction mixture was placed in the photochemical reactor and was subjected to UV-Vis light irradiation in the wavelength range of (370-400 nm), under stirring condition. All the reactions were carried out in borosilicate round bottom flasks. Throughout the process, the reaction temperature was recorded to be within a range of 28 to 32 °C using a thermostat. After completion of the reaction as understood from TLC, the reaction mixture was filtered to separate and regain the catalyst. The desired compound was obtained by solvent extraction with ethyl acetate after being washed with NH₄Cl and brine solution thrice. The extracted organic phase was evaporated under reduced vacuum condition. The obtained compounds were purified by column chromatography and then characterised by various spectroscopic techniques.

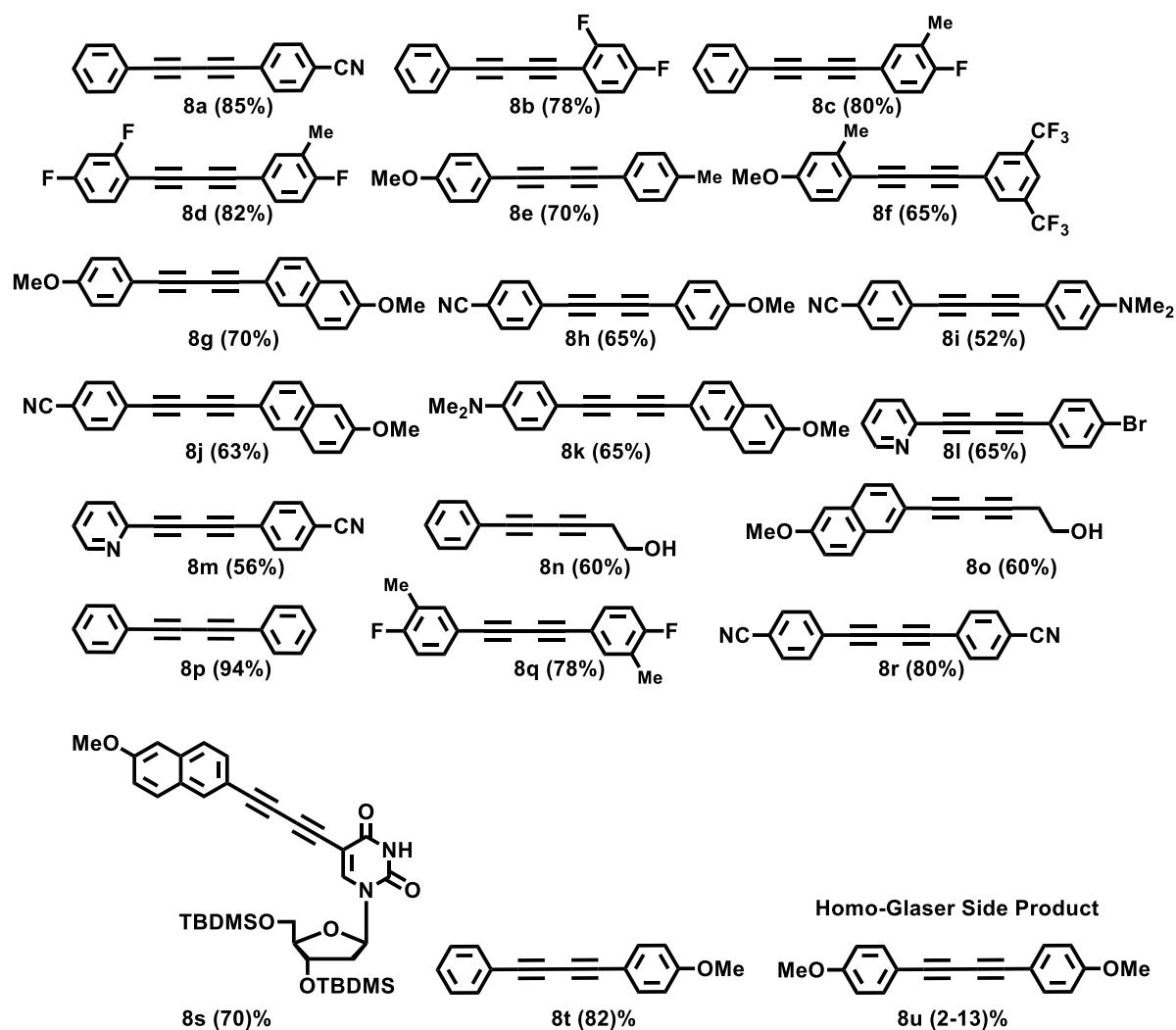


Figure S16. Chemical structures of the synthesized hetero-/homo-Glaser products through photocatalytic route.

10. Recyclability and Stability of The Photocatalyst

Finally, recyclability of the photocatalyst was tested for a total of five cycles for both the Hetero-Glaser with alkynes **7a/7l** couple and Homo-Glaser with alkynes **7a** couples. We observed that a maximum of 3-5 % loss in product yield was observed in all the cases after the 5th/6th cycle under air and in H₂O:^tBuOH solvent. The catalyst showed excellent stability even after the 5th/6th cycle (**Figure S17**). The similar stability was observed in the case of THF used as solvent under N₂ or air. In each step the catalyst was isolated from reaction mixture through filtration using whatmann filter paper. It was thoroughly and carefully washed with methanol and water several times and dried in hot air oven at 55-60 °C for 10 h. After complete drying the catalyst was re-weighed. Fortunately not much loss in catalyst was recorded (a negligible loss between 0.3 mg to 0.1 mg was observed).

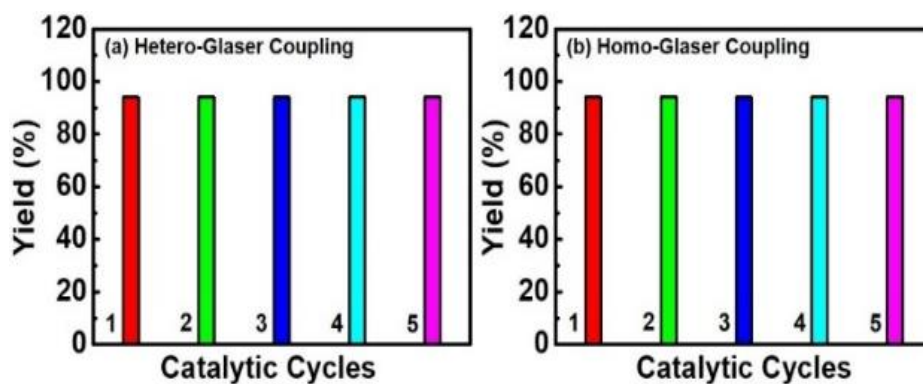


Figure S17. Reusability of $\text{Cu}^{2+}@\text{TiO}_2$ photocatalyst in water: $^t\text{BuOH}$ in the open air- (a) is for hetero-Glaser, (b) is for homo-Glaser.

Physical characteristics also remained similar before and after the reaction as was observed from TEM. After reaction from **Figure S18** we can observe that the integrity of the catalyst remained intact. The Cu^{2+} cores surrounded by TiO_2 shell is clearly visible for $\text{Cu}^{2+}@\text{TiO}_2$ photocatalyst, when isolated from the reaction mixture.

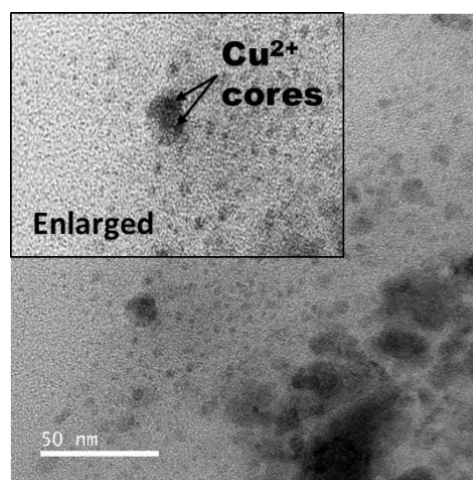


Figure S18. TEM image of recovered catalyst.

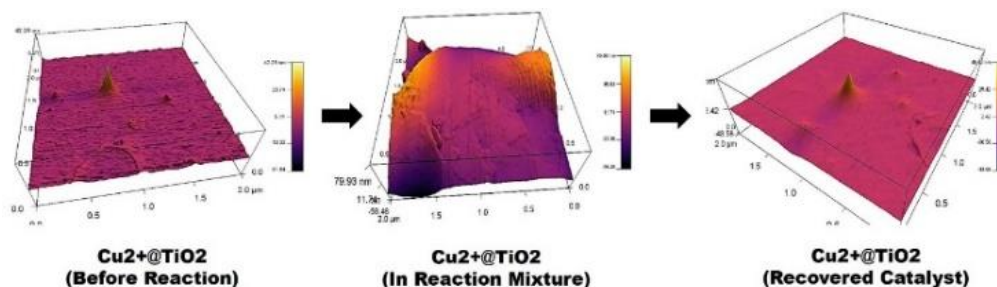


Figure S19. Recyclability of catalyst: topography of the catalyst at various stages (lateral view).

11.Procedures for Atomic Absorption Spectroscopic Measurement to Test the Leached out Concentration of Cu^{2+}

The leaching experiment was carried out in $\text{H}_2\text{O}/\text{BuOH}$ solvent system as shown in. $\text{Cu}^{2+}/\text{TiO}_2$ was stirred in reaction mixture for 6 h and sample was drawn from the reaction chamber every 1 h. Thereafter leached out concentration was checked using Atomic Absorption Spectrophotometer (Varian). Method settings was carried out using the inbuilt software. Cu (Flame) method was selected for analysis. Prior to feeding of test samples, a standard curve was plotted by feeding the machine with known concentration of Cu^{2+} (0, 2, 4, 6, 8 and 10) ppm. The standard was prepared from CuSO_4 in same solvent system. The analysis of atomic absorption spectroscopy (AAS) of the crude reaction mixtures at various time intervals showed no leached out copper in the solution indicating the added advantage as heterogeneous catalyst (**Figure S20**). This observation also suggested the excellent performance of the catalysts during several catalytic cycles. This stability might be due to continuous regeneration of Cu(I) from Cu(II) as the light falls on the photocatalyst and the oxidation of Cu(I) to Cu(II) by the air or hole to maintain the feed of the photocatalyst making possible to use for both the Glaser reactions.

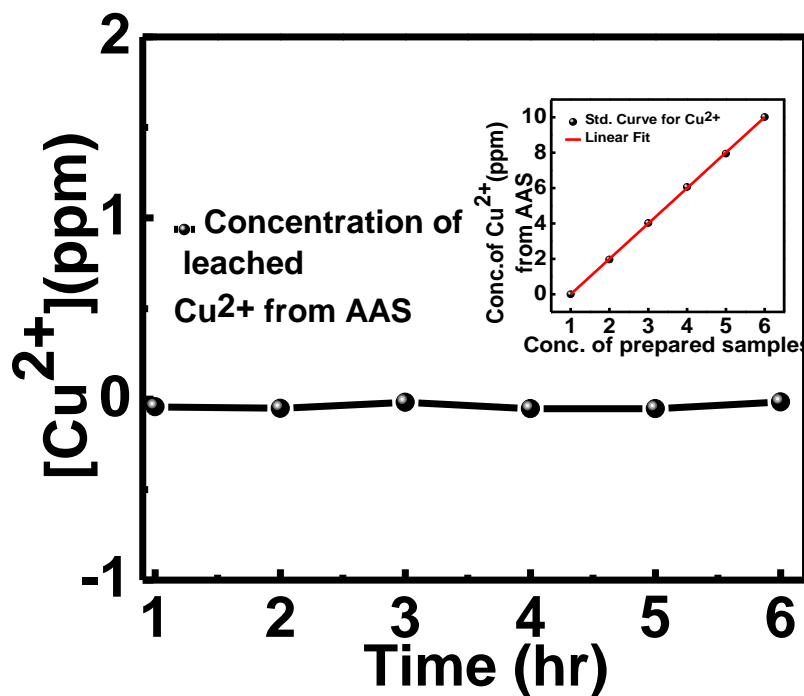


Figure S20. The analysis of the crude reaction mixtures by AAS showing no leached out copper in the solution

12.Characterisation of Synthesized Glaser Products

4-(phenylbuta-1,3-diyne-1-yl)benzonitrile (8a): Phenylacetylene (0.035 g, 0.35 mmol) (**7a**) and 0.030 g (0.23 mmol) of 4-ethynylbenzonitrile (**7l**) was taken in a 1:1 t-BuOH and water system. 15 mg of catalyst was added and the reaction was subjected to light for 3-6 h. After finishing starting material, the reaction mixture was evaporated to remove t-BuOH completely and it was partitioned by EtOAc and NH₄Cl solution. The organic layer was washed with brine, dried over Na₂SO₄. Pure product **8a** (0.045 g, 0.19 mmol) was isolated as a pale yellowish white gummy material in pure form by column chromatography (Si-gel, Hex:EA = 90:1, R_f=0.35). Yield 85%. IR (KBr) $\tilde{\nu}$ 3434, 2940, 2716, 2258, 2068, 1720, 1630, 1585, 1395, 1375, 1355, 1205, 923, 693cm⁻¹. ¹H NMR (CDCl₃, 400 MHz) δ 7.64 – 7.58 (m, 4H), 7.54 (d, J = 6.8 Hz, 2H), 7.40 (d, J = 7.1 Hz, 3H). ¹³C NMR (CDCl₃, 100 MHz) 133.1, 132.8, 132.2, 129.9, 128.7, 127.0, 121.3, 118.3, 112.5, 84.1, 79.5, 78.3, 76.9, 73.4. +ESI-HRMS calcd. for C₁₇H₁₀N [M + H]⁺ 228.0807, found 228.0820.

2,4-difluoro-1-(phenylbuta-1,3-diyne-1-yl)benzene (8b): 0.052 g (0.59 mmol) of phenylacetylene (**7a**) and 0.04 g (0.29 mmol) of 1-ethynyl-2,4-difluorobenzene (**7i**) was taken in a 1:1 t-BuOH and water system. 15 mg of catalyst was added and the reaction was subjected to light for 3-6 h. After finishing starting material, the reaction mixture was evaporated to remove t-BuOH completely and it was partitioned by EtOAc and NH₄Cl solution. The organic layer was washed with brine, dried over Na₂SO₄. Pure product **8b** (0.053 g, 0.22 mmol) was isolated as white solid powder in pure form by column chromatography (Si-gel, Hexane, R_f=0.68). Yield 78 %; m.p.80°C. IR (KBr) $\tilde{\nu}$ 3449, 2987, 2923, 2066, 1637, 1485cm⁻¹. ¹H NMR (CDCl₃, 400 MHz) δ 7.53 (dd, J = 7.9, 1.6 Hz, 4H), 7.41 – 7.30 (m, 3H), 6.87 (ddt, J = 11.5, 9.3, 2.7 Hz, 1H). ¹³C NMR (CDCl₃, 150 MHz) δ 165.2, 165.2, 164.2, 164.1, 163.5, 163.5, 162.5, 162.5, 135.4, 135.3, 132.7, 132.6, 129.6, 129.3, 128.6, 128.6, 121.9, 121.6, 112.1, 111.9, 104.8, 104.7, 104.5, 82.8, 81.7, 74.04. ¹⁹F NMR (470 MHz, CDCl₃) δ 103.86 (d, J = 9.2 Hz), -104.11 (d, J = 8.9 Hz), -104.19 (d, J = 9.1 Hz), -104.70 (d, J = 9.1 Hz). +ESI-HRMS calcd. for C₁₆H₉F₂ [M + H]⁺ 239.0667, found 239.0669.

1-fluoro-2-methyl-4-(phenylbuta-1,3-diyne-1-yl)benzene(8c): 0.061 g (0.59 mmol) of phenylacetylene (**7a**) and 0.04 g (0.29 mmol) of 4-ethynyl-1-fluoro-2-methylbenzene (**7j**) was taken in a 1:1 t-BuOH and water system. 15 mg of catalyst was added and the reaction was subjected to light for 3-6 h. After finishing starting material, the reaction mixture was evaporated to remove t-BuOH completely and it was partitioned by EtOAc and NH₄Cl solution. The organic layer was washed with brine, dried over Na₂SO₄. Pure product **8c** (0.055 g, 0.23 mmol) was isolated as white powder in pure form by column chromatography (Si-gel, Hexane, R_f=0.7). Yield 80 %; m.p.67 °C. IR (KBr) $\tilde{\nu}$ 3448, 2925, 2854, 2066, 1634, 1499cm⁻¹. ¹H NMR (CDCl₃, 500 MHz) δ 7.56 – 7.51 (m, 2H), 7.40 – 7.31 (m, 5H), 6.97 (t, J = 8.9 Hz, 1H), 2.26 (s, 3H); ¹³C NMR (CDCl₃, 100 MHz) δ 163.0, 160.5, 135.8, 135.7, 135.7, 135.7, 132.5, 132.5, 131.9, 131.8, 129.2, 128.4, 125.6, 125.4, 121.8, 121.8, 117.5, 117.5, 117.5, 117.5, 115.6, 115.3, 81.6, 81.3, 80.8, 80.6, 73.9, 73.9, 73.3, 73.3, 73.3, 14.9, 14.3. ¹⁹F NMR (CDCl₃, 470 MHz) δ 113.15 (d, J = 5.8 Hz). +ESI-HRMS calcd. for C₁₇H₁₂F [M + H]⁺ 235.0918, found 235.0959.

4-((2,4-difluorophenyl)buta-1,3-diyne-1-yl)-1-fluoro-2-methylbenzene (8d): 0.08 g (0.59 mmol) of 1-ethynyl-2,4-difluorobenzene (**7i**) and 0.04 g (0.29 mmol) of 4-ethynyl-1-fluoro-2-methylbenzene (**7j**), was taken in a 1:1 t-BuOH and water system. 15 mg of catalyst was added and the reaction was subjected to light for 3-6 h. After finishing starting material, the reaction

mixture was evaporated to remove t-BuOH completely and it was partitioned by EtOAc and NH₄Cl solution. The organic layer was washed with brine, dried over Na₂SO₄. Pure product **8d** (0.066 g, 0.24 mmol) was isolated as white solid

powder in pure form by column chromatography (Si-gel, Hexane, R_f = 0.56). Yield 82 %; m.p. 165 °C. IR (KBr) $\tilde{\nu}$ 3454, 2924, 2118, 1637, 1219 cm⁻¹. ¹H NMR (CDCl₃, 400 MHz) δ 7.50 (h, *J* = 6.0 Hz, 1H), 7.39 – 7.30 (m, 1H), 6.97 (td, *J* = 8.8, 3.5 Hz, 1H), 6.87 (tt, *J* = 9.0, 3.8 Hz, 3H), 2.26 (s, 3H). ¹³C NMR (CDCl₃, 150 MHz) δ 165.3, 165.2, 164.4, 164.3, 163.6, 163.5, 162.7, 162.6, 161.2, 135.9, 135.9, 135.4, 135.4, 135.4, 135.4, 135.3, 135.3, 132.1, 132.1, 125.8, 125.7, 115.7, 115.6, 112.2, 112.2, 112.1, 112.1, 112.0, 112.0, 111.9, 111.9, 106.9, 106.9, 106.8, 106.8, 104.9, 104.8, 104.7, 104.7, 104.6, 104.5, 82.0, 78.6, 78.2, 74.9, 73.6, 73.0, 14.5, 14.5. ¹⁹F NMR (CDCl₃, 470 MHz) δ 103.88 (d, *J* = 9.2 Hz), -104.17 (d, *J* = 9.1 Hz), -104.23 (d, *J* = 9.1 Hz), -104.73 (d, *J* = 9.0 Hz), -112.70, -113.16. +ESI-HRMS calcd. for C₁₇H₁₀F₃[M + H]⁺ 271.0729, found 271.0749.

1-methoxy-4-(p-tolylbuta-1,3-diyne-1-yl)benzene (8e): 0.059 g (0.45 mmol) of 1-ethynyl-4-methoxybenzene (**7c**) and 0.035 g (0.30 mmol) of 4-ethynyltoluene (**7b**) was taken in a 1:1 t-BuOH and water system. 15 mg of catalyst was added and the reaction was subjected to light for 3-6 h. After finishing starting material, the reaction mixture was evaporated to remove t-BuOH

completely and it was partitioned by EtOAc and NH₄Cl solution. The organic layer was washed with brine, dried over Na₂SO₄. Pure product **8e** (0.052 g, 0.21 mmol) was isolated as a pale yellowish solid material in pure form by column chromatography (Si-gel, Hex:EA = 50:1, R_f = 0.3). Yield 70%; m.p. 133 °C. IR (KBr) $\tilde{\nu}$ 3434, 2940, 2361, 2215, 2138, 1585, 1395, 1375, 1355 cm⁻¹. ¹H NMR (CDCl₃, 400 MHz) δ 7.46 (d, *J* = 8.8 Hz, 2H), 7.41 (d, *J* = 8.0 Hz, 1H), 7.14 (d, *J* = 7.8 Hz, 1H), 6.85 (d, *J* = 8.7 Hz, 2H), 3.82 (s, 3H), 2.17 (s, 3H). +ESI-HRMS calcd. for C₁₈H₁₅O[M + H]⁺ 247.111, found 247.120.

1-((3,5-bis(trifluoromethyl)phenyl)buta-1,3-diyne-1-yl)-4-methoxy-2-methylbenzene (8f): 0.036 g (0.25 mmol) of 1-ethynyl-4-methoxy-2-methylbenzene (**7d**) and 0.04 g (0.16 mmol) of 1-ethynyl-3,5-bis(trifluoromethyl)benzene (**7k**) was taken in a 1:1 t-BuOH and water system. 15 mg of catalyst was added and the reaction was subjected to light for 3-6 h. After finishing starting

material, the reaction mixture was evaporated to remove t-BuOH completely and it was partitioned by EtOAc and NH₄Cl solution. The organic layer was washed with brine, dried over Na₂SO₄. Pure product **8f** (0.038 g, 0.09 mmol)

was isolated as light yellowish gummy material in pure form by column chromatography (Si-gel, Hexane, R_f = 0.68). Yield 65 %. IR (KBr) $\tilde{\nu}$ 3433, 2956, 2922, 2852, 2109, 1635, 1467, 1219 cm⁻¹. ¹H NMR (CDCl₃, 500 MHz) δ 7.43 (d, *J* = 8.6 Hz, 2H), 6.75 (d, *J* = 2.8 Hz, 2H), 6.69 (dd, *J* = 8.5, 2.8 Hz, 2H), 3.81 (s, 3H), 2.47 (s, 3H). ¹³C NMR (CDCl₃, 126 MHz) δ 160.2, 143.6, 134.5, 115.4, 114.3, 111.6, 80.9, 76.7, 55.4, 21.2. ¹⁹F NMR (CDCl₃, 470 MHz) δ 62.99, -63.22. +ESI-HRMS calcd. for C₂₀H₁₃F₆O[M + H]⁺ 383.0865, found 383.0873.

2-methoxy-7-((4-methoxyphenyl)buta-1,3-diyne-1-yl)naphthalene (8g): 0.050 g (0.38 mmol) of 4-ethynylanisole (**7c**) and 0.045 g (0.25 mmol) of 2-ethynyl-6-methoxynaphthalene (**7e**) was taken in a 1:1 t-BuOH and water system. 15 mg of catalyst was added and the reaction was subjected to light for 3-6 h. After finishing starting material, the reaction mixture was evaporated

to remove t-BuOH completely and it was partitioned by EtOAc and NH₄Cl

solution. The organic layer was washed with brine, dried over Na₂SO₄. Pure product **8g** (0.054 g, 0.17mmol) was isolated as a yellow white solid in pure form by column chromatography (Si-gel, Hex:EA = 20:1, R_f=0.7, FL). Yield 70%; m.p. 174°C. IR (KBr) $\tilde{\nu}$ 3448, 2925, 2069, 1634, 1383, 1107, 536 cm⁻¹. ¹H NMR (CDCl₃, 400 MHz) δ 7.99 (d, J = 10.8 Hz, 1H), 7.69 (td, J = 9.5, 5.4 Hz, 2H), 7.54 – 7.44 (m, 3H), 7.17 (dt, J = 8.9, 2.9 Hz, 1H), 7.11 (t, J = 2.7 Hz, 1H), 6.87 (d, J = 8.8 Hz, 2H), 3.93 (d, J = 2.1 Hz, 3H), 3.82 (d, J = 3.3 Hz, 3H). ¹³C NMR (CDCl₃, 100 MHz) δ 160.5, 158.9, 134.2, 134.2, 132.9, 132.8, 129.6, 129.3, 128.5, 127.1, 119.8, 114.3, 114.0, 106.0, 82.4, 81.9, 74.0, 73.2, 55.5, 55.5. +ESI-HRMS calcd. for HRMS calcd. for C₂₂H₁₇O₂ [M + H]⁺ 313.1223, found 313.1221.

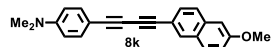
4-((4-methoxyphenyl)buta-1,3-diyne-1-yl)benzotrile (8h): 0.03 g (0.24mmol) of 4-ethynylbenzotrile (**7i**) and 0.02 g (0.15mmol) of 1-ethynyl-4-methoxybenzene (**7c**), was taken in a 1:1 t-BuOH and water system. 15 mg of catalyst was added and the reaction was subjected to light for 3-6 h. After finishing starting material, the reaction mixture was evaporated to remove t-BuOH completely and it was partitioned by EtOAc and NH₄Cl solution. The organic layer was washed with brine, dried over Na₂SO₄. The pure product **8h** (0.031 g, 0.12mmol) was isolated as a pale yellowish white solid powder in pure form by column chromatography (Si-gel, Hexane, R_f=0.3). Yield 80%; m.p. 213°C. IR (KBr): $\tilde{\nu}$ 3433.18, 2955.95, 2922.39, 2852.20 2109.37, 1635.02, 1466.98, 1219.16. ¹H NMR (CDCl₃, 400 MHz) δ 7.60 (dt, J = 15.4, 7.2 Hz, 4H), 7.47 (dd, J = 10.6, 8.7 Hz, 2H), 6.89 – 6.83 (m, 2H), 3.83 (d, J = 5.2 Hz, 4H). ¹³C NMR (CDCl₃, 100 MHz) δ 160.9, 160.4, 134.5, 134.2, 133.2, 132.9, 132.3, 132.2, 127.3, 114.4, 114.3, 114.2, 113.2, 112.3, 81.4, 79.1, 78.7, 73.13, 72.36, 55.53. +ESI-HRMS calcd. for C₁₈H₁₂NO [M + H]⁺ 258.0913, found 258.0925.

4-((4-(dimethylamino)phenyl)buta-1,3-diyne-1-yl)benzotrile (8i): 0.053 g (0.41 mmol) of 4-ethynylbenzotrile (**7i**) and 0.040 g (0.27 mmol) of 4-ethynyl-N,N-dimethylaniline (**7g**) was taken in a 1:1 t-BuOH and water system. 15 mg of catalyst was added and the reaction was subjected to light for 3-6 h. After finishing starting material, the reaction mixture was evaporated to remove t-BuOH completely and it was partitioned by EtOAc and NH₄Cl solution. The organic layer was washed with brine, dried over Na₂SO₄. Pure product **8i** (0.038 g, 0.14 mmol) was isolated as a brown gummy material in pure form by column chromatography (Si-gel, Hex:EA = 90:1, R_f=0.3). Yield 52%. IR (KBr) $\tilde{\nu}$ 3448, 2229, 2085, 1638, 1382, 1353, 573 cm⁻¹. ¹H NMR (CDCl₃, 400 MHz) δ 7.62 (d, J = 8.5 Hz, 2H), 7.57 (d, J = 8.5 Hz, 2H), 7.36 (d, J = 8.9 Hz, 2H), 6.62 (d, J = 8.9 Hz, 2H), 2.97 (s, 6H). ¹³C NMR (CDCl₃, 100 MHz) δ 150.6, 133.4, 132.8, 132.2, 130.7, 111.8, 110.8, 108.9, 85.0, 82.0, 81.7, 74.89, 40.30. +ESI-HRMS calcd. for C₁₉H₁₅N₂ [M + H]⁺ 271.1229, found 271.1240. ¹³C NMR (101 MHz, CDCl₃) δ

4-((7-methoxynaphthalen-2-yl)buta-1,3-diyne-1-yl)benzotrile (8j): 0.040 g (0.31 mmol) of 4-ethynylbenzotrile (**7i**) and 0.038 g (0.21 mmol) of 2-ethynyl-6-methoxynaphthalene (**7e**) was taken in a 1:1 t-BuOH and water system. 15 mg of catalyst was added and the reaction was subjected to light for 3-6 h. After finishing starting material, the reaction mixture was evaporated to remove t-BuOH completely and it was partitioned by EtOAc and NH₄Cl solution. The organic layer was washed with brine, dried over Na₂SO₄. Pure product **8j** (0.045 g, 0.14 mmol) was isolated as a brownish white solid in pure form by column chromatography (Si-gel, Hex:EA = 50:1, R_f=0.15, FL). Yield 70%; m.p. 220°C. IR (KBr) $\tilde{\nu}$ 3361, 2898, 2748, 2229, 1578, 1396, 1375, 1355, 762, 573 cm⁻¹. ¹H NMR (CDCl₃, 400 MHz) δ 8.01 (s, 1H), 7.71 (d, J = 8.3 Hz, 2H), 7.67 (d, J = 3.5 Hz, 1H), 7.66 – 7.57 (m, 3H), 7.54 – 7.48 (m, 1H),

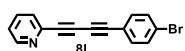
7.21 – 7.15 (m, 1H), 7.11 (s, 1H), 3.93 (s, 3H). ¹³C NMR (CDCl₃, 100 MHz) δ 159.2, 135.1, 133.0, 132.9, 132.2, 129.6, 129.58, 129.14, 127.25, 127.11, 119.97, 119.77, 118.41, 79.40, 78.68, 74.04, 73.12, 55.54. +ESI-HRMS calcd. for C₂₂H₁₄NO [M + H]⁺ 308.1069, found 308.1067.

4-((7-methoxynaphthalen-2-yl)buta-1,3-diyne-1-yl)-N,N-dimethylaniline (8k): 0.040 g (0.27 mmol) of 4-ethynyl-N,N-dimethylaniline (**7g**) and 0.033 g (0.18 mmol) of 2-ethynyl-6-methoxynaphthalene (**7e**) was taken in a 1:1 t-BuOH and water system. 15 mg of catalyst was



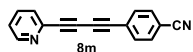
added and the reaction was subjected to light for 3-6 h. After finishing starting material, the reaction mixture was evaporated to remove t-BuOH completely and it was partitioned by EtOAc and NH₄Cl solution. The organic layer was washed with brine, dried over Na₂SO₄. Pure product **8k** (0.038 g, 0.11 mmol) was isolated as a greenish brown solid in pure form by column chromatography (Si-gel, Hex:EA = 50:1, R_f=0.3). Yield 65%; m.p. 179°C. IR (KBr) $\tilde{\nu}$ 3434, 2940, 2716, 2258, 2068, 1720, 1630, 1585, 1395, 1375, 1355, 1205, 923, 693 cm⁻¹. ¹H NMR (CDCl₃, 400 MHz) δ 8.00 (s, 1H), 7.69 (q, J = 10.1, 9.7 Hz, 2H), 7.54 – 7.47 (m, 1H), 7.40 (dd, J = 13.5, 8.9 Hz, 2H), 7.20 – 7.13 (m, 1H), 7.11 (dd, J = 5.7, 2.3 Hz, 1H), 6.62 (dd, J = 8.8, 6.0 Hz, 2H), 3.93 (d, J = 3.5 Hz, 3H), 2.99 (d, J = 6.5 Hz, 6H). ¹³C NMR (CDCl₃, 100 MHz) δ 158.9, 150.7, 134.8, 134.5, 133.9, 133.8, 132.9, 132.6, 129.5, 129.3, 127.1, 127.0, 119.8, 119.6, 111.8, 106.1, 83.5, 82.4, 74.1, 72.5, 55.5, 40.2. +ESI-HRMS calcd. for C₂₃H₂₀NO [M + H]⁺ 326.1539, found 326.1553.

2-((4-bromophenyl)buta-1,3-diyne-1-yl)pyridine (8l): 0.030 g (0.29 mmol) of 2-ethynylpyridine (**7f**) and 0.08 g (0.44 mmol) of 1-ethynyl-4-bromobenzene (**7h**) was taken in a 1:1 t-BuOH and water system. 15 mg of catalyst was added and the reaction was subjected to light for 3-6 h. After finishing starting material, the reaction mixture was evaporated to remove t-BuOH completely and it was partitioned by EtOAc and NH₄Cl solution. The organic layer was washed with brine,



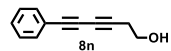
dried over Na₂SO₄. Pure product **8l** (0.05 g, 0.18 mmol) was isolated as a dark brownish gummy material in pure form by column chromatography (Si-gel, Hex:EA = 5:1, R_f=0.5). Yield 65%. IR (KBr) $\tilde{\nu}$ 3448, 2940, 2256, 2064, 1721, 1636, 1396, 1374, 1204, 1039, 921 cm⁻¹. ¹H NMR (CDCl₃, 400 MHz) δ 8.72 (d, J = 4.7 Hz, 1H), 8.04 (d, J = 7.9 Hz, 2H), 7.62 (d, J = 8.8 Hz, 2H), 7.50 – 7.35 (m, 1H), 7.22 – 7.16 (m, 1H), 6.95 (t, J = 6.9 Hz, 1H). ¹³C NMR (CDCl₃, 100 MHz) δ 135.9, 135.8, 132.7, 132.1, 131.9, 129.3, 128.6, 125.8, 125.6, 121.9, 121.9, 117.7, 117.6, 117.6, 81.7, 81.5, 80.9, 80.7, 74.1. +ESI-HRMS calcd. for C₁₅H₉BrN [M + H]⁺ 281.9913, found 281.9920.

4-(pyridin-2-ylbuta-1,3-diyne-1-yl)benzotrile (8m): 0.035 g (0.28 mmol) of 4-ethynylbenzotrile (**7i**) and 0.018 g (0.18 mmol) of 2-ethynylpyridine (**7f**) was taken in a 1:1 t-BuOH and water system. 15 mg of catalyst was added and the reaction was subjected to light for 3-6 h. After finishing starting material, the reaction mixture was evaporated to remove t-BuOH completely and it was partitioned by EtOAc and NH₄Cl solution. The organic layer was washed



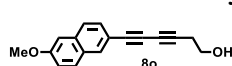
with brine, dried over Na₂SO₄. Pure product **8m** (0.02 g, 0.1 mmol) was isolated as a reddish brown gummy material in pure form by column chromatography (Si-gel, Hex:EA = 5:1, R_f=0.2). Yield 56%. IR (KBr) $\tilde{\nu}$ 3452, 2919, 2849, 2229, 2073, 1637, 1468, 1368, 1117, 614 cm⁻¹. ¹H NMR (CDCl₃, 400 MHz) δ 10.01 (d, J = 7.1 Hz, 1H), 7.85 (d, J = 8.2 Hz, 2H), 7.77 (d, J = 8.2 Hz, 2H), 7.64 (d, J = 8.8 Hz, 1H), 7.25 – 7.20 (m, 1H), 6.99 (t, J = 6.9 Hz, 1H). ¹³C NMR (CDCl₃, 100 MHz) δ 135.9, 135.8, 132.7, 132.1, 131.9, 129.3, 128.6, 125.8, 125.6, 121.9, 121.9, 117.7, 117.6, 117.6, 115.7, 115.5, 81.7, 81.5, 80.9, 80.7, 74.1. +ESI-HRMS calcd. for C₁₆H₉N₂ [M + H]⁺ 229.0760, found 229.0728.

6-phenylhexa-3,5-diyne-1-ol (8n): 0.08 g (0.44mmol) of phenyl acetylene (**7a**) and 0.04 g (0.57mmol) of 3-butyn-1-ol (**7m**) was taken in a 1:1 t-BuOH and water system. 15 mg of catalyst was added and the reaction was subjected to light for 3-6 h. After finishing starting material, the reaction mixture was evaporated to remove t-BuOH completely and it was partitioned by EtOAc and NH₄Cl solution. The organic layer was washed with brine, dried over Na₂SO₄.



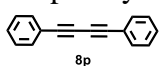
Pure product **8n** (0.05 g, 0.18 mmol) was isolated as a yellowish gummy material in pure form by column chromatography (Si-gel, Hexane, R_f=0.35). Yield 60%. IR (KBr) $\tilde{\nu}$ 3452, 2063, 1633, 1396, 1377, 1356, 609cm⁻¹. ¹H NMR (CDCl₃, 400 MHz) δ 7.48 (dd, J = 8.0, 1.6 Hz, 2H), 7.35 – 7.28 (m, 3H), 3.80 (t, J = 6.2 Hz, 2H), 3.18 (t, J = 5.3 Hz, 1H), 2.64 (t, J = 6.2 Hz, 2H). ¹³C NMR (CDCl₃, 100 MHz) δ 132.7, 129.2, 128.5, 121.9, 81.1, 75.5, 74.1, 67.0, 60.9, 29.8. +ESI-HRMS calcd. for C₁₂H₁₁O[M + H]⁺ 171.0809, found 171.0857.

6-(7-methoxynaphthalen-2-yl)hexa-3,5-diyne-1-ol (8o): 0.050 g (0.27mmol) of 2-ethynyl-6-methoxynaphthalene (**7e**) and 0.028 g (0.41mmol) of 3-butyn-1-ol (**7m**) was taken in a 1:1 t-BuOH and water system. 15 mg of catalyst was added and the reaction was subjected to light for



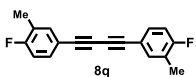
3-6 h. After finishing starting material, the reaction mixture was evaporated to remove t-BuOH completely and it was partitioned by EtOAc and NH₄Cl solution. The organic layer was washed with brine, dried over Na₂SO₄. Pure product **8o** (0.054 g, 0.17mmol) was isolated as a reddish brown gummy material in pure form by column chromatography (Si-gel, Hex:EA = 5:1, R_f=0.2). Yield 60%. IR (KBr) $\tilde{\nu}$ 3444, 2925, 2854, 2077, 1631, 1394, 1377, 1357, 573cm⁻¹. ¹H NMR (CDCl₃, 500 MHz) δ 7.94 (s, 1H), 7.66 (dd, J = 13.6, 8.8 Hz, 2H), 7.45 (d, J = 7.2 Hz, 1H), 7.15 (dd, J = 8.9, 2.3 Hz, 1H), 7.10 – 7.08 (m, 1H), 3.92 (s, 3H), 3.81 (t, J = 6.2 Hz, 2H), 3.19 – 3.14 (m, 1H), 2.66 (t, J = 6.2 Hz, 2H). ¹³C NMR (CDCl₃, 126 MHz) δ 158.8, 134.7, 132.9, 129.5, 129.4, 128.5, 127.1, 119.6, 116.7, 106.1, 80.9, 76.3, 73.8, 67.3, 61.0, 55.5, 48.1. +ESI-HRMS calcd. for C₁₇H₁₅O₂[M + H]⁺ 251.1066, found 251.1079.

1,4-diphenylbuta-1,3-diyne (8p): 0.1 g (0.98mmol) of phenylacetylene (**7a**) was taken in a 1:1 t-BuOH and water system. 15 mg of catalyst was added and the reaction was subjected to light for 3-6 h. After finishing starting material, the reaction mixture was evaporated to remove t-BuOH completely and it was partitioned by EtOAc and NH₄Cl solution. The organic layer was washed



with brine, dried over Na₂SO₄. Pure product **8p** (0.17g, 0.84mmol) was isolated as a white solid crystal in pure form by column chromatography (Si-gel, Hexane, R_f = 0.85). Yield 94%; m.p.87°C. IR (KBr) $\tilde{\nu}$ 3436, 2149, 1634, 1105, 971, 755, 523cm⁻¹. ¹H NMR (CDCl₃, 400 MHz) δ 7.58 – 7.53 (m, 4H), 7.37 (t, J = 7.6 Hz, 6H). ¹³C NMR (CDCl₃, 100 MHz) δ 132.6, 129.3, 128.6, 121.9, 81.7, 74.10. +ESI-HRMS calcd. for C₁₆H₁₁ [M + H]⁺ 203.0855, found 203.0860.

1,4-bis(4-fluoro-3-methylphenyl)buta-1,3-diyne (8q): 0.04 g (0.29mmol) of 4-ethynyl-1-fluoro-2-methylbenzene (**7j**), was taken in a 1:1 t-BuOH and water system. 15 mg of catalyst was added and the reaction was subjected to light for 3-6 h. After finishing starting material, the reaction mixture was evaporated to remove t-BuOH completely and it was partitioned by EtOAc and NH₄Cl solution. The organic layer was washed with brine, dried over



Na₂SO₄. Pure product **8q** (0.061 g, 0.23 mmol) was isolated as yellow needle shaped solid in pure form by column chromatography (Si-gel, Hexane, R_f=0.56). Yield 78%; m.p.167°C. IR (KBr) $\tilde{\nu}$ 3462, 2076, 1637, 1495cm⁻¹. ¹H NMR (CDCl₃, 500 MHz) δ 7.38 – 7.30 (m, 4H), 6.97 (t, J = 8.9 Hz, 2H), 2.26 (s, 6H). ¹³C NMR (CDCl₃, 100 MHz) δ 163.2, 160.7, 135.9, 135.8, 132.1, 131.9, 125.8, 125.6, 117.7, 117.6, 115.7, 115.5, 73.4, 14.5. ¹⁹F NMR (CDCl₃, 470 MHz) δ -113.11. +ESI-HRMS calcd. for C₁₈H₁₆F₂N[M + NH₄]⁺ 284.1245,

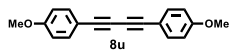
found 284.1234.

4,4'-(buta-1,3-diyne-1,4-diyl)dibenzonitrile (8r): 0.04 g (0.31mmol) 4-ethynylbenzonitrile (**7l**) was taken in a 1:1 t-BuOH and water system. 15 mg of catalyst was added and the reaction was subjected to light for 3-6 h. After finishing starting material, the reaction mixture was evaporated to remove t-BuOH completely and it was partitioned by EtOAc and NH₄Cl solution. The organic layer was washed with brine, dried over Na₂SO₄. Pure product **8r** (0.063 g, 0.25mmol) was isolated as pale whitish powder in pure form by column chromatography (Si-gel, Hex:EA = 10:1, R_f=0.7). Yield 80%; m.p.184°C. IR (KBr): $\tilde{\nu}$ 3628.89, 3276.86, 1636.40, 1219.40. ¹H NMR (600 MHz, δ)7.62 (d, J = 8.3 Hz, 4H), 7.57 (d, J = 8.1 Hz, 4H). ¹³C NMR (CDCl₃, 100 MHz) δ 132.8, 132.2, 127.1, 118.4, 112.4, 81.9, 81.7. +ESI-HRMS calcd. for C₁₈H₉N₂[M + H⁺] 253.0760, found 253.0790.

4-(phenylbuta-1,3-diyne-1-yl)benzonitrile (8s): 0.040 g (0.08 mmol) of 3',5'-di-*o*-tert-butylsilyl-5-ethynyl-2'-deoxyuridine (**7n**) and 0.022 g (0.12 mmol) of 2-ethynyl-6-methoxynaphthalene (**7e**) was taken in a 1:1 t-BuOH and water system. 15 mg of catalyst was added and the reaction was subjected to light for 3-6 h. After finishing starting material, the reaction mixture was evaporated to remove t-BuOH completely and it was partitioned by EtOAc and NH₄Cl solution. The organic layer was washed with brine, dried over Na₂SO₄. Pure product **8s** (0.038 g, 0.057mmol) was isolated as a pale yellowish white gummy material in pure form by column chromatography (Si-gel, Hex:EA = 5:1, R_f=0.2). Yield 70%. IR (KBr) $\tilde{\nu}$ 3436, 2085, 1637, 1396, 1377, 1356, 1118, 616 cm⁻¹. ¹H NMR (CDCl₃, 400 MHz) δ 7.94 (s, 1H), 7.68 (dd, J = 11.4, 8.9 Hz, 2H), 7.45 (d, J = 8.5 Hz, 1H), 7.17 (d, J = 2.5 Hz, 1H), 7.15 (d, J = 2.4 Hz, 1H), 7.10 (d, J = 2.2 Hz, 1H), 6.29 (t, J = 6.5 Hz, 1H), 4.42 (dt, J = 5.6, 2.7 Hz, 1H), 4.00 (d, J = 2.3 Hz, 1H), 3.95 (d, J = 2.3 Hz, 0H), 3.93 (s, 3H), 3.78 (dd, J = 11.5, 1.9 Hz, 1H), 2.35 (ddd, J = 13.2, 5.9, 3.0 Hz, 1H), 2.06 (dt, J = 13.2, 6.4 Hz, 1H), 0.98 (s, 9H), 0.90 (s, 9H), 0.18 (d, J = 8.5 Hz, 6H), 0.09 (d, J = 2.7 Hz, 6H); ¹³C NMR (CDCl₃, 100 MHz) δ 161.1, 158.9, 148.9, 144.5, 134.8, 132.9, 129.6, 129.2, 128.4, 127.1, 119.8, 116.5, 106.0, 99.5, 88.7, 86.2, 83.2, 79.2, 77.2, 73.7, 72.7, 72.3, 63.0, 55.5, 42.4, 29.8, 26.2, 25.9, 18.6, 18.1, -4.2, -4.7, -5.2, -5.3. +ESI-HRMS calcd. for C₃₆H₄₉N₂O₆Si₂ [M + H]⁺ 661.312, found 661.320.

1-methoxy-4-(phenylbuta-1,3-diyne-1-yl)benzene (8t): 0.054 g (0.53mmol) 4-ethynylbenzonitrile (**7l**) and 1-ethynyl-4-methoxybenzene (**7c**) was taken in a 1:1 t-BuOH and water system. 15 mg of catalyst was added and the reaction was subjected to light for 3-6 h. After finishing the starting material, the reaction mixture was evaporated to remove t-BuOH completely and it was partitioned by EtOAc and NH₄Cl solution. The organic layer was washed with brine, dried over Na₂SO₄. Pure product **8t** (0.067 g, 0.29 mmol) was isolated as pale whitish powder in pure form by column chromatography (Si-gel, Hex=100% R_f=0.35). Yield 82%; m.p.96.4°C. IR (KBr): $\tilde{\nu}$ 3628.89, 2361, 2212, 2138 cm⁻¹. ¹H NMR (500 MHz, δ)7.53 (d, J = 7.6 Hz, 2H), 7.48 (d, J = 8.8 Hz, 2H), 7.35 (t, J = 8.9 Hz, 3H), 6.86 (d, J = 8.8 Hz, 2H), 3.82 (s, 3H). ¹³C NMR (CDCl₃, 100 MHz) δ 160.5, 134.3, 132.6, 129.1, 128.5, 122.2, 114.3, 113.9, 81.9, 81.2, 77.4, 76.9, 74.4, 72.9, 55.5. +ESI-HRMS calcd. for C₁₇H₁₃O [M + H]⁺ 233.0961, found 233.0956.

1,4-bis(4-methoxyphenyl)buta-1,3-diyne (8u):8u is the side product obtained during standardization of hetero Glaser reactions. ¹H NMR (400 MHz, δ) 7.46 (d, J = 8.8 Hz, 4H), 6.85 (d, J = 8.8 Hz, 4H), 3.82 (s, 6H). ¹³C NMR (CDCl₃, 100 MHz) δ 160.4, 134.2, 114.3, 81.4, 77.5, 76.8, 73.1, 55.5.



13.NMR ^1H and ^{13}C of Glaser Derivatives Synthesized Through Photocatalytic Route

SSB-SS-377-1H

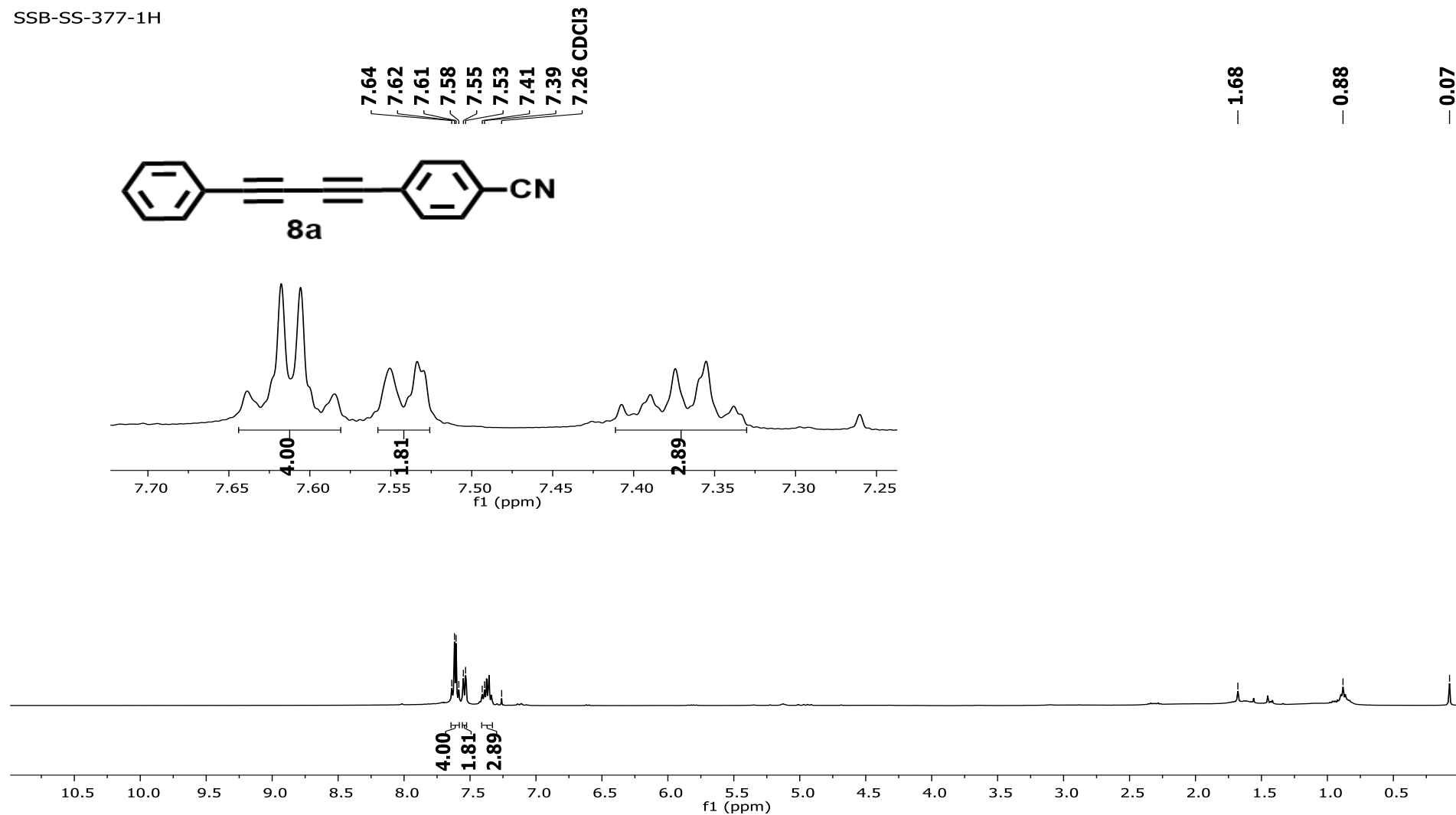


Figure S21. ^1H NMR spectrum of 4-(phenylbuta-1,3-diyne-1-yl)benzonitrile (8a).

SSB-SS-377-13C

133.06
132.77
132.24
129.87
128.69
127.01
121.35
118.35
112.55

84.11
79.46
78.32
77.48
77.16 CDCl₃
76.84
73.40

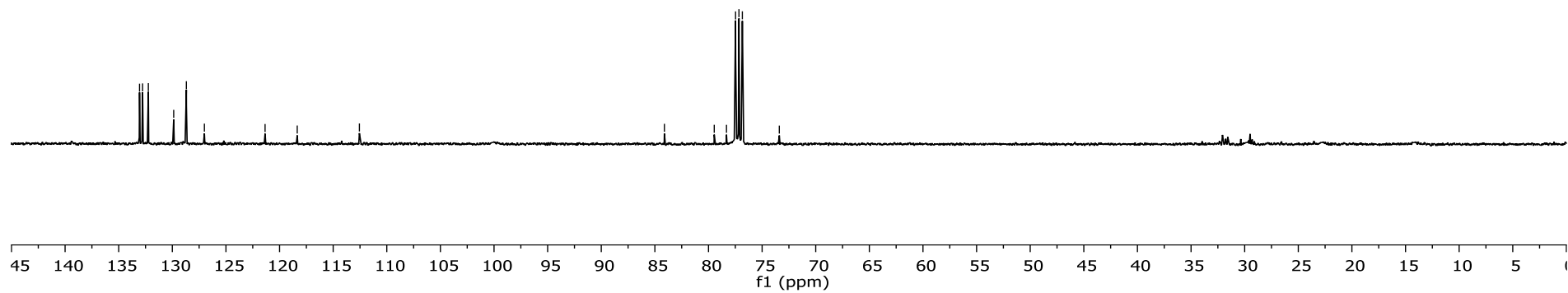
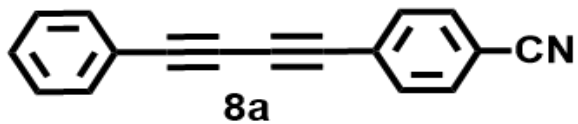


Figure S22. ¹³C NMR spectrum of 4-(phenylbuta-1,3-dyn-1-yl)benzonitrile (8a).

SSB-SS-166-1H

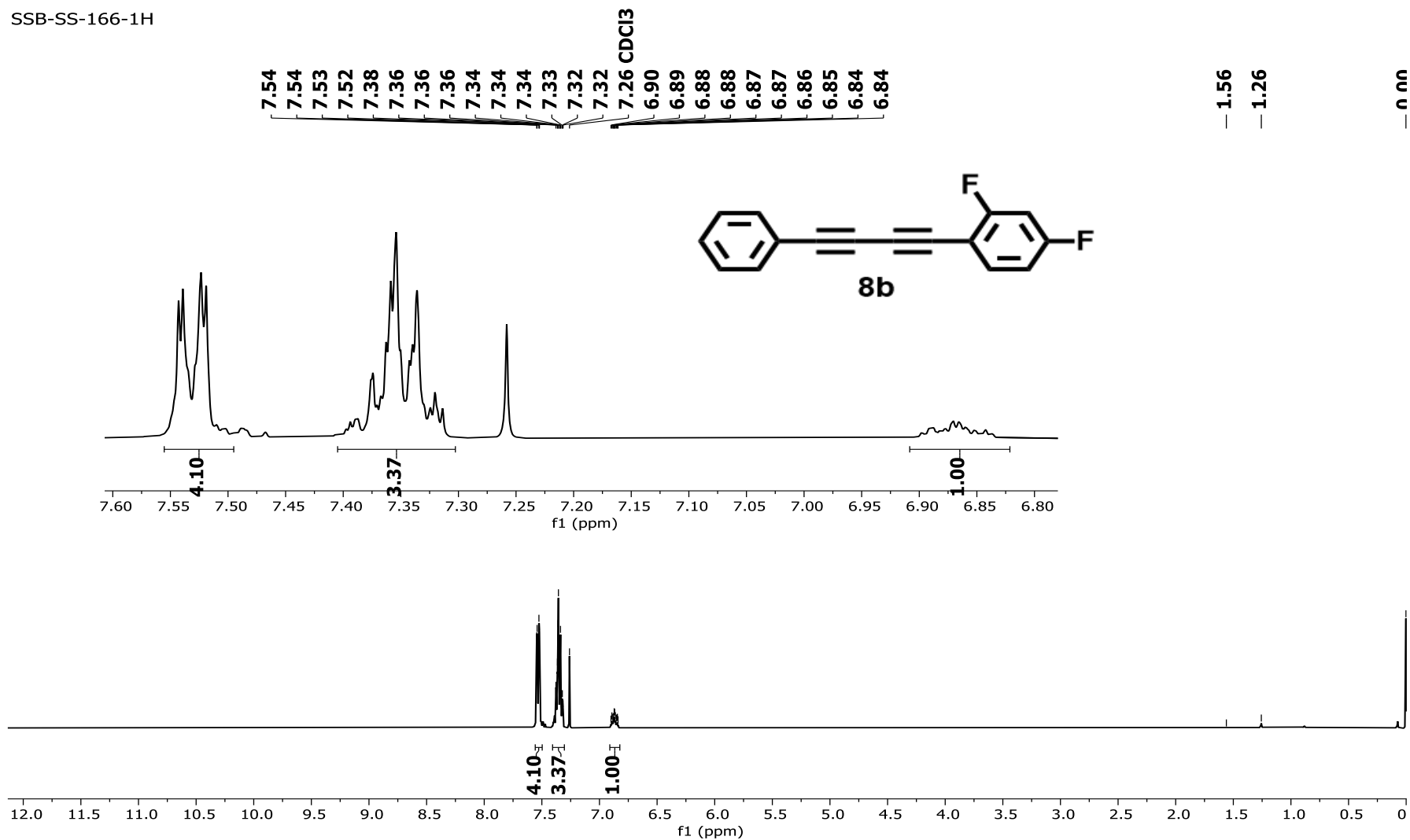


Figure S23. ¹H NMR spectrum of 2,4-difluoro-1-(phenylbuta-1,3-diyne-1-yl)benzene (**8b**).

SSB-SS-166-13C

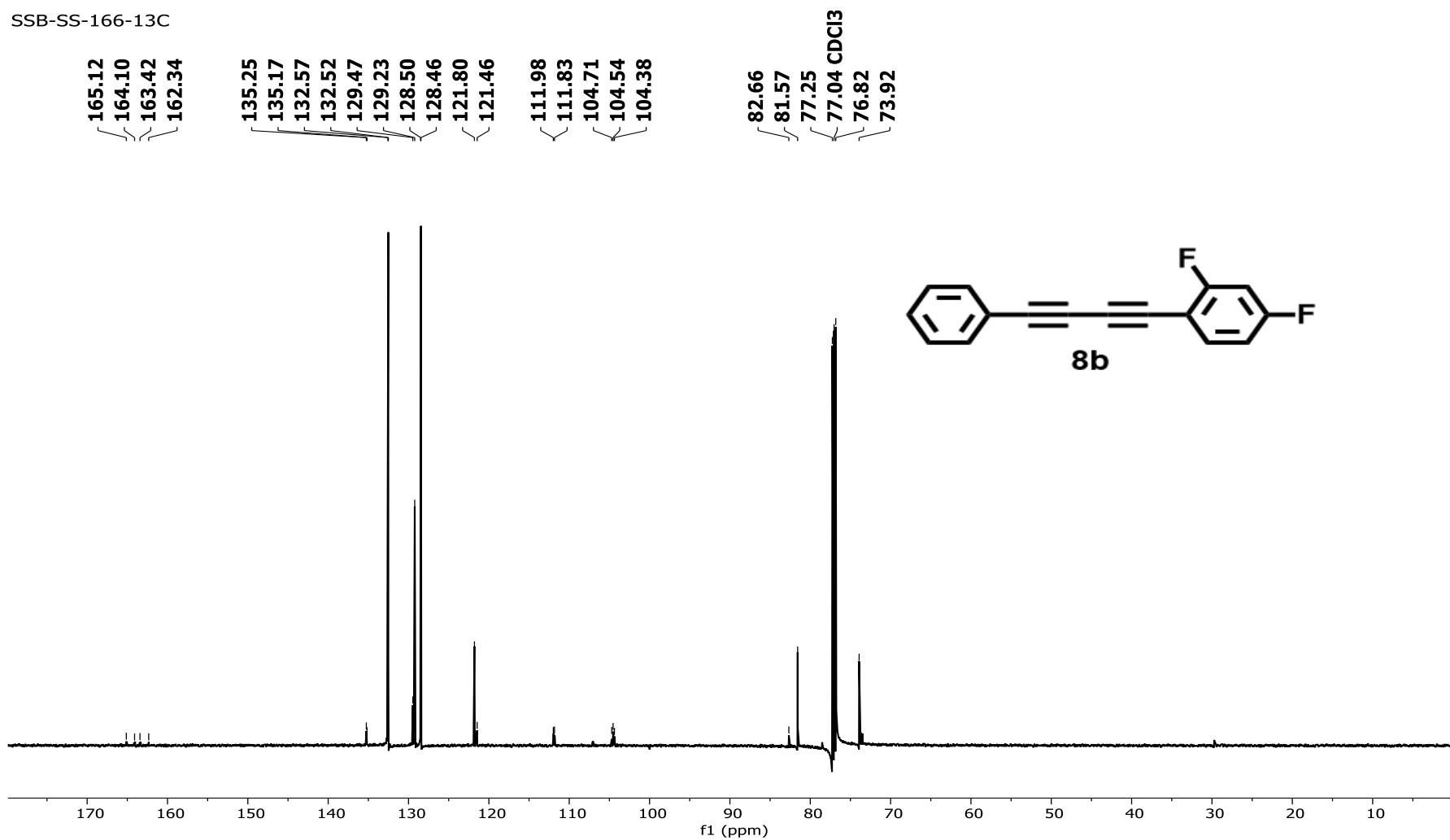


Figure S24. ¹³C NMR spectrum of 2,4-difluoro-1-(phenylbuta-1,3-diyne-1-yl)benzene (8b).

SSB-SS-166-19F

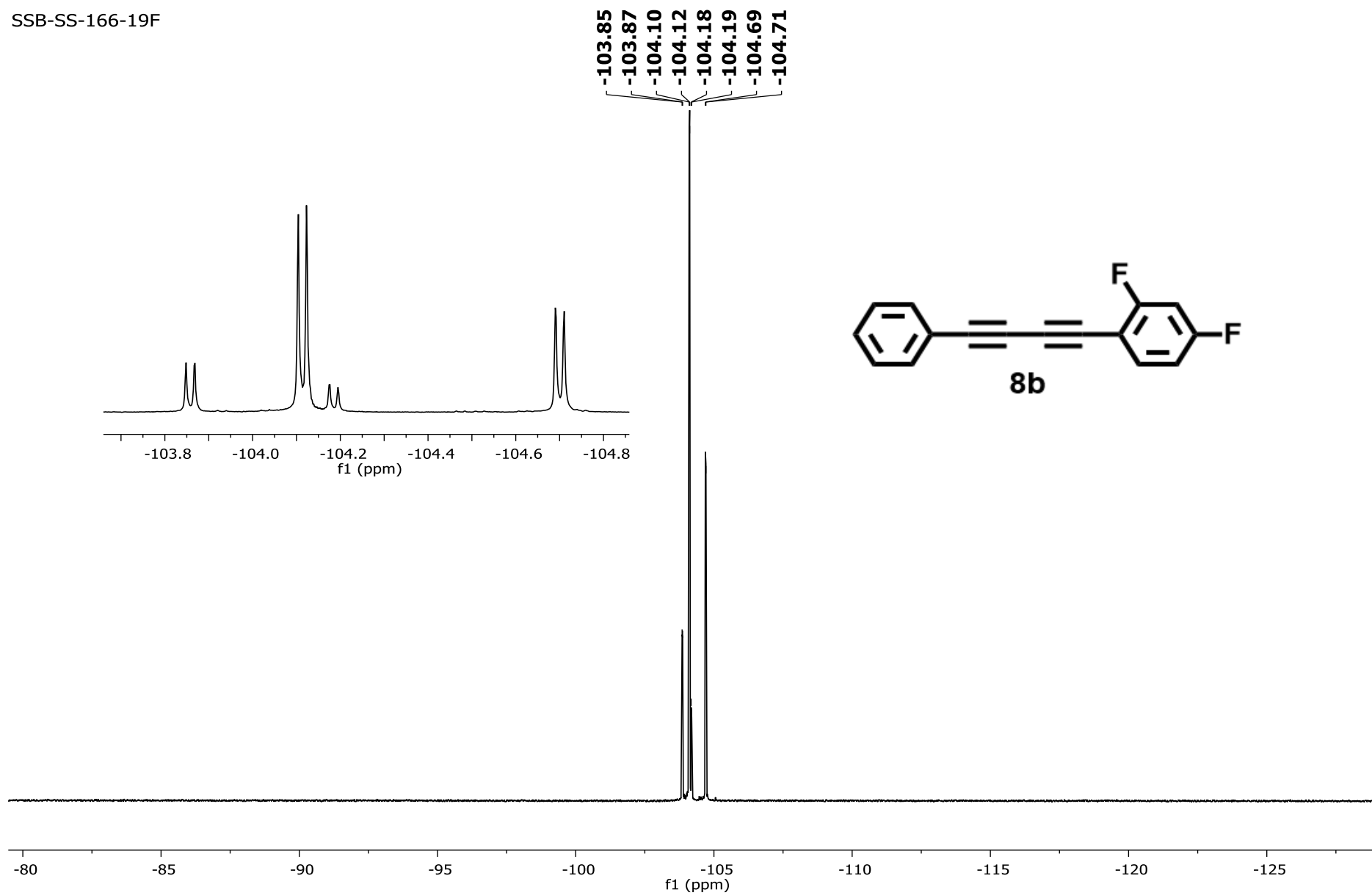


Figure S25. ^{19}F NMR spectrum of 2,4-difluoro-1-(phenylbuta-1,3-diyne-1-yl)benzene (**8b**).

SSB-SS-165-1H

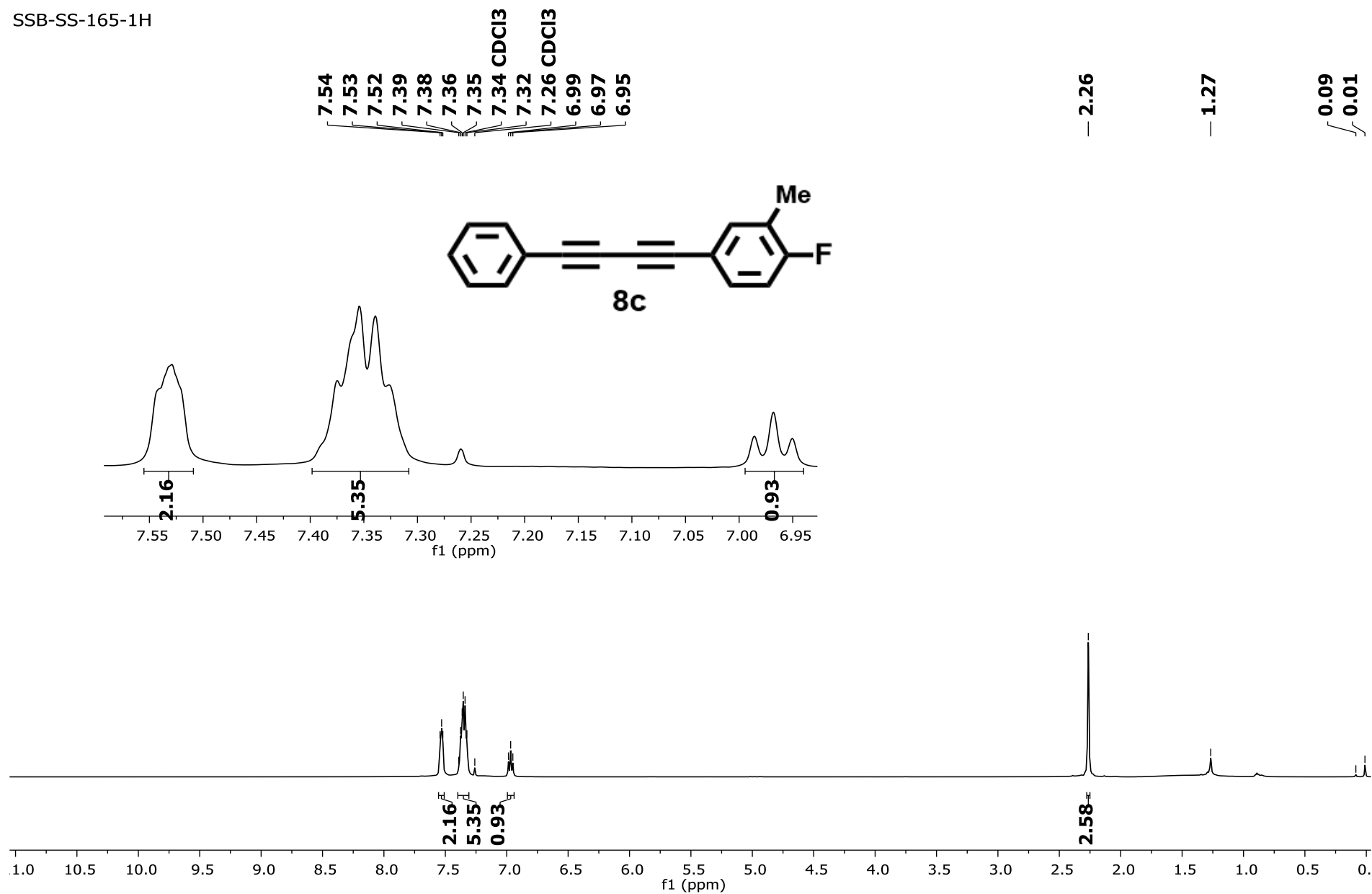


Figure S26. spectrum of *1-fluoro-2-methyl-4-(phenylbuta-1,3-diyne-1-yl)benzene* (**8c**).

SSB-SS-165-13C

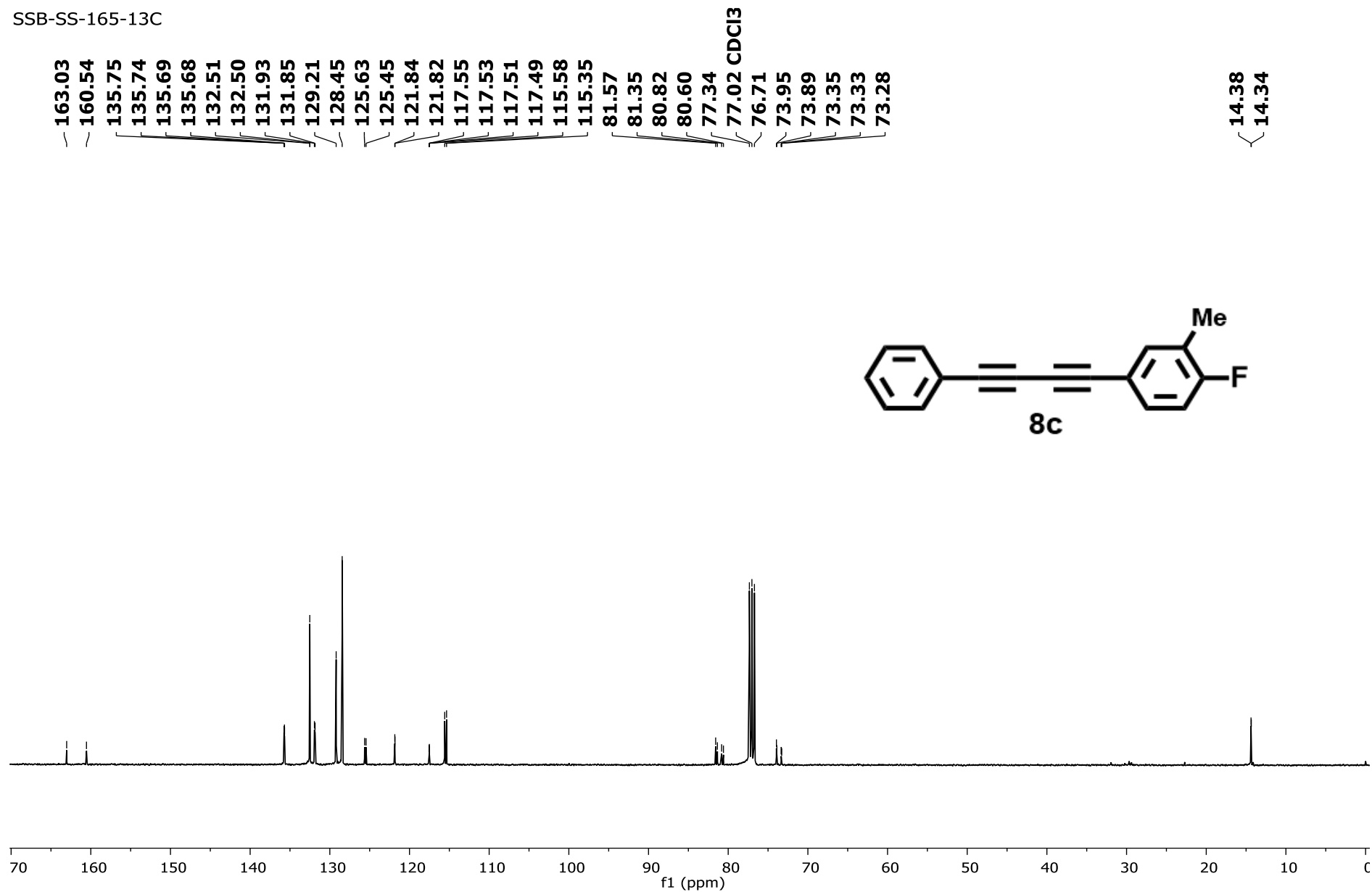


Figure S27. ¹³C NMR spectrum of 1-fluoro-2-methyl-4-(phenylbuta-1,3-diy-1-yl)benzene (8c).

SSB-SS-165-19F

-113.14
-113.15

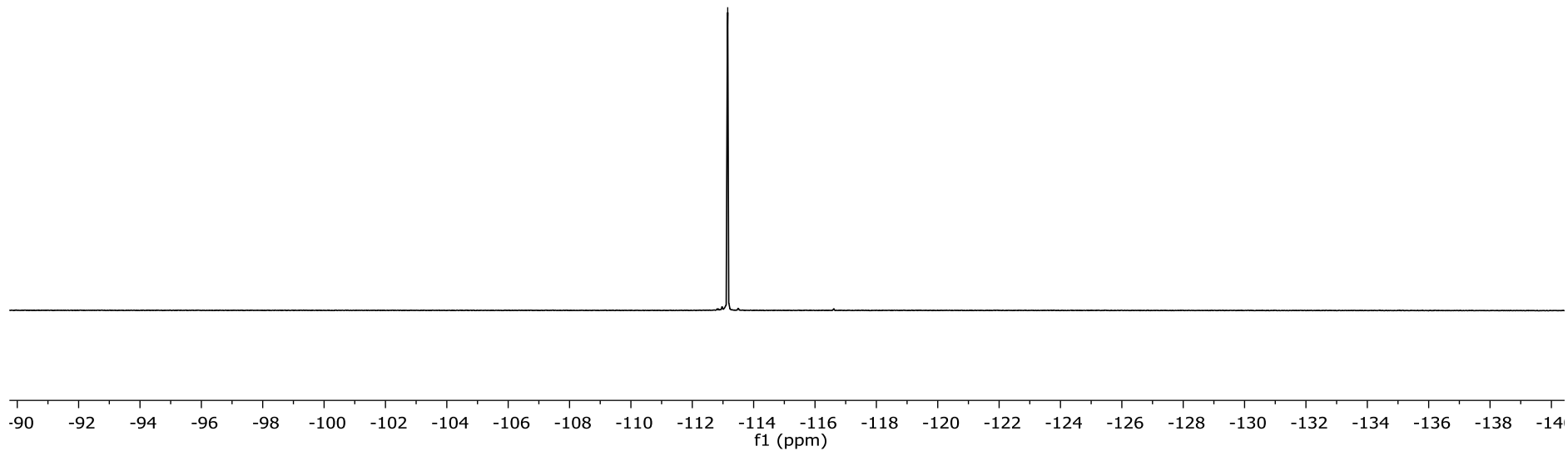
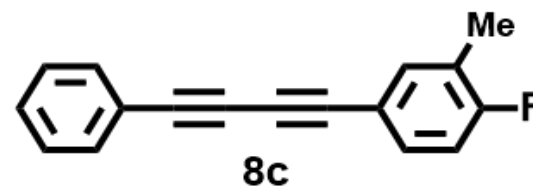
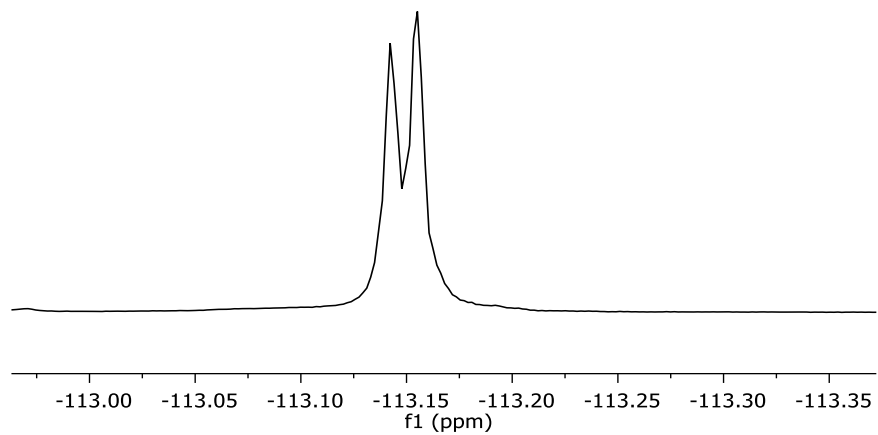


Figure S28. ¹⁹F NMR spectrum of 1-fluoro-2-methyl-4-(phenylbuta-1,3-diyne-1-yl)benzene (8c).

SSB-SS-167-1H

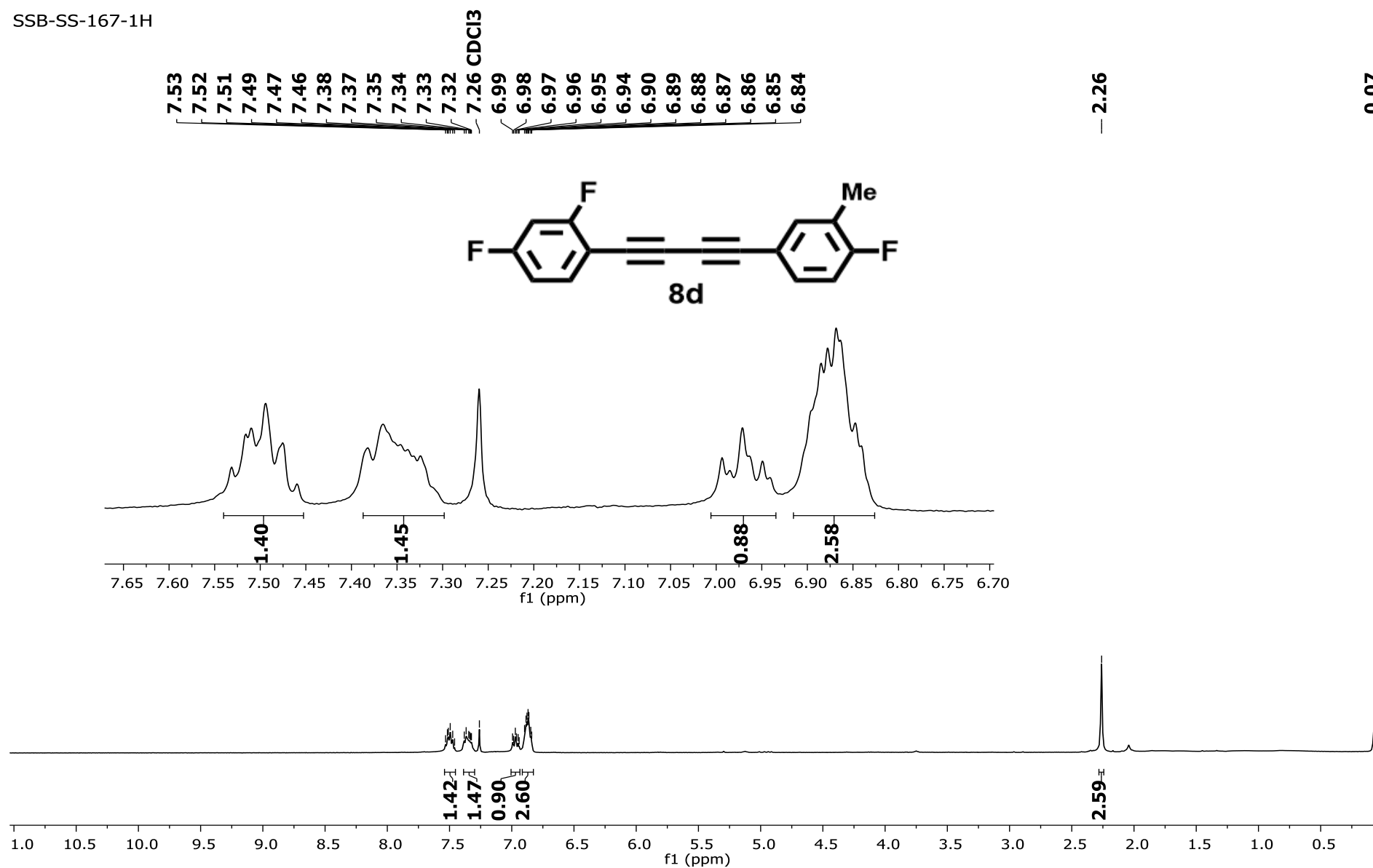


Figure S29. ¹H NMR spectrum of 4-((2,4-difluorophenyl)buta-1,3-dien-1-yl)-1-fluoro-2-methylbenzene (8d).

SSB-SS-167-13C

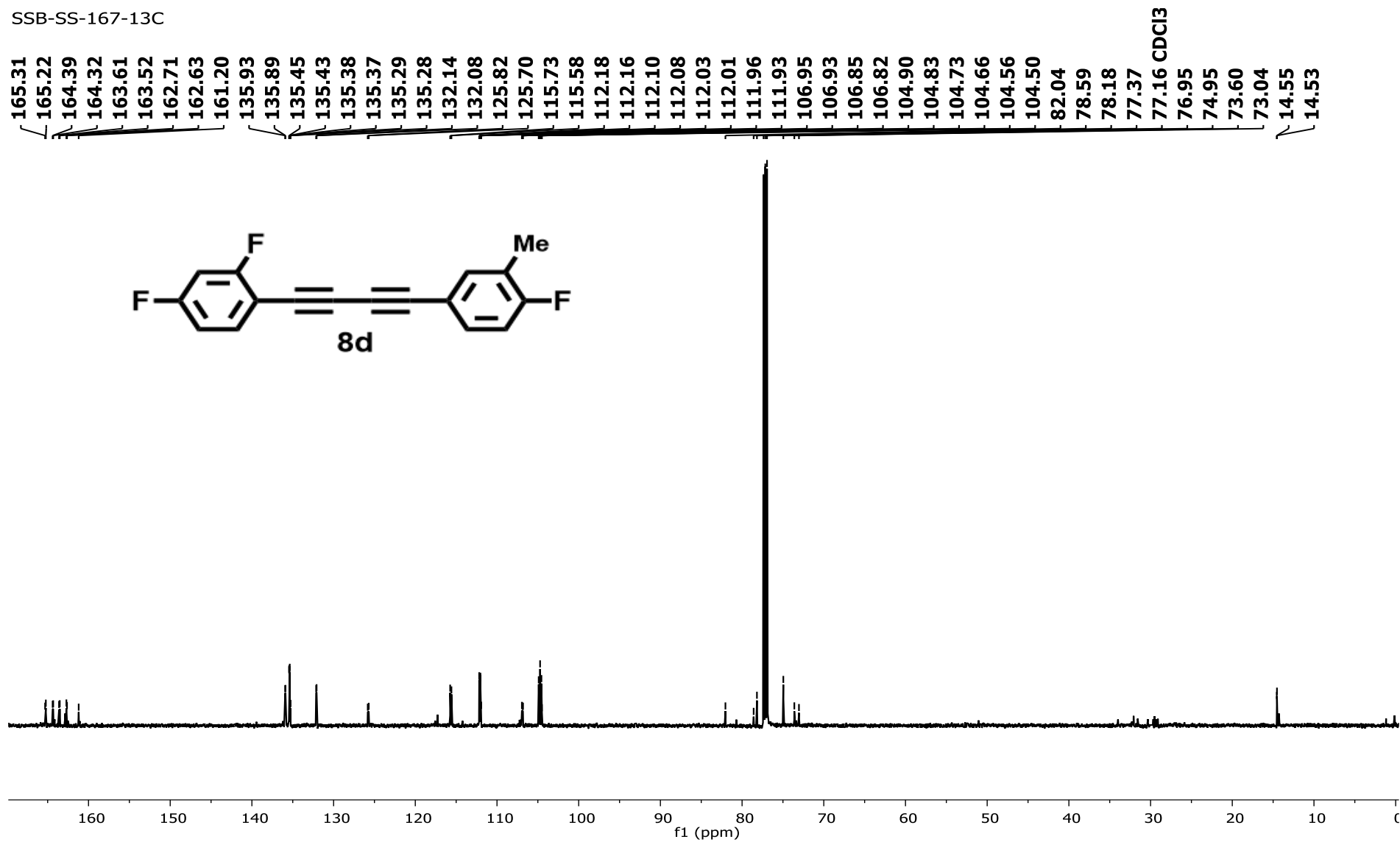


Figure S30. ^{13}C NMR spectrum of 4-((2,4-difluorophenyl)buta-1,3-diyne-1-yl)-1-fluoro-2-methylbenzene (8d).

SSB-SS-167-19F

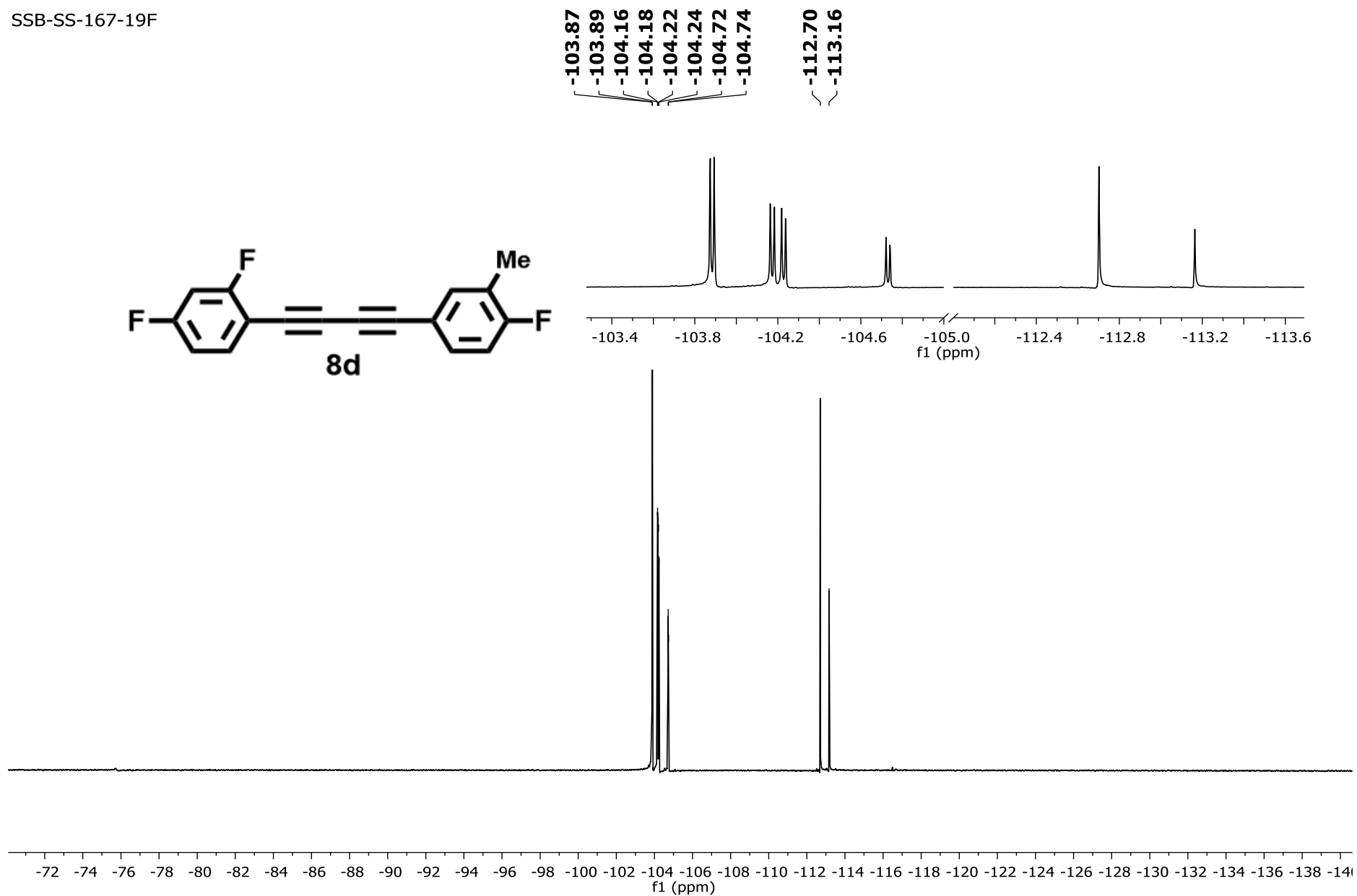


Figure S31. ^{19}F NMR spectrum of 4-((2,4-difluorophenyl)buta-1,3-diyne-1-yl)-1-fluoro-2-methylbenzene (8d).

SSB-SS-392-1H

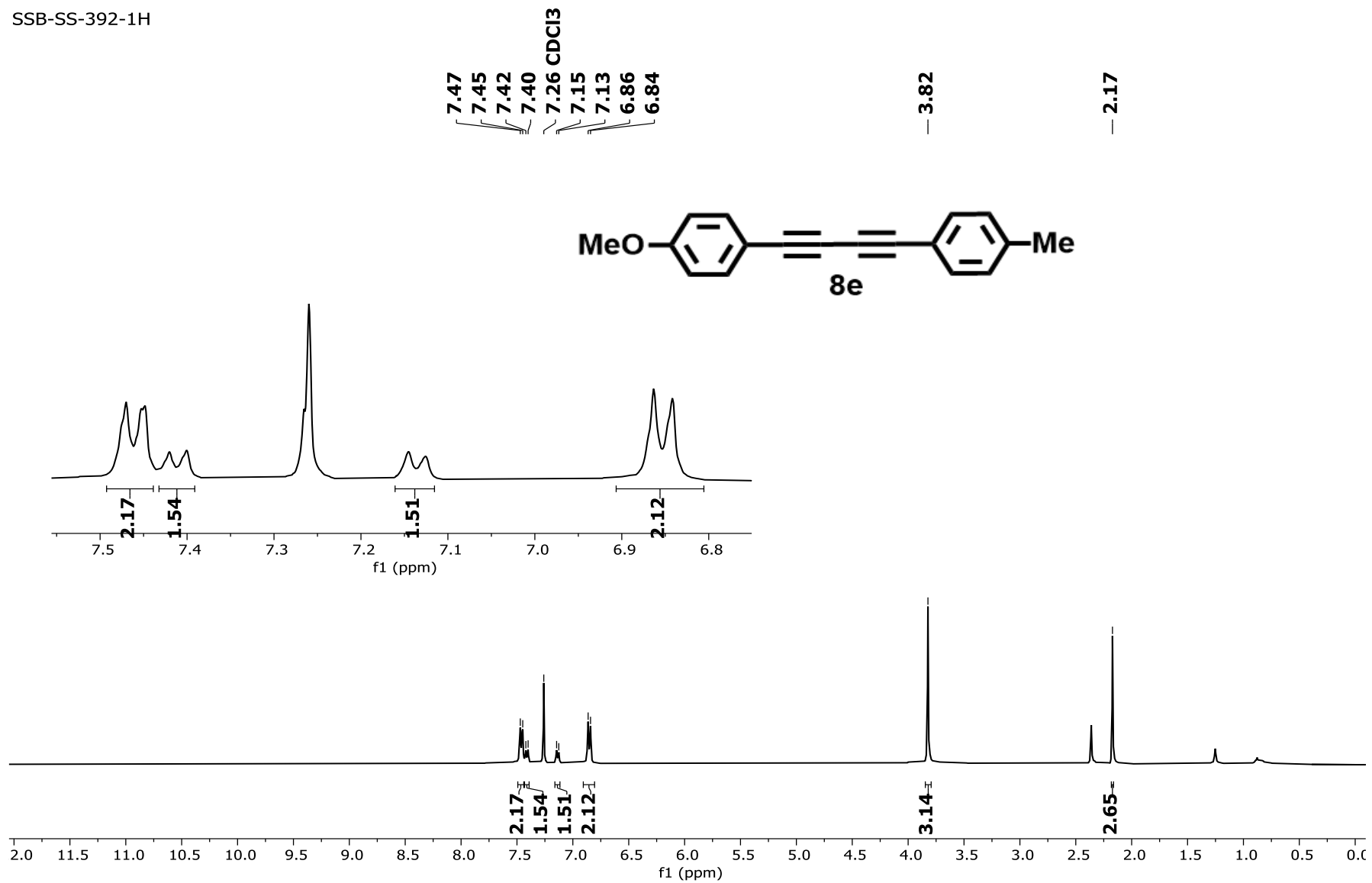


Figure S32. ¹H NMR spectrum of *1-methoxy-4-(p-tolylbuta-1,3-diyne-1-yl)benzene (8e)*.

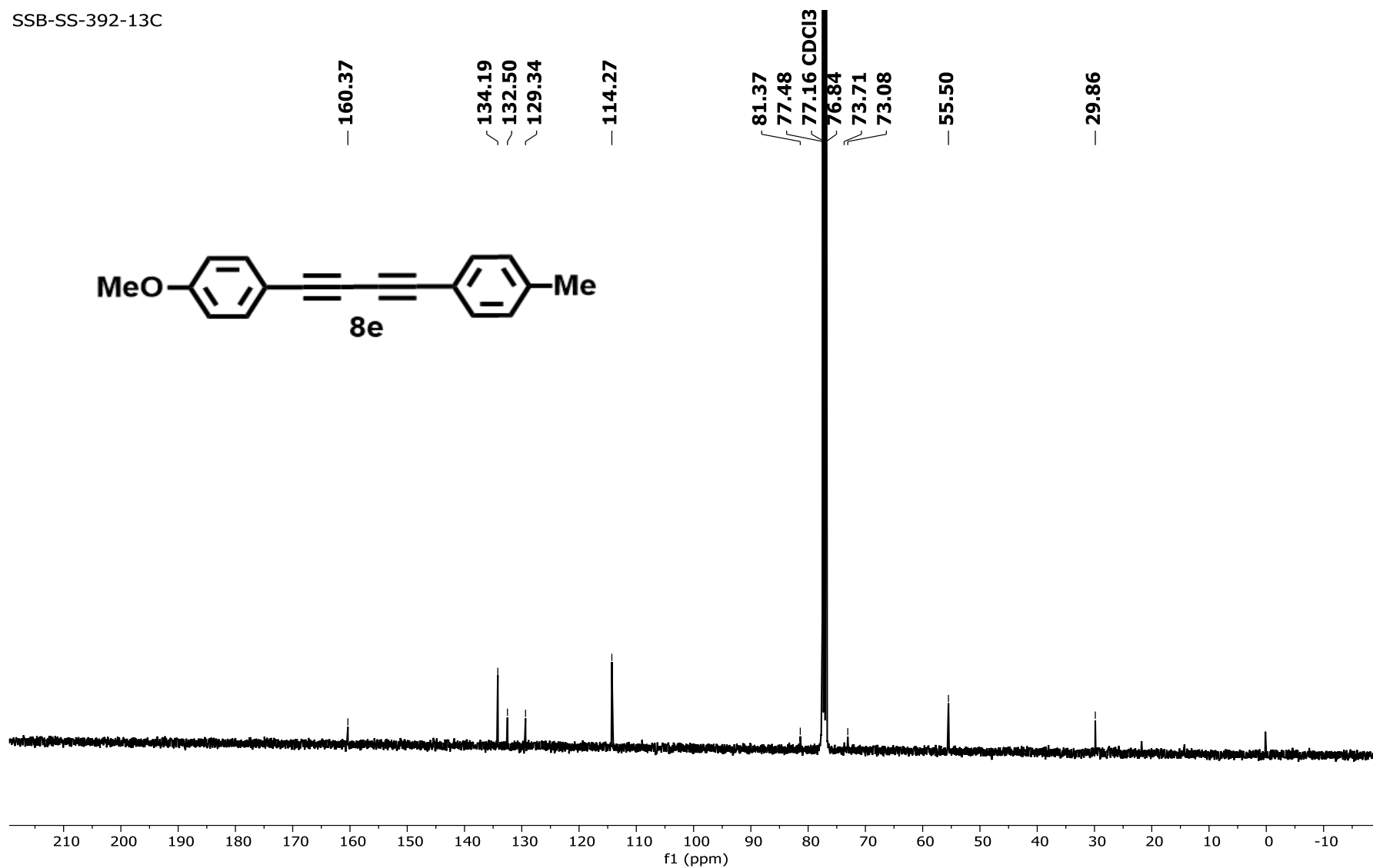


Figure S33. ¹³C NMR spectrum of *1-methoxy-4-(p-tolylbuta-1,3-diy-1-yl)benzene (8e)*.

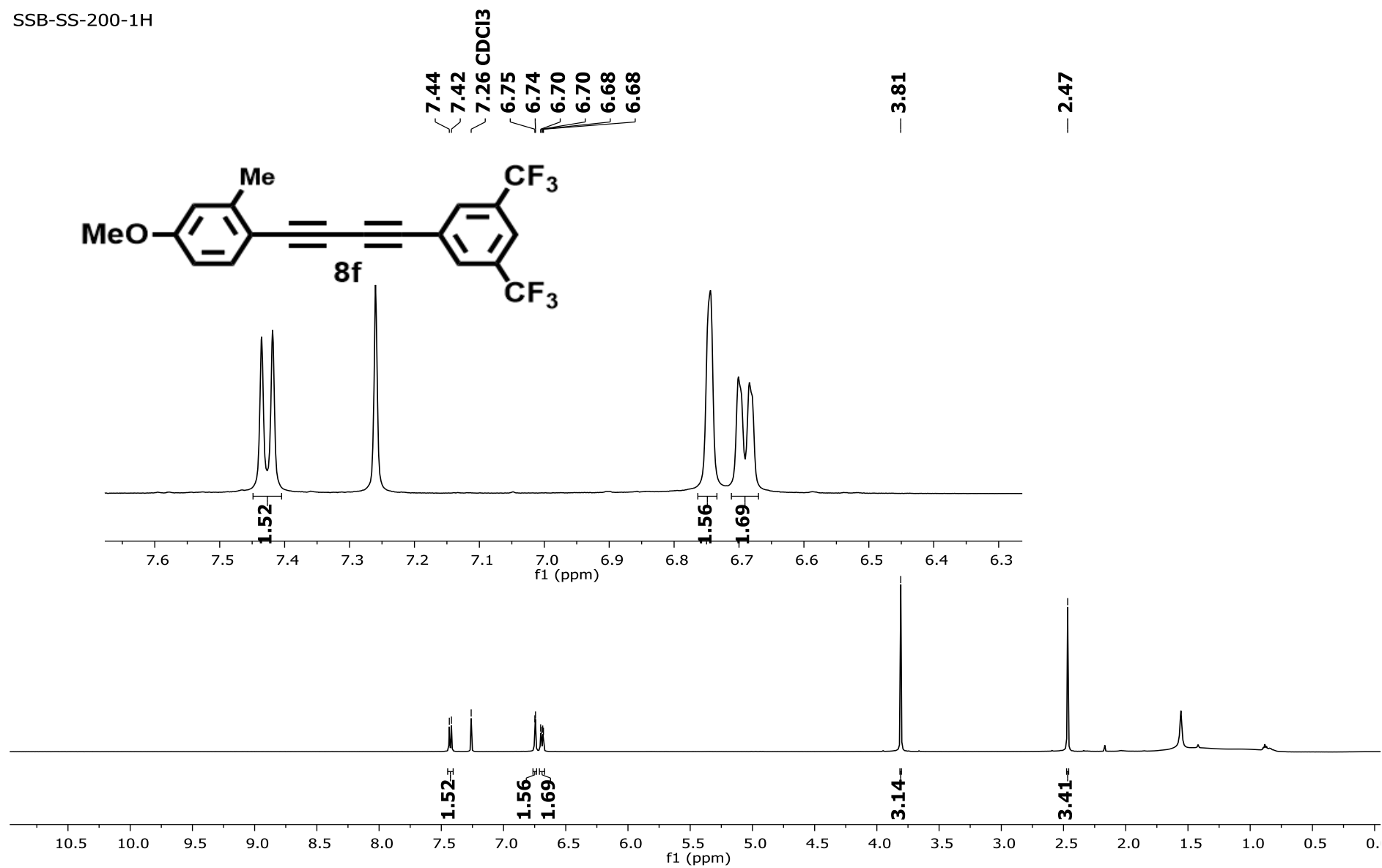


Figure S34. ¹H NMR spectrum of *1-((3,5-bis(trifluoromethyl)phenyl)buta-1,3-dien-1-yl)-4-methoxy-2-methylbenzene* (**8f**).

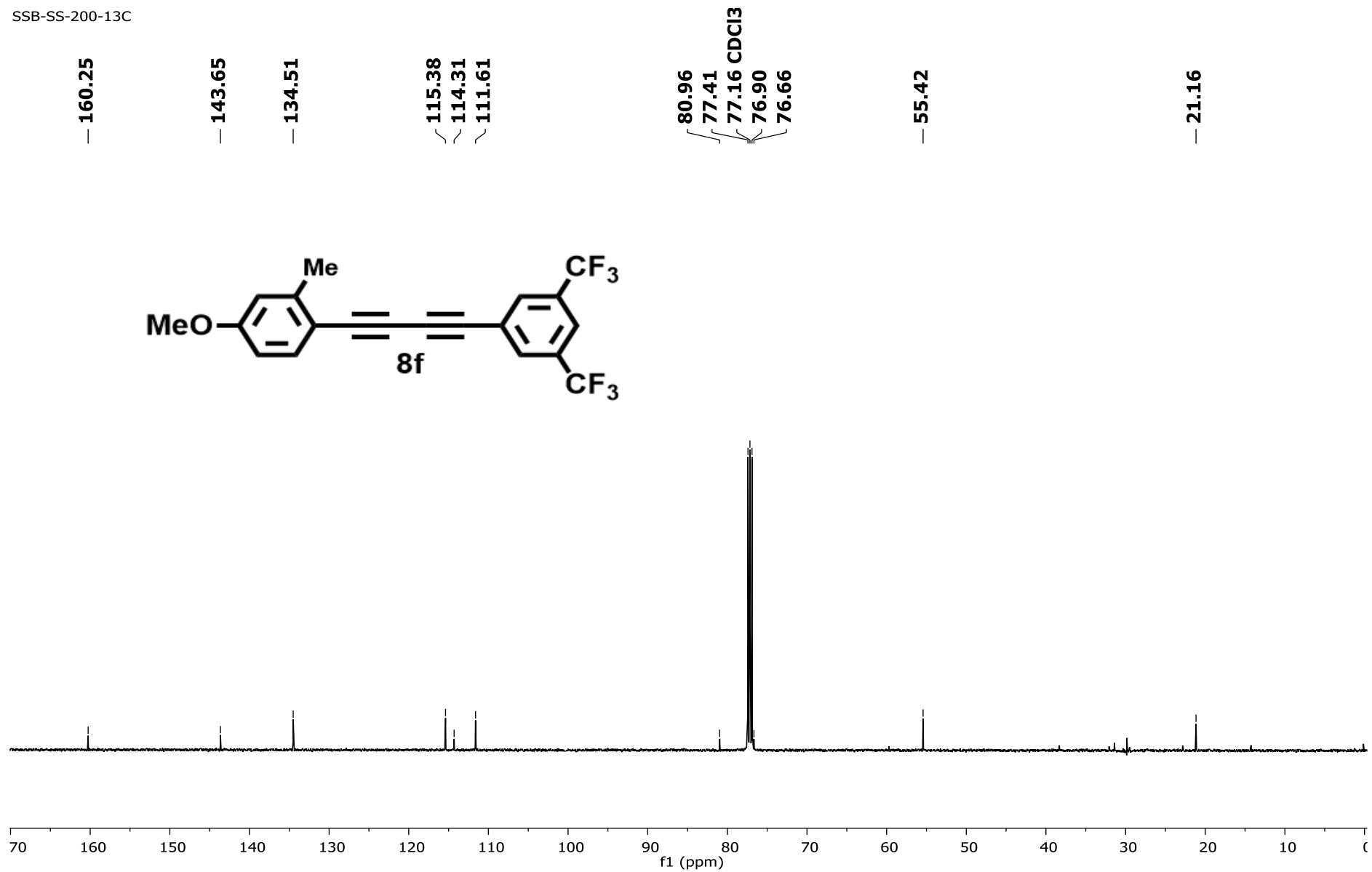


Figure S35. ¹³C NMR spectrum of *1-((3,5-bis(trifluoromethyl)phenyl)buta-1,3-diyne-1-yl)-4-methoxy-2-methylbenzene* (**8f**).

SSB-SS-200-19F

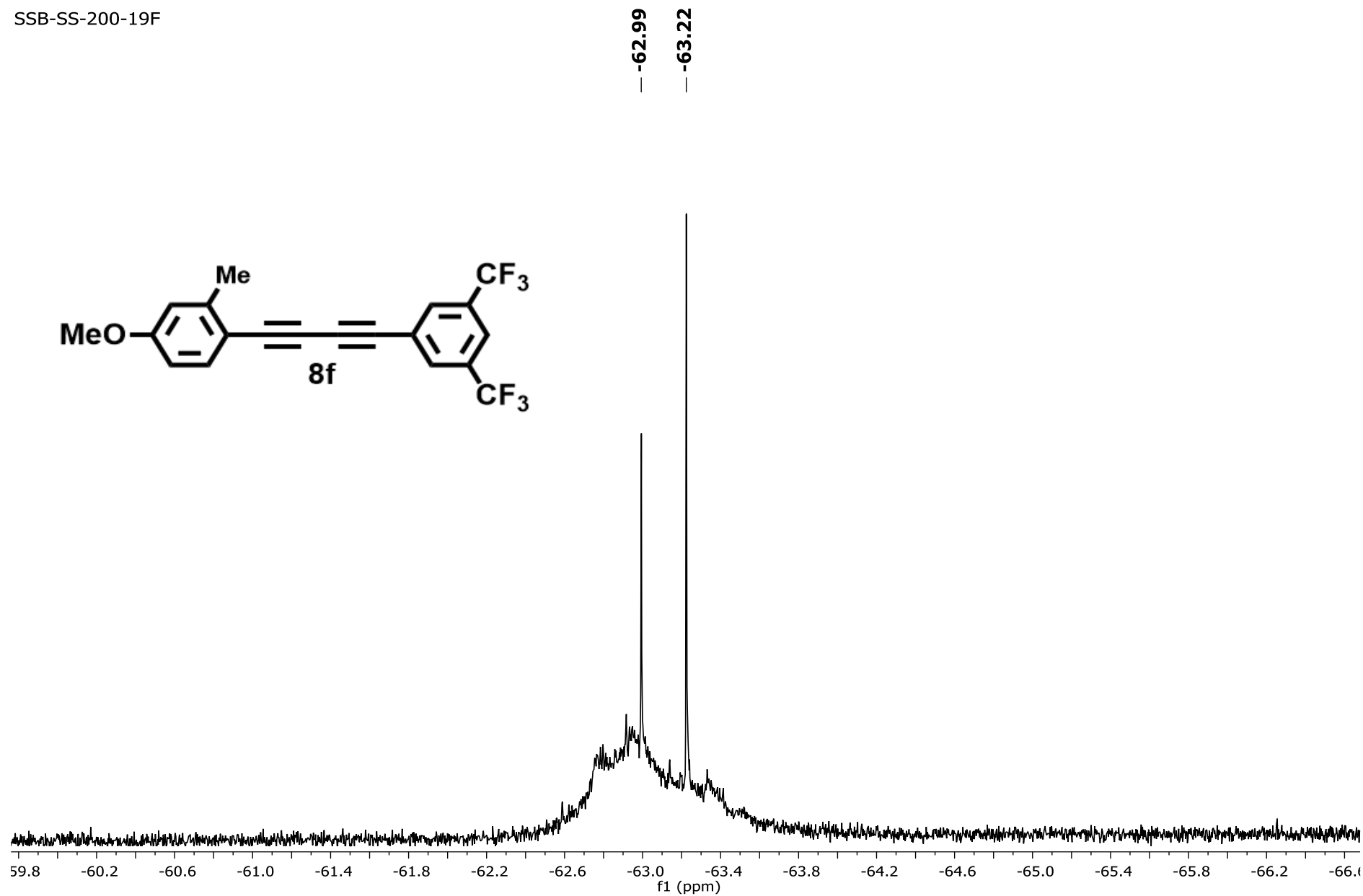


Figure S36. ¹⁹F NMR spectrum of 1-((3,5-bis(trifluoromethyl)phenyl)buta-1,3-diyne-1-yl)-4-methoxy-2-methylbenzene (**8f**).

SSB-SS-327-1H

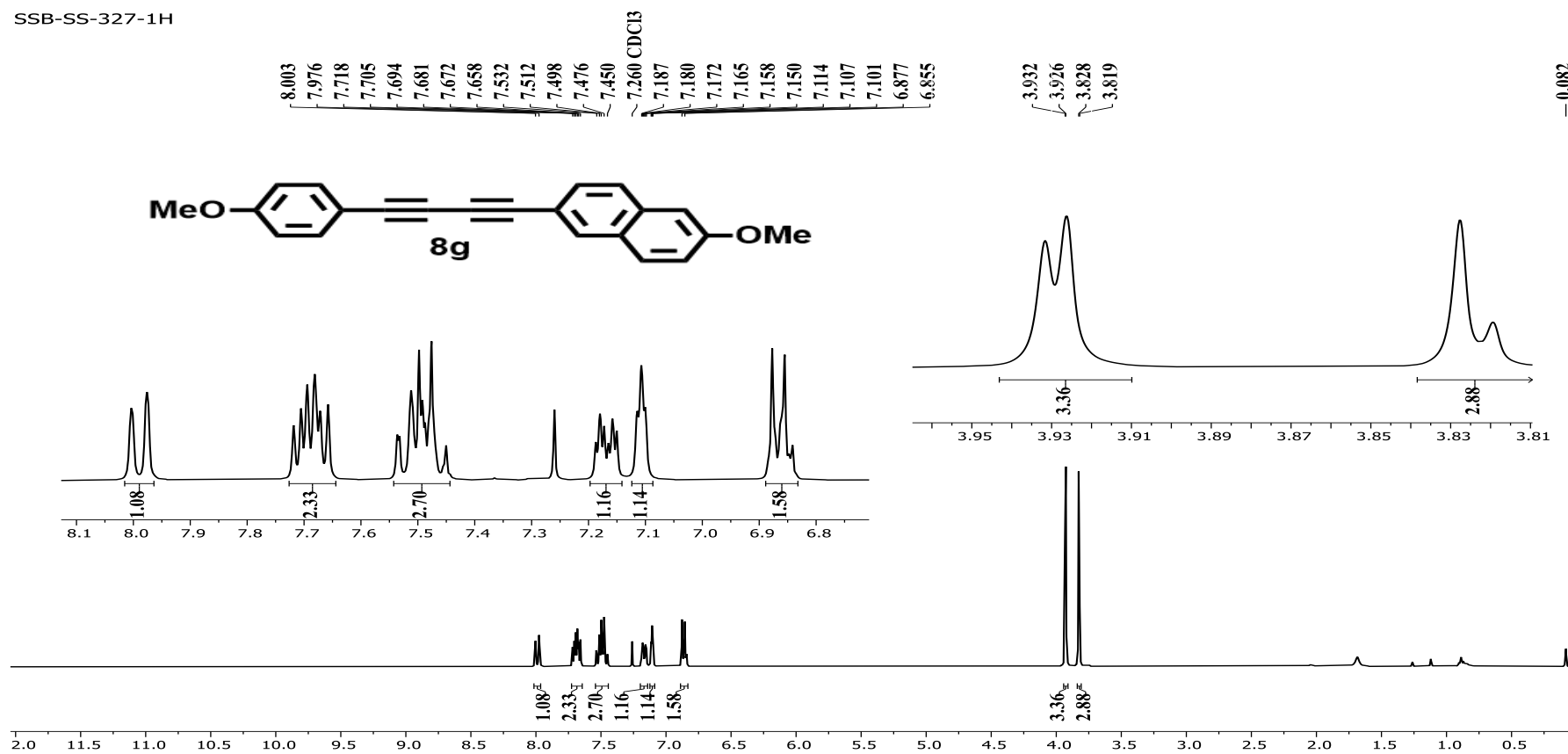


Figure S37. ¹H NMR spectrum of 2-methoxy-7-((4-methoxyphenyl)buta-1,3-diyne-1-yl)naphthalene (8g).

SSB-SS-327-13C

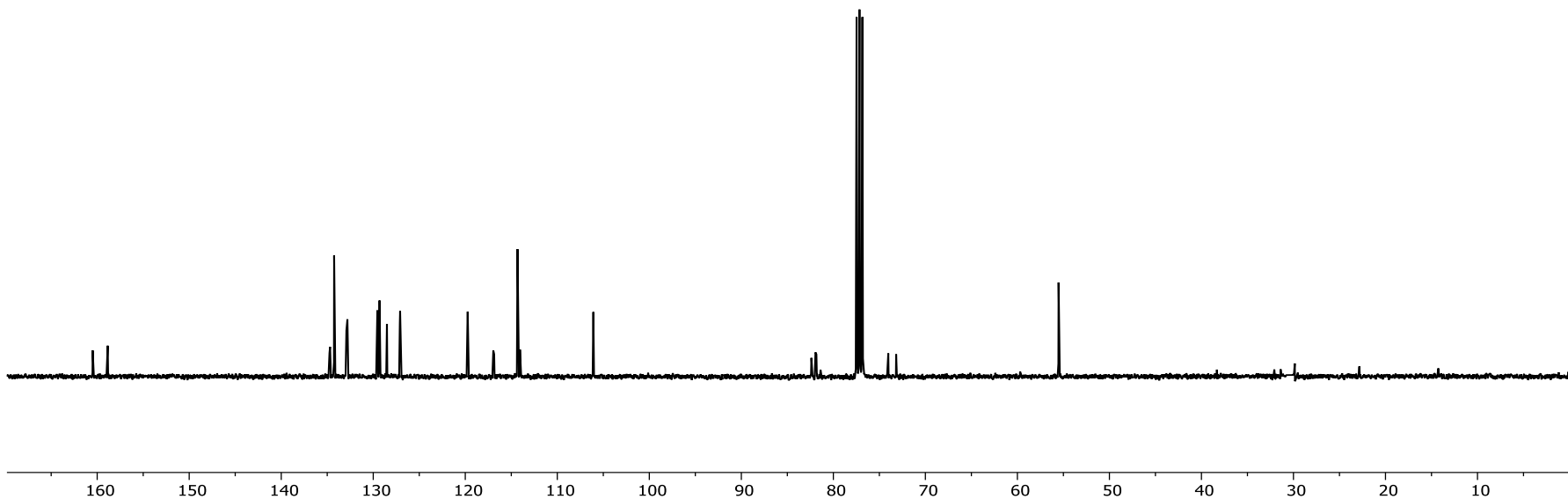
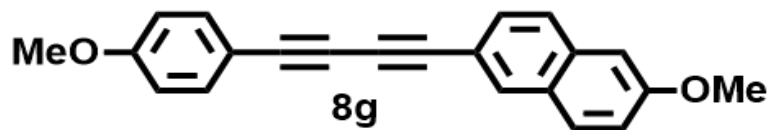
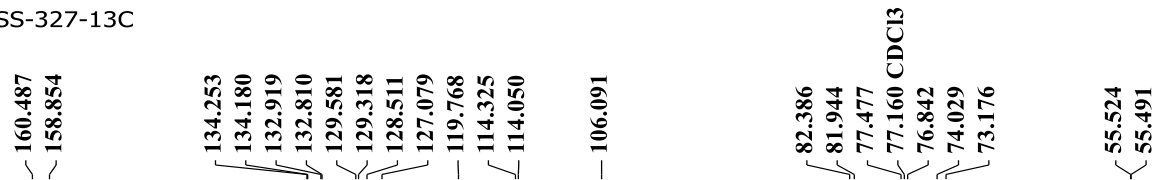


Figure S38. ¹³C NMR spectrum of 2-methoxy-7-((4-methoxyphenyl)buta-1,3-diyne-1-yl)naphthalene (8g).

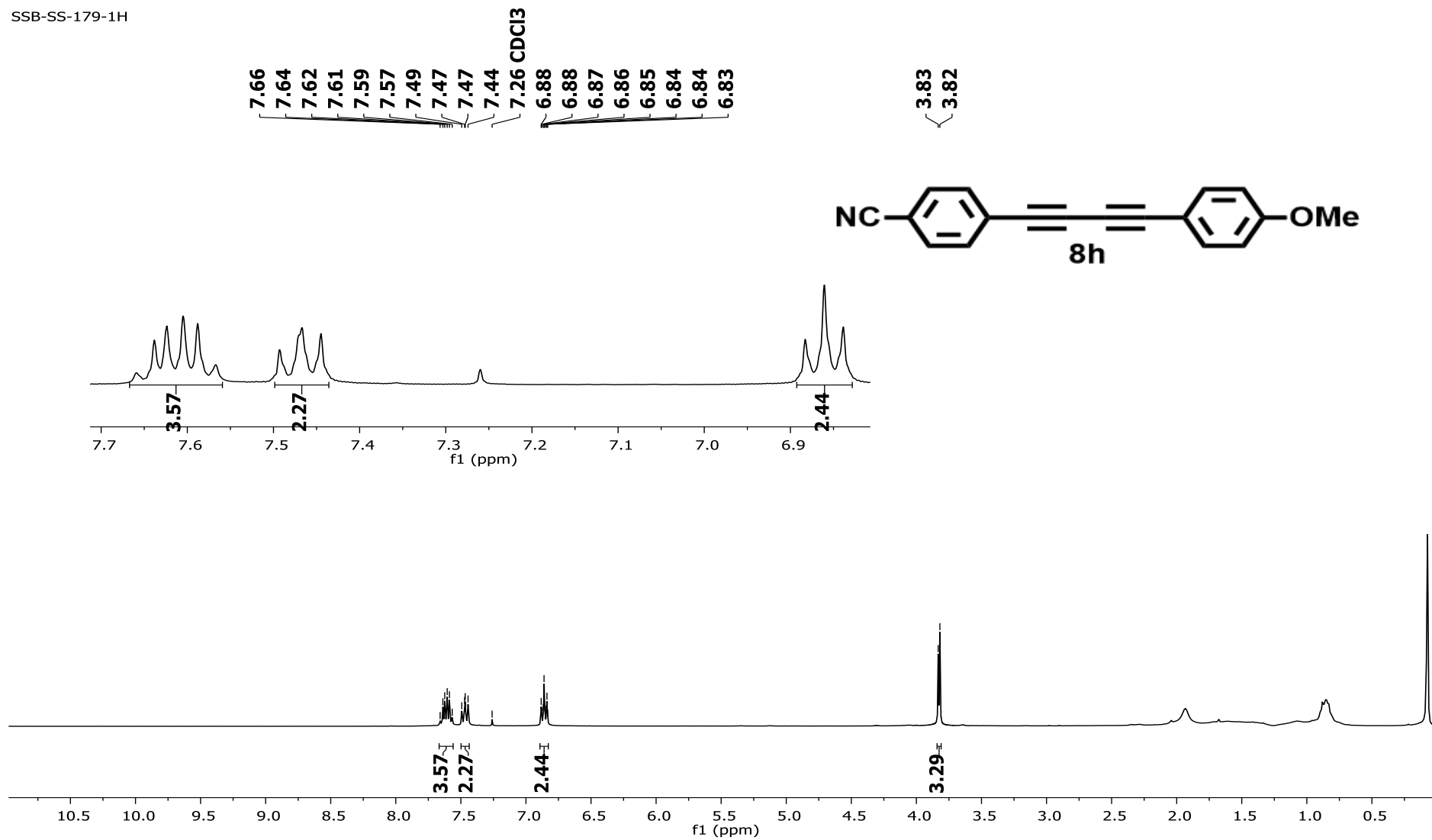


Figure S39. ¹H NMR spectrum of 4-((4-methoxyphenyl)buta-1,3-diyne-1-yl)benzonitrile (8h).

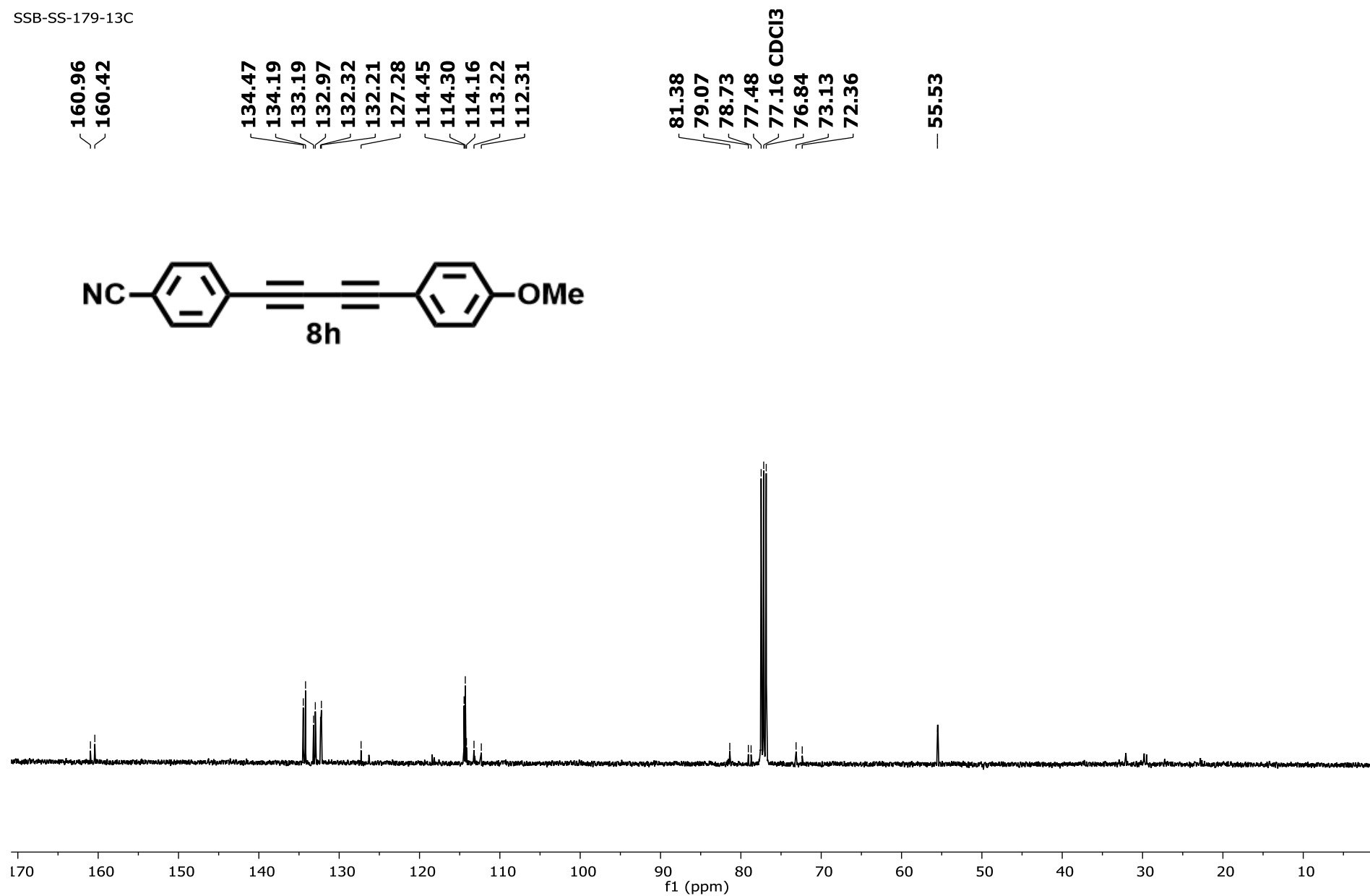


Figure S40. ¹³C NMR spectrum of 4-((4-methoxyphenyl)buta-1,3-diyne-1-yl)benzonitrile (8h).

SSB-SS-320-1H

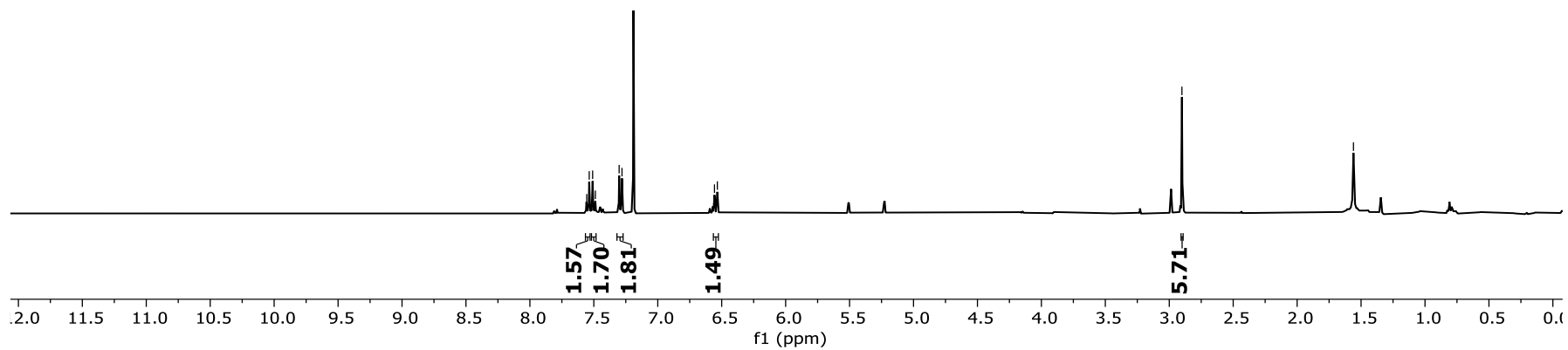
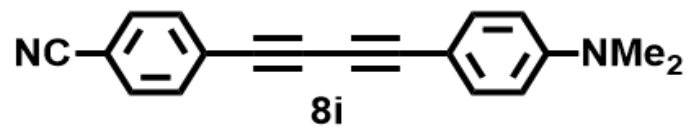
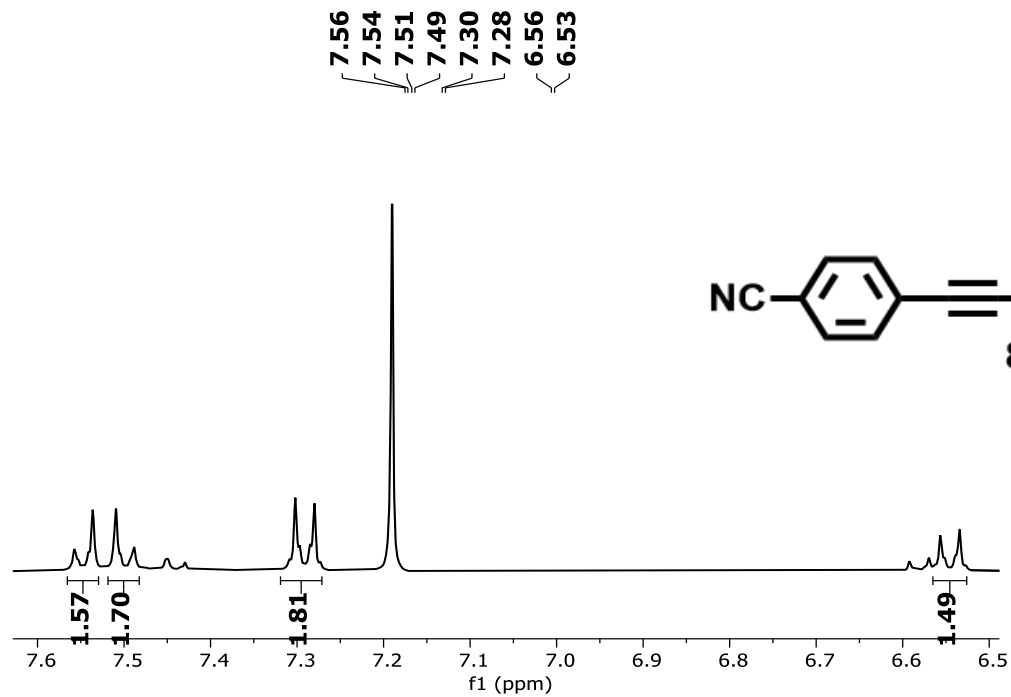


Figure S41. ^1H NMR spectrum of 4-((4-(dimethylamino)phenyl)buta-1,3-diyne-1-yl)benzotrile (8i).

SSB-SS-320-13C

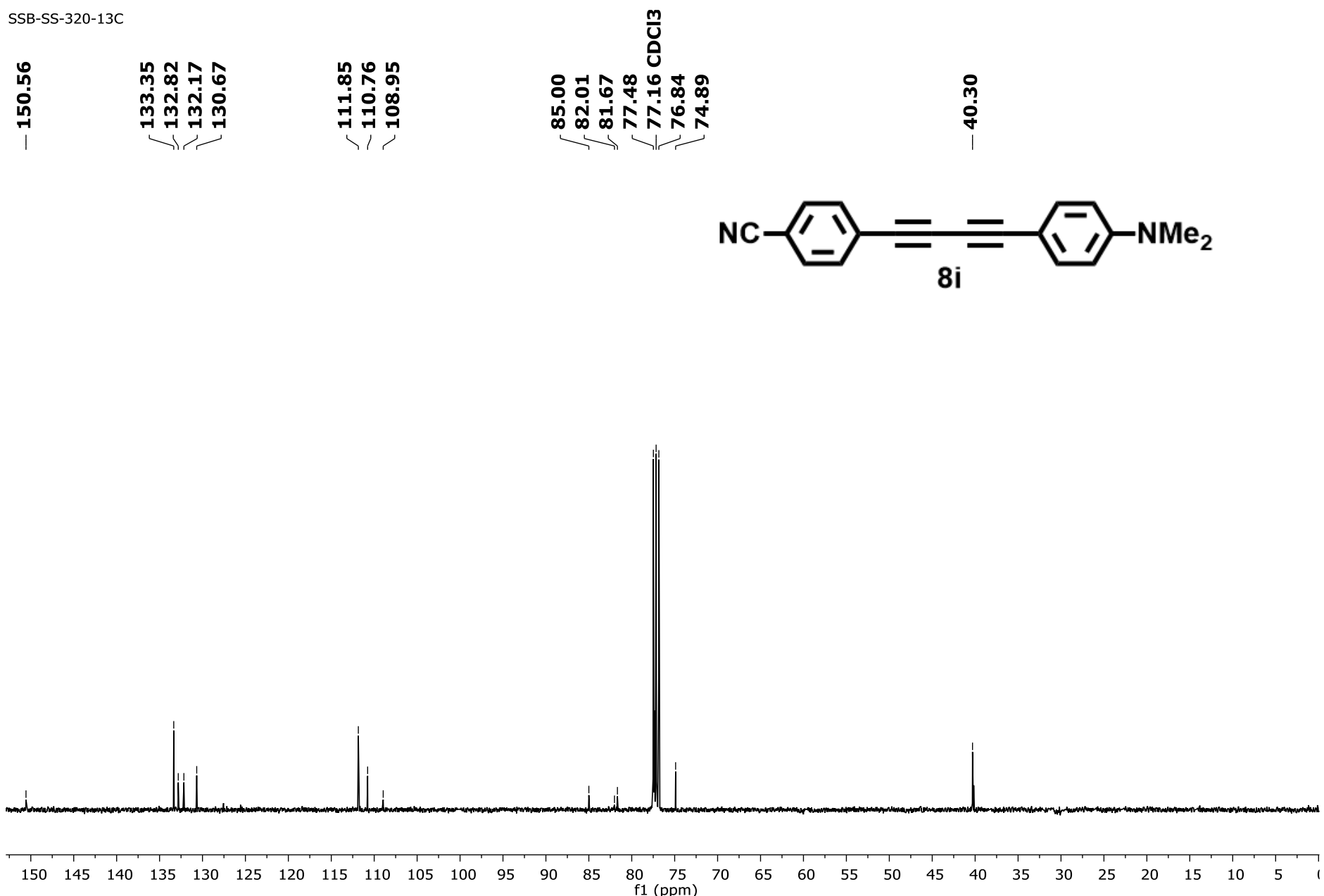


Figure S42. ¹³C NMR spectrum of 4-((4-(dimethylamino)phenyl)buta-1,3-diy-1-yl)benzonitrile (**8i**).

SSB-SS-325-1H

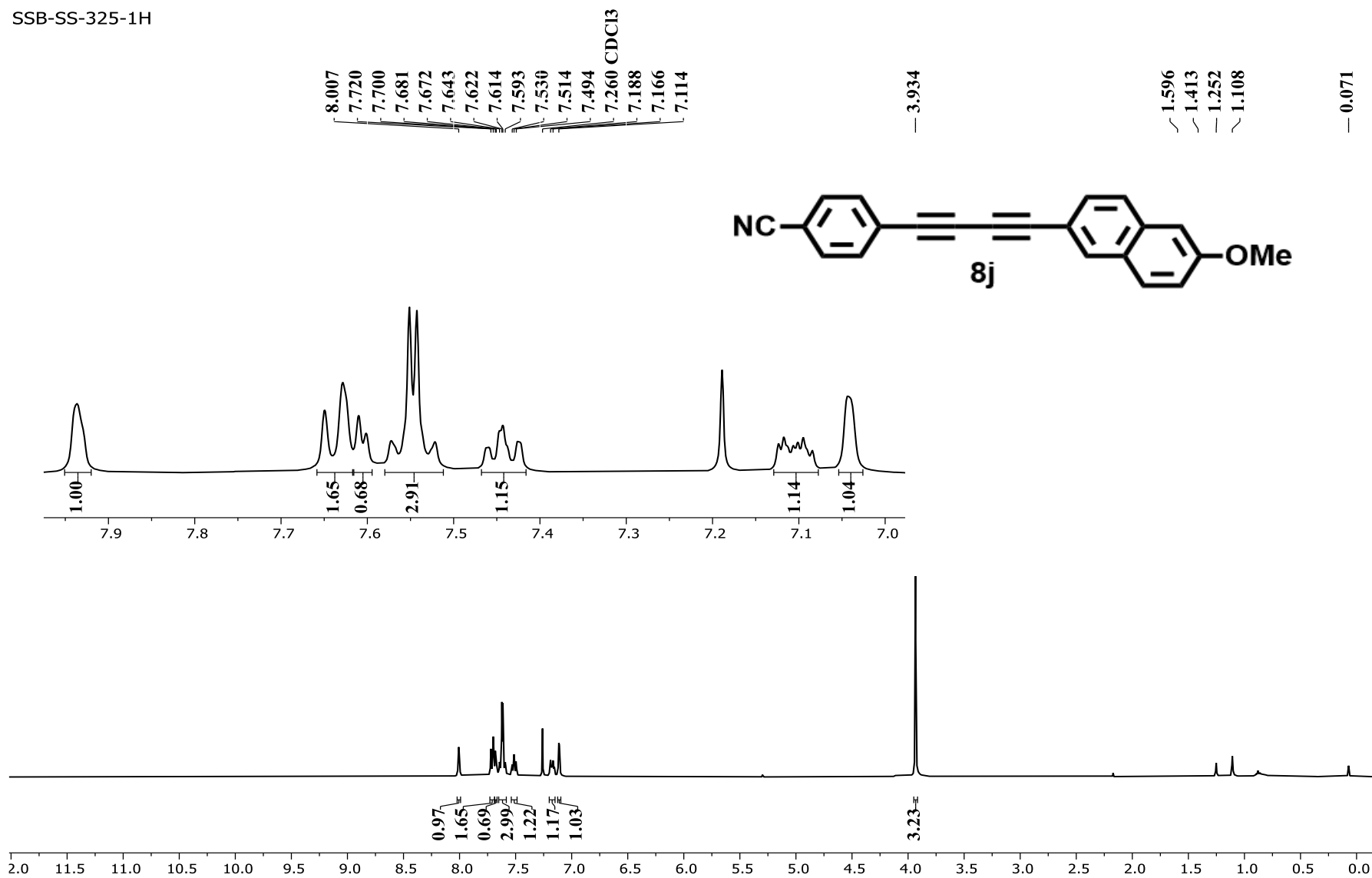


Figure S43. ¹H NMR spectrum of 4-((7-methoxynaphthalen-2-yl)buta-1,3-dyn-1-yl)benzotrile (**8j**).

SSB-SS-235-13C

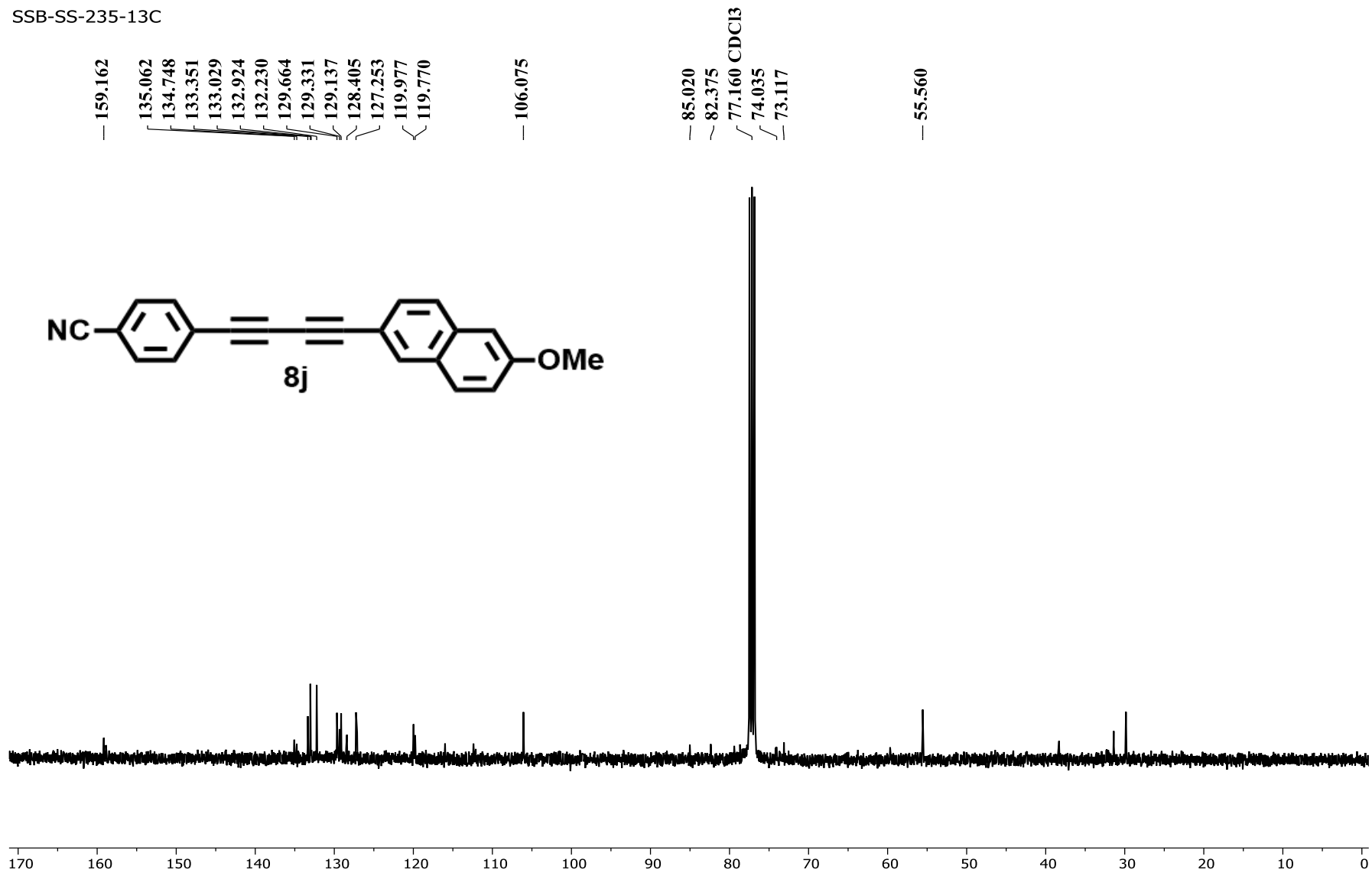


Figure S44. ¹³C NMR spectrum of 4-((7-methoxynaphthalen-2-yl)buta-1,3-diy-1-yl)benzonitrile (**8j**).

SSB-SS-332-1H

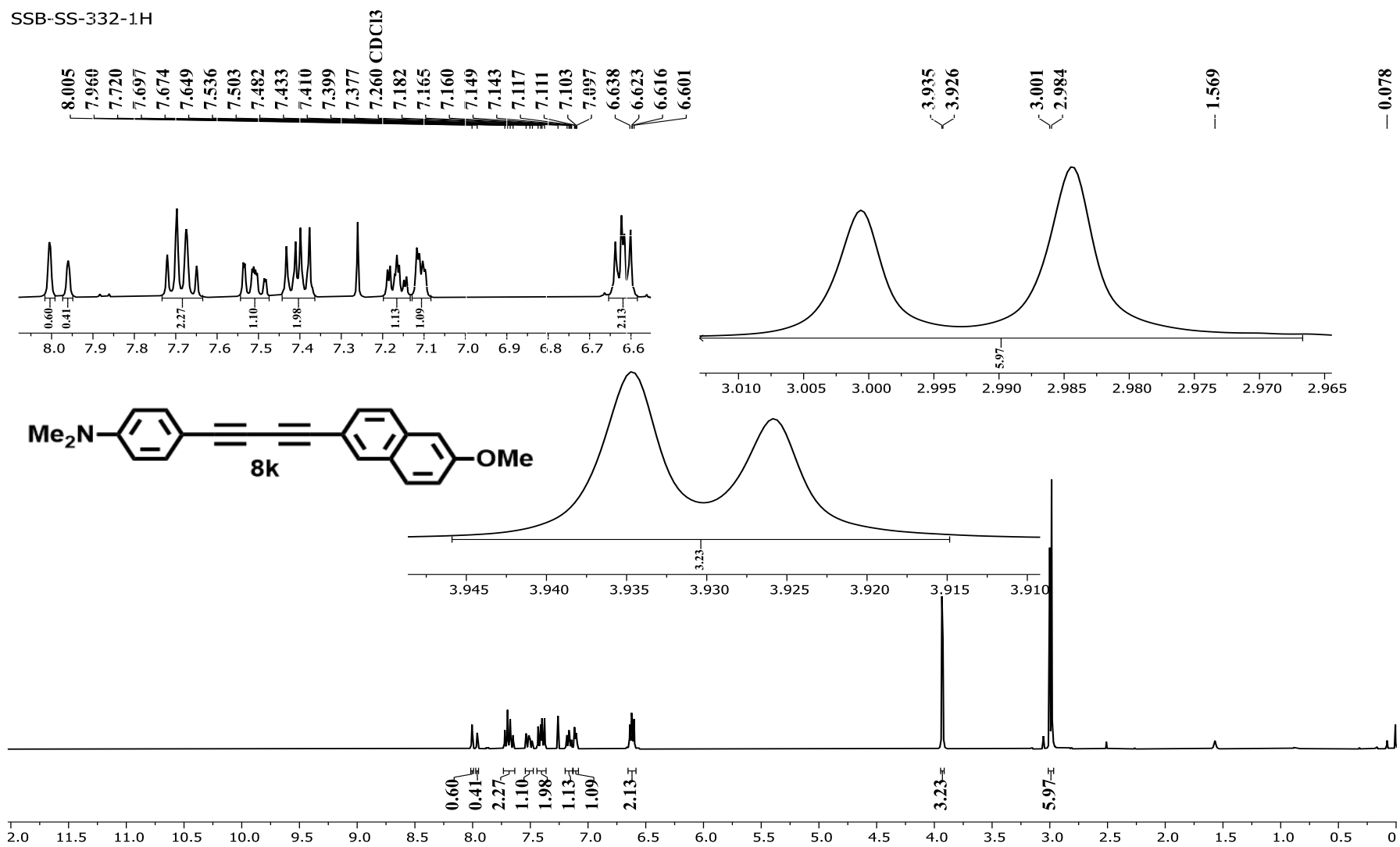


Figure S45. ¹H NMR spectrum of 4-((7-methoxynaphthalen-2-yl)buta-1,3-dyn-1-yl)-N,N-dimethylaniline (**8k**).

SSB-SS-332-13C

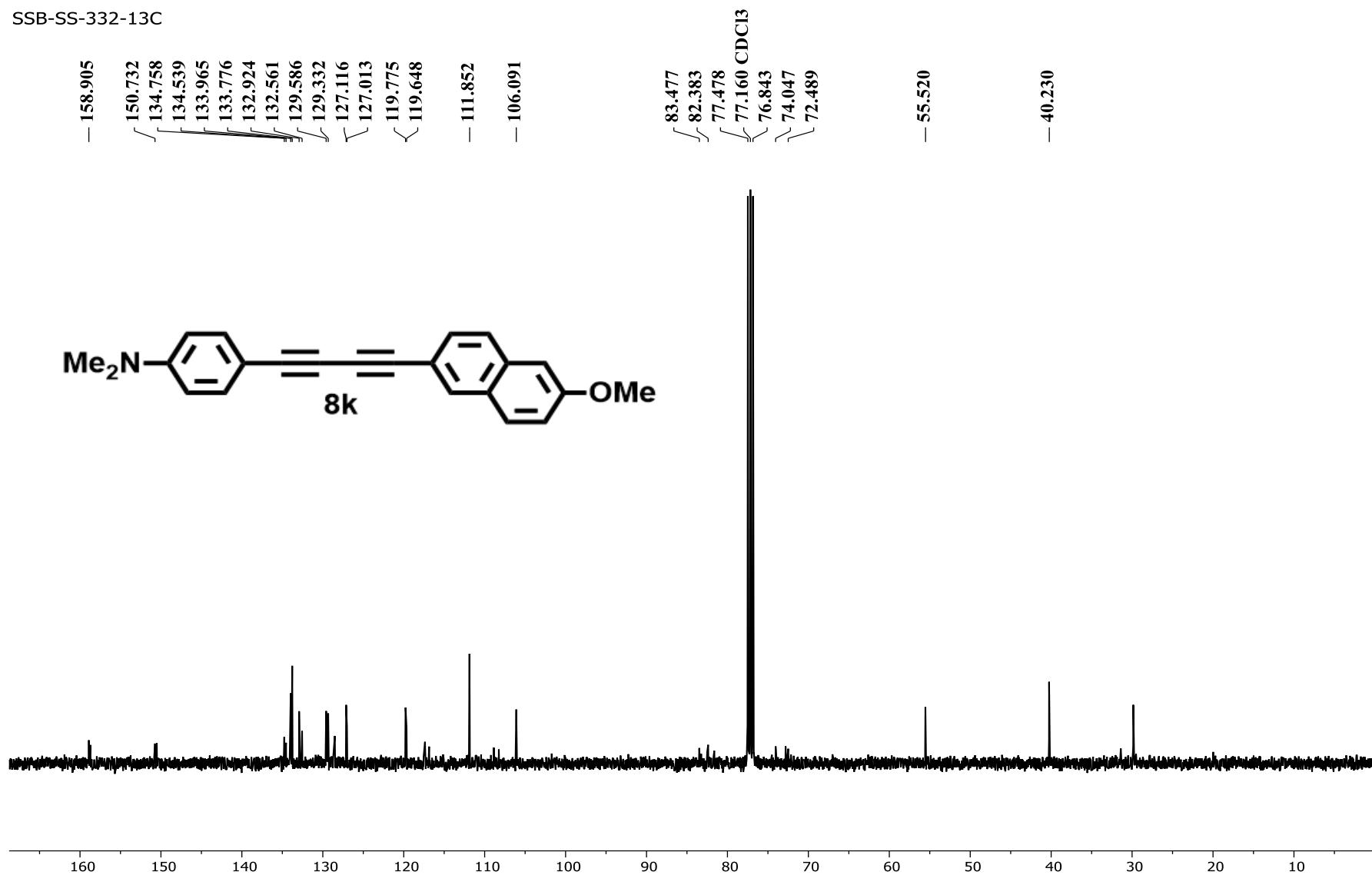
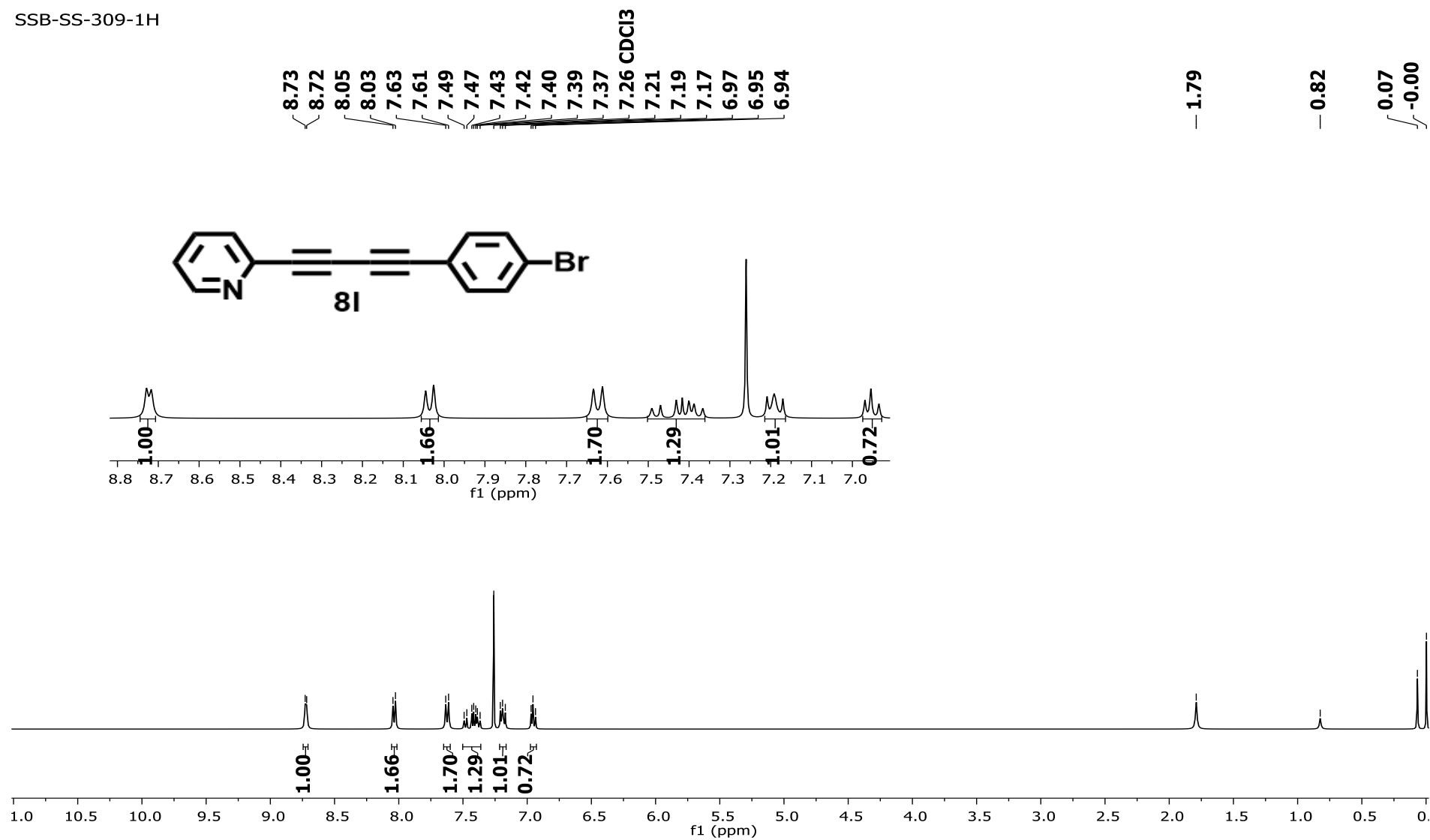


Figure S46. ¹³C NMR spectrum of 4-((7-methoxynaphthalen-2-yl)buta-1,3-diy-1-yl)-N,N-dimethylaniline (8k).



SSB-SS-309-13C

135.88
135.82
132.65
132.07
131.99
129.34
128.58
125.77
125.59
121.98
121.96
117.68
117.64
117.62

81.71
81.49
80.96
80.73
77.48
77.16 CDCl3
76.84
74.08

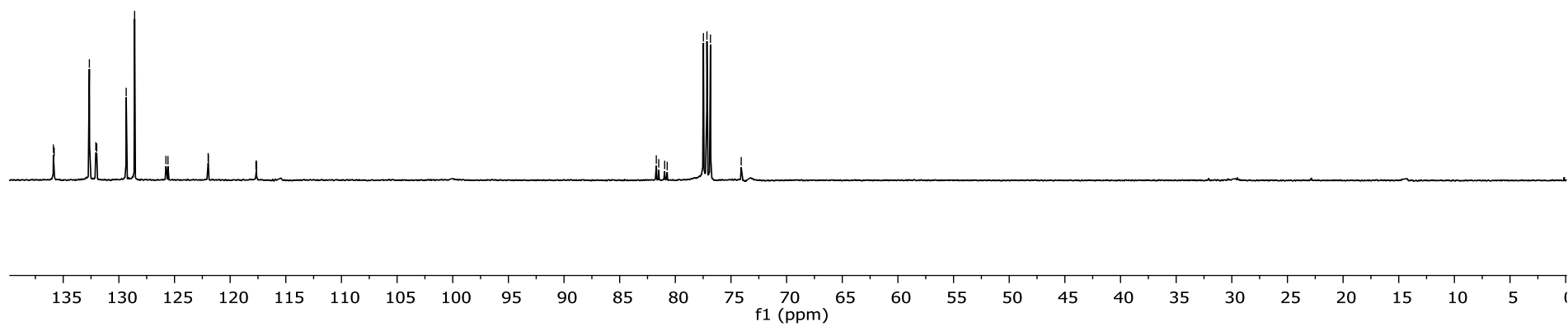
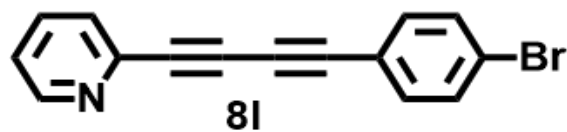


Figure S48. ^{13}C NMR spectrum of 2-((4-bromophenyl)buta-1,3-diyne-1-yl)pyridine (**81**).

SSB-SS-314-1H

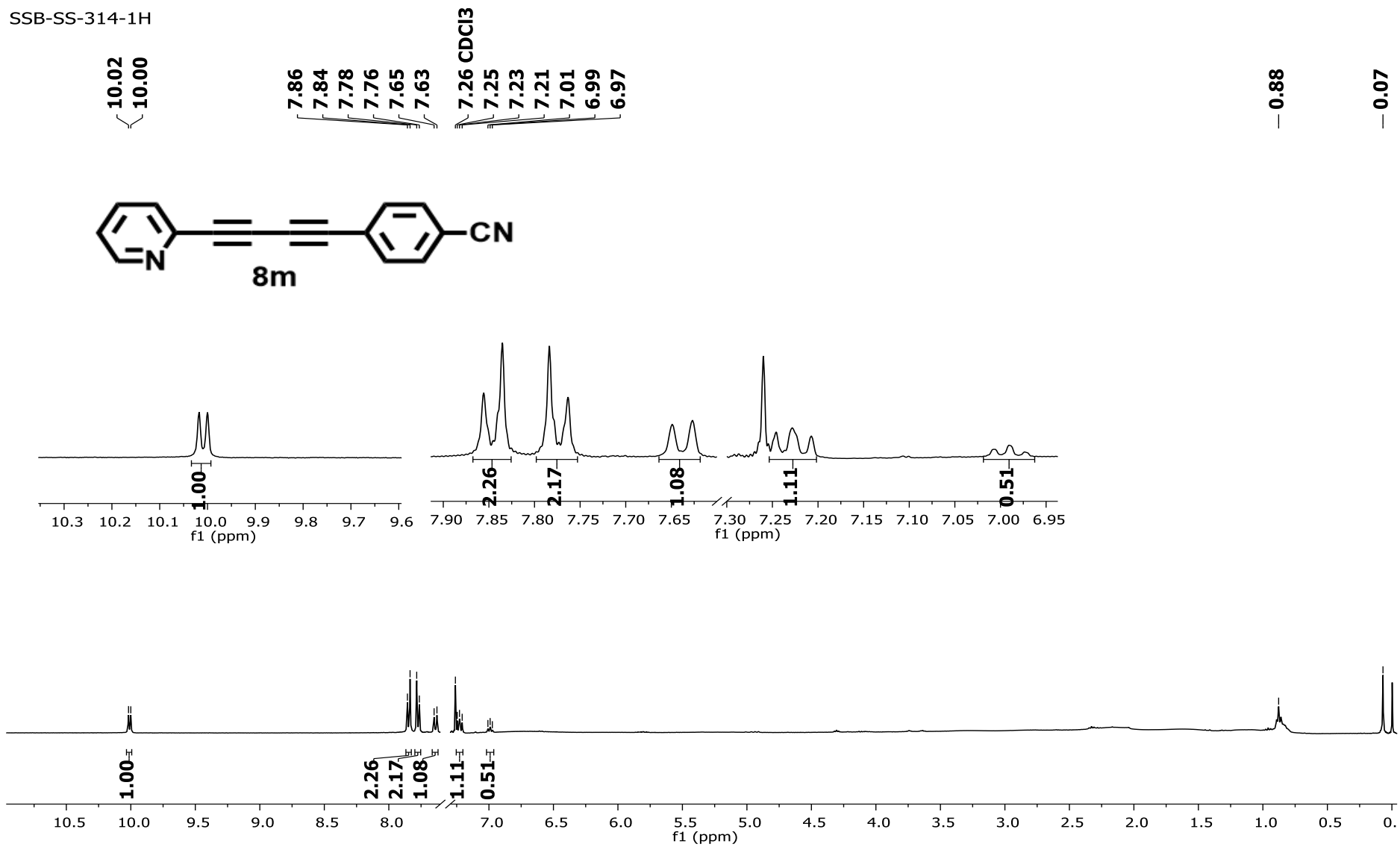


Figure S49. ¹H NMR spectrum of 6-phenylhexa-3,5-diyne-1-ol (8m).

SSB-SS-314-13C

135.88
135.82
132.65
132.07
131.99
129.34
128.58
125.77
125.59
121.98
121.96
117.68
117.64
117.62
115.72
115.48

81.71
81.49
80.96
80.73
77.48
77.16 CDCl3
76.84
74.08

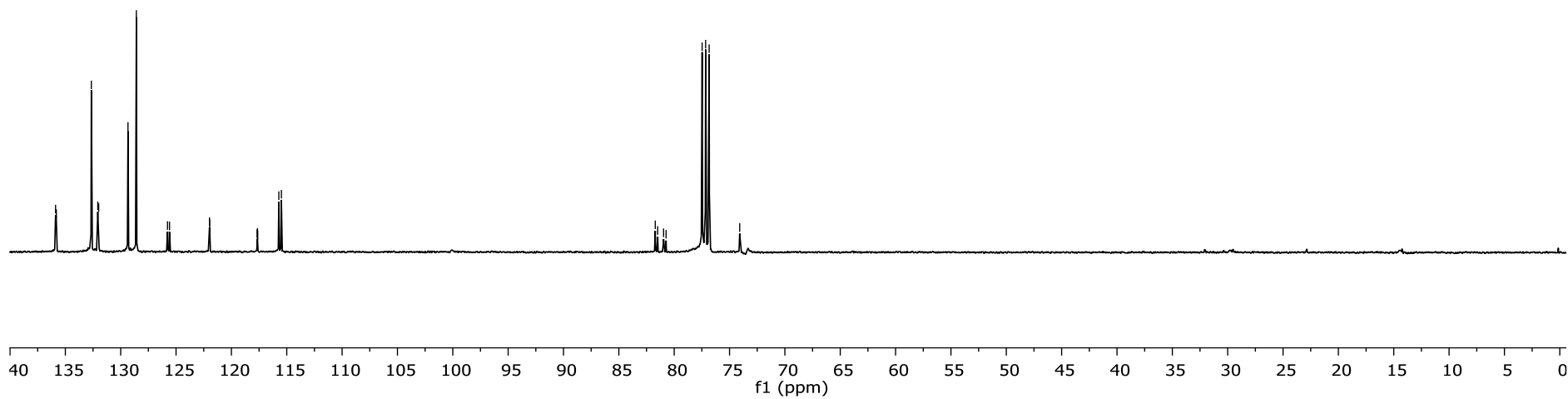
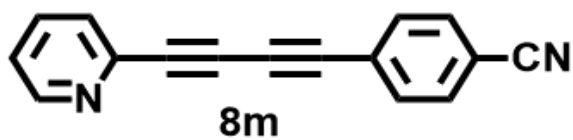


Figure S50. ¹³C NMR spectrum of 26-phenylhexa-3,5-diyne-1-ol (8m)

SSB-SS-308-1H

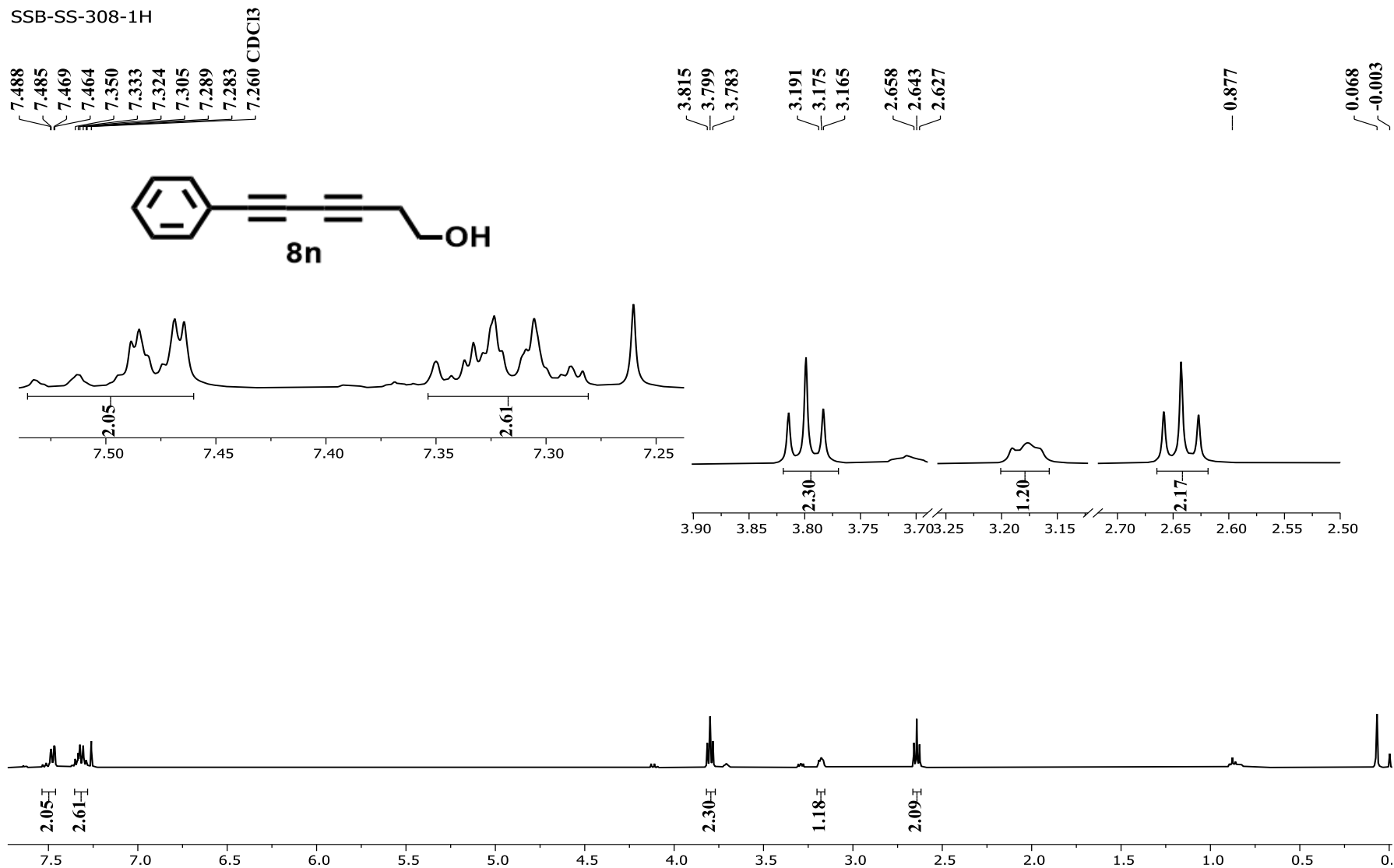


Figure S51. ¹H NMR spectrum of 6-phenylhexa-3,5-dyn-1-ol (8n).

SSB-SS-308-13C

132.686
129.187
128.521
121.892

81.106
77.478
77.160 CDCl₃
76.843
75.529
74.076

67.014

60.930

48.116

29.843

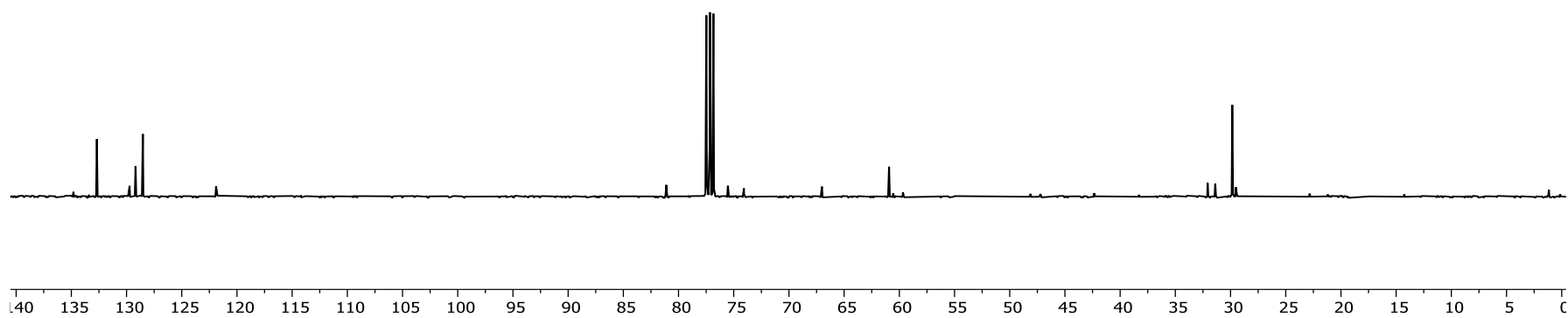
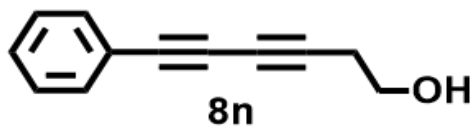


Figure S52. ¹³C NMR spectrum of 26-phenylhexa-3,5-diyne-1-ol (8n).

SSB-SS-330-1H

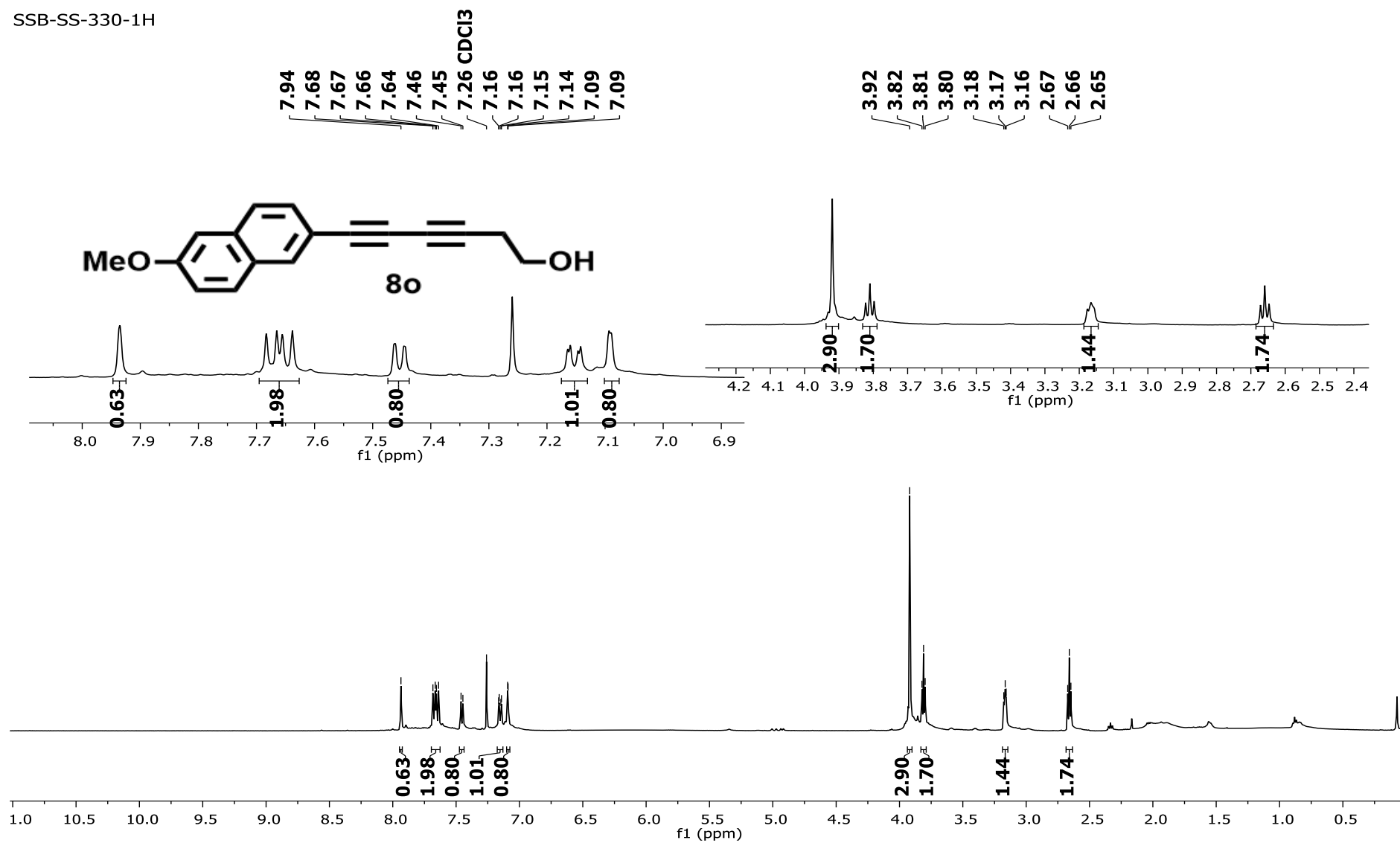


Figure S53. ¹H NMR spectrum of 6-(7-methoxynaphthalen-2-yl)hexa-3,5-diyne-1-ol (8o).

SSB-SS-330-13C

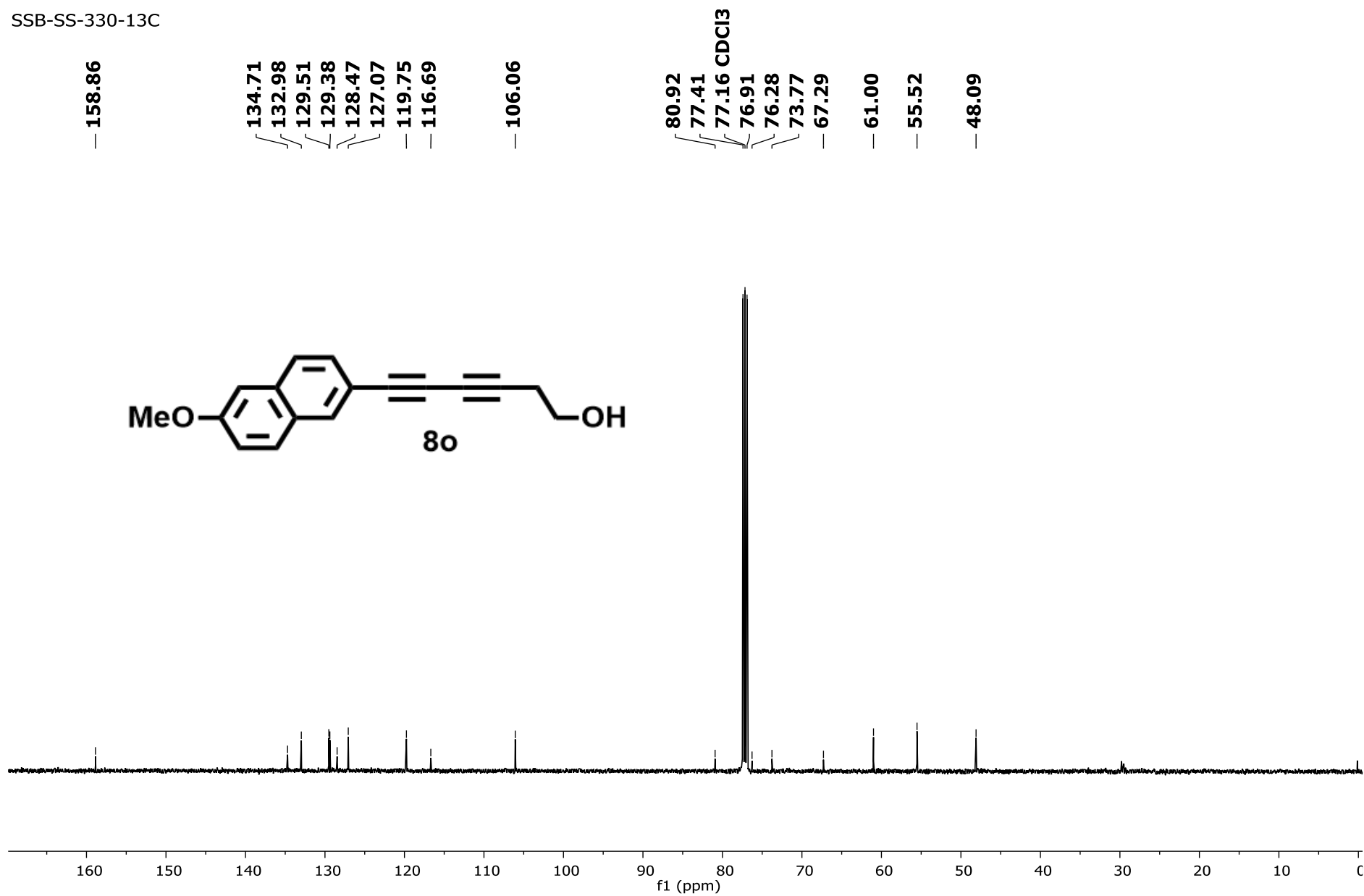
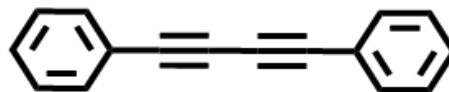


Figure S54. ^{13}C NMR spectrum of 6-(7-methoxynaphthalen-2-yl)hexa-3,5-diyne-1-ol (2o).

SSB-SS-334-1H

7.564
7.561
7.546
7.542
7.408
7.390
7.370
7.352
7.336
7.330
7.260 CDCl₃



8p

1.549
1.287
1.150

0.114

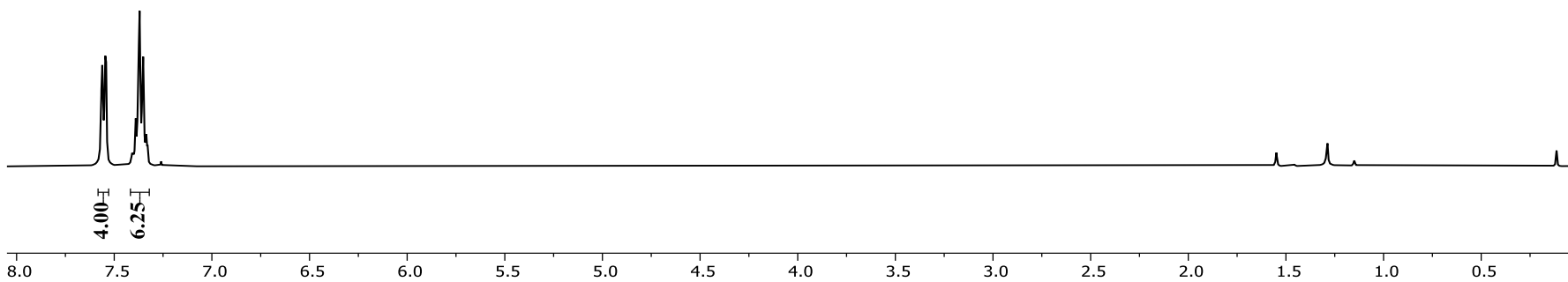
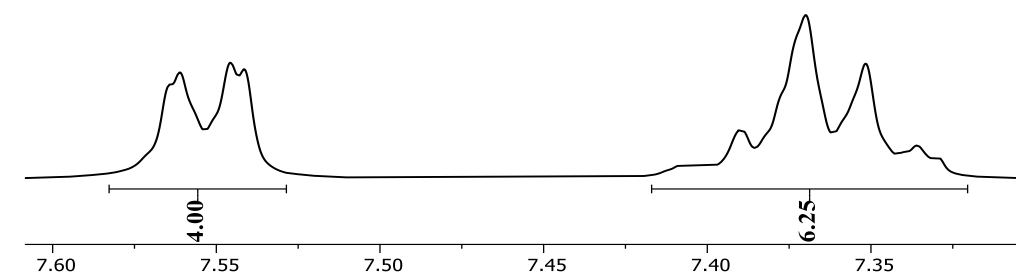
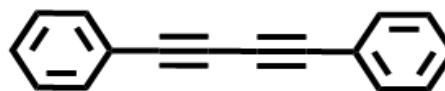


Figure S55. ¹H NMR spectrum of 1,4-diphenylbuta-1,3-diyne (8p).

SSB-SS-334-13C

~ 132.624
~ 129.326
~ 128.566
— 121.943

81.713
77.478
77.160 CDCl₃
76.843
74.096



8p

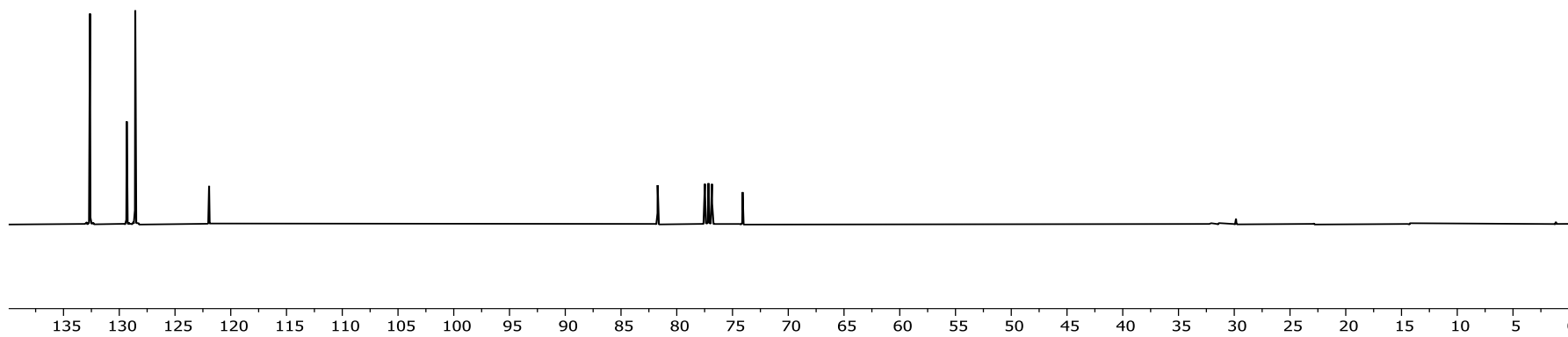


Figure S56. ¹³C NMR spectrum of 1,4-diphenylbuta-1,3-diyne (8p).

SSB-SS-164-1H

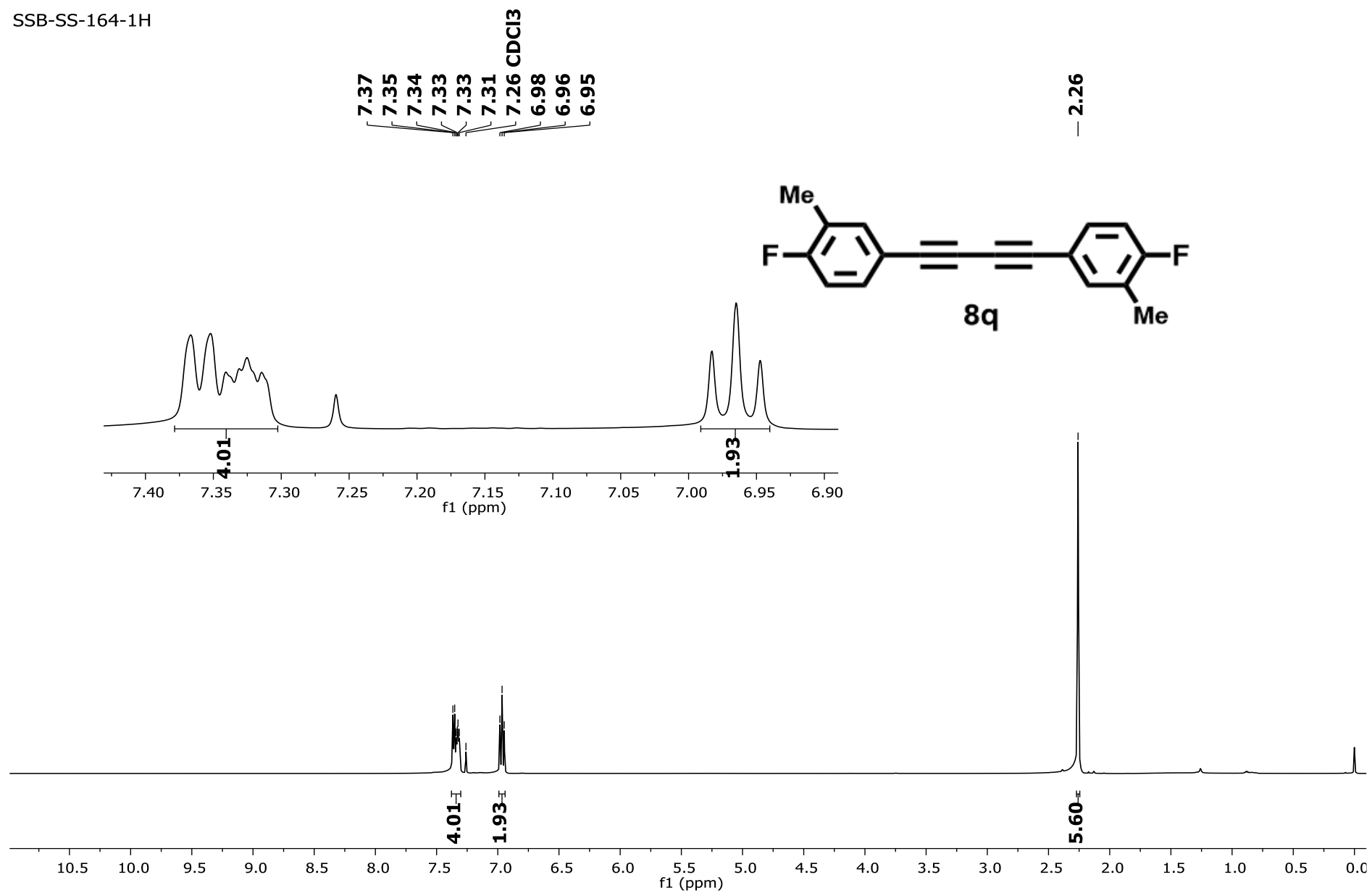


Figure S57. ¹H NMR spectrum of 1,4-bis(4-fluoro-3-methylphenyl)buta-1,3-diyne (8q).

SSB-SS-164-13C

163.16
160.68

135.87
135.81
132.07
131.98
125.77
125.59
117.67
117.63
115.72
115.48

77.48
77.16 CDCl₃
76.84
73.42

14.47

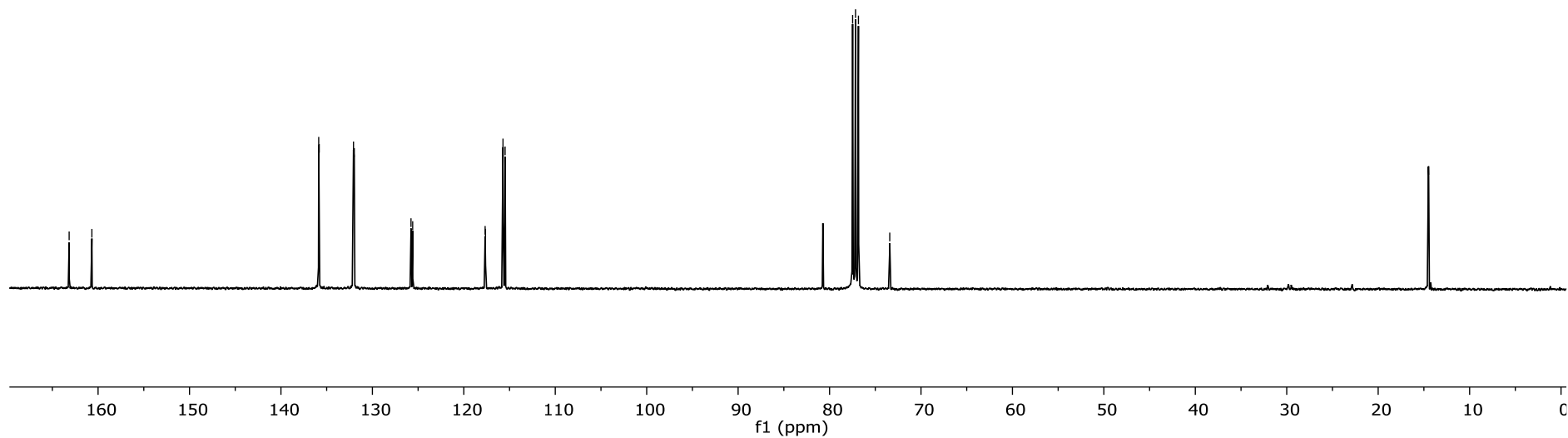
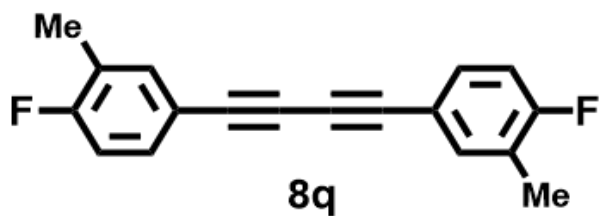


Figure S58. ¹³C NMR spectrum of *1,4-bis(4-fluoro-3-methylphenyl)buta-1,3-diyne* (8q).

SSB-SS-164-19F

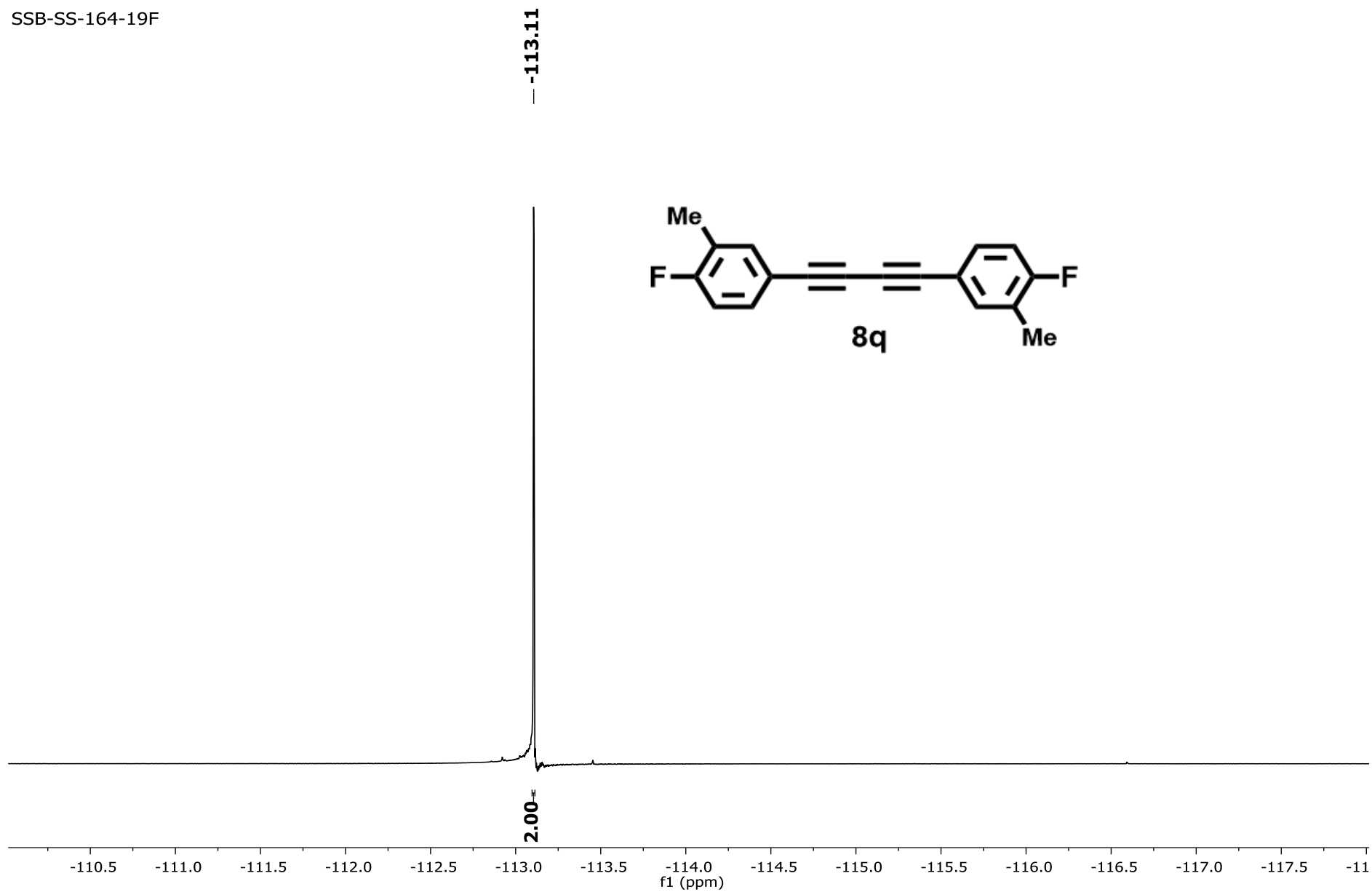


Figure S59. ^{19}F NMR spectrum of 1,4-bis(4-fluoro-3-methylphenyl)buta-1,3-diyne (8q).

SSB-SS-97-1H

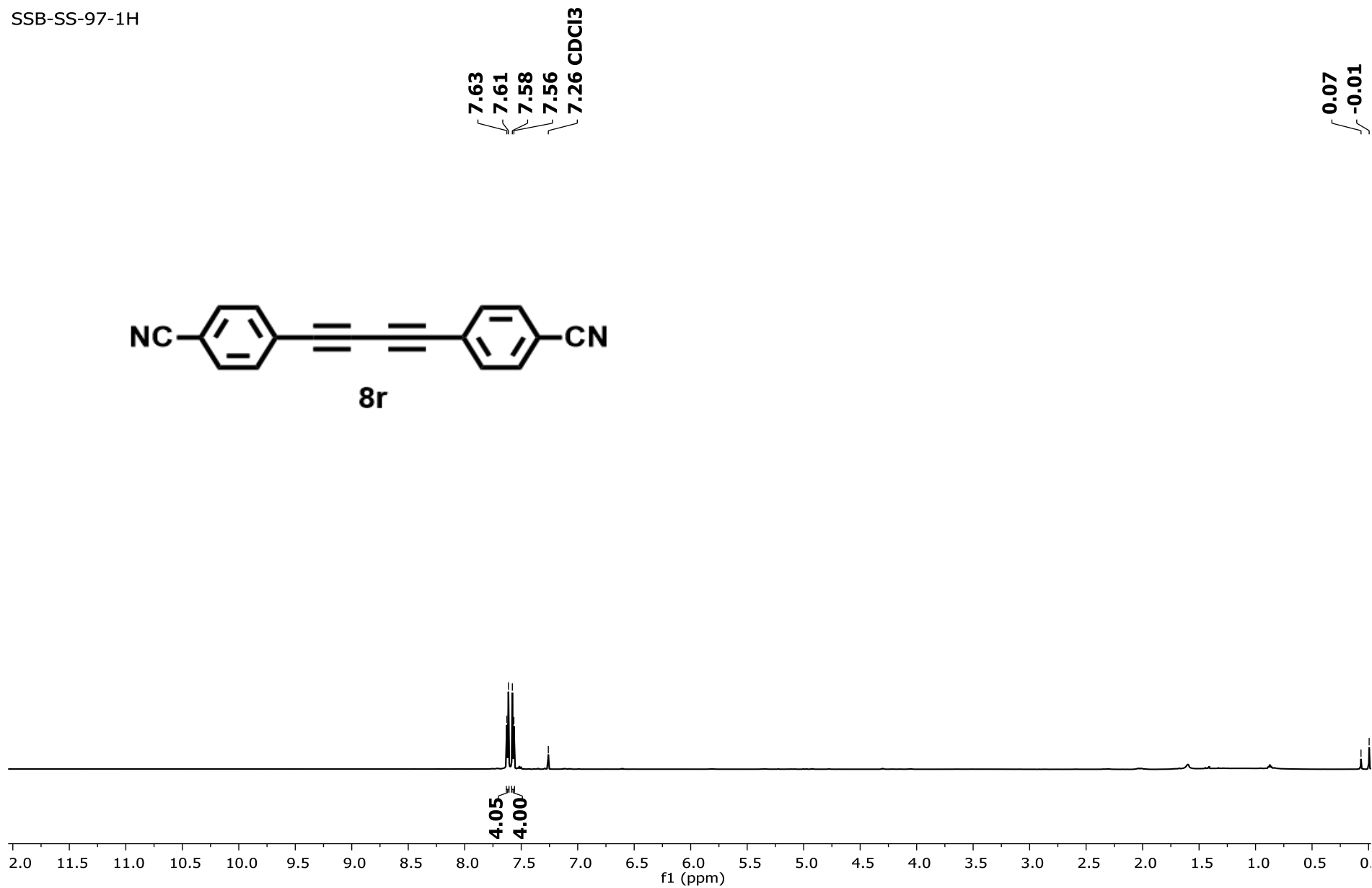


Figure S60. ¹H NMR spectrum of 4,4'-(buta-1,3-diyne-1,4-diyl)dibenzonitrile (**8r**).

SSB-SS-97-13C

132.801
132.161

127.107

118.413

112.418

81.978

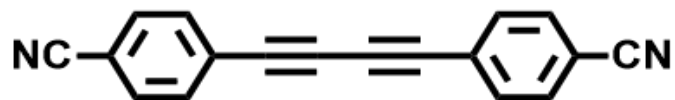
81.699

77.373

77.160

76.948

CDCCl₃



8r

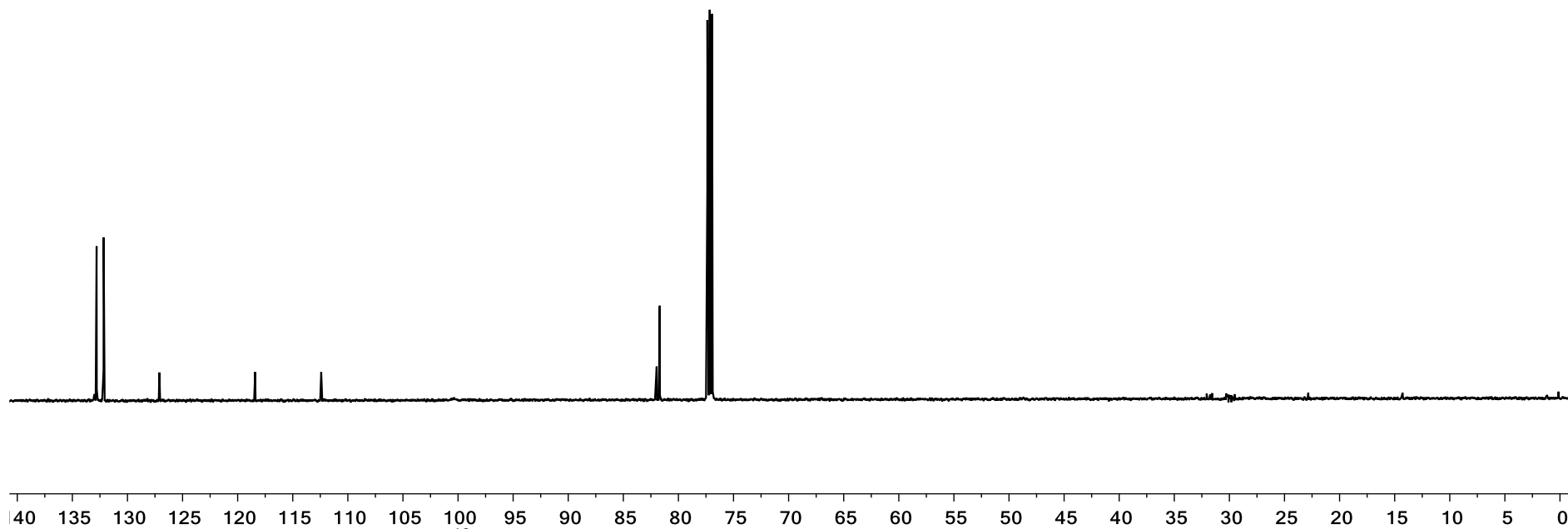


Figure S61. ¹³C NMR spectrum of 4,4'-(buta-1,3-diyne-1,4-diyl)dibenzonitrile (8r).

SSB-SS-367-1H

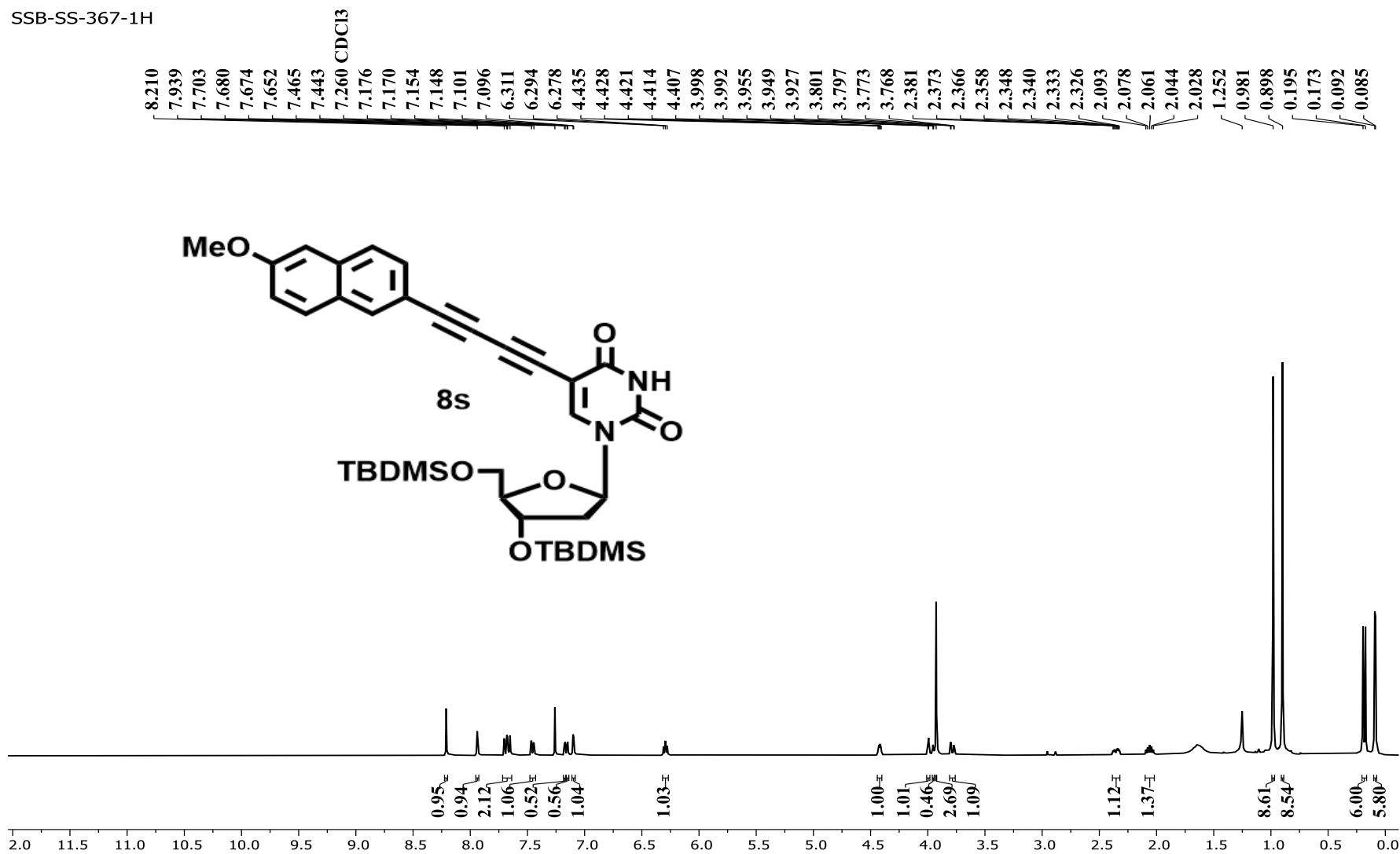


Figure S62. ¹H NMR spectrum of 4-(phenylbuta-1,3-dien-1-yl)benzointrile (**8s**).

SSB-SS-367-13C

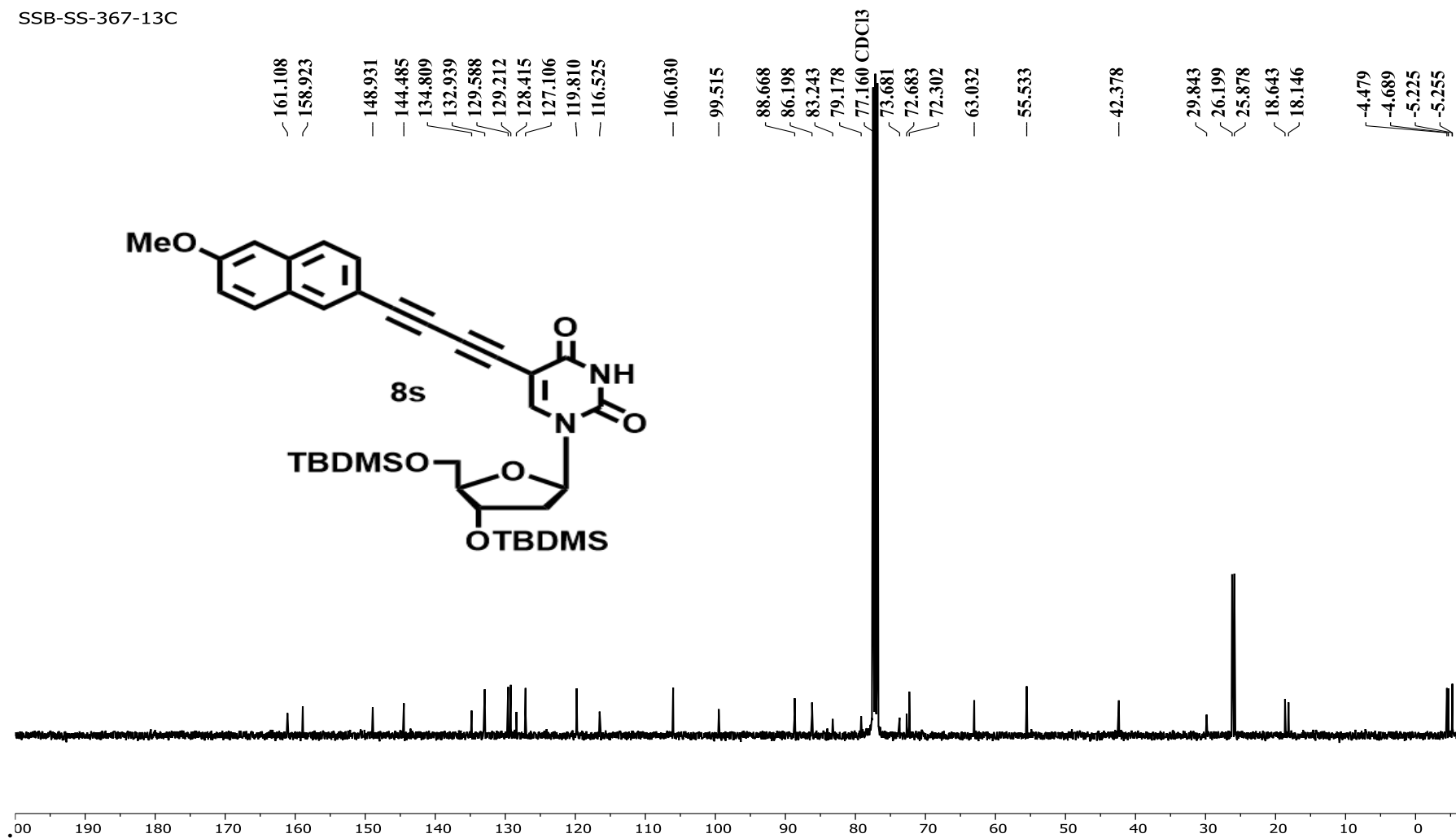


Figure S63. ^{13}C NMR spectrum of 4-(phenylbuta-1,3-diy-1-yl)benzonitrile (*8s*).

SSB-SS-386-1H

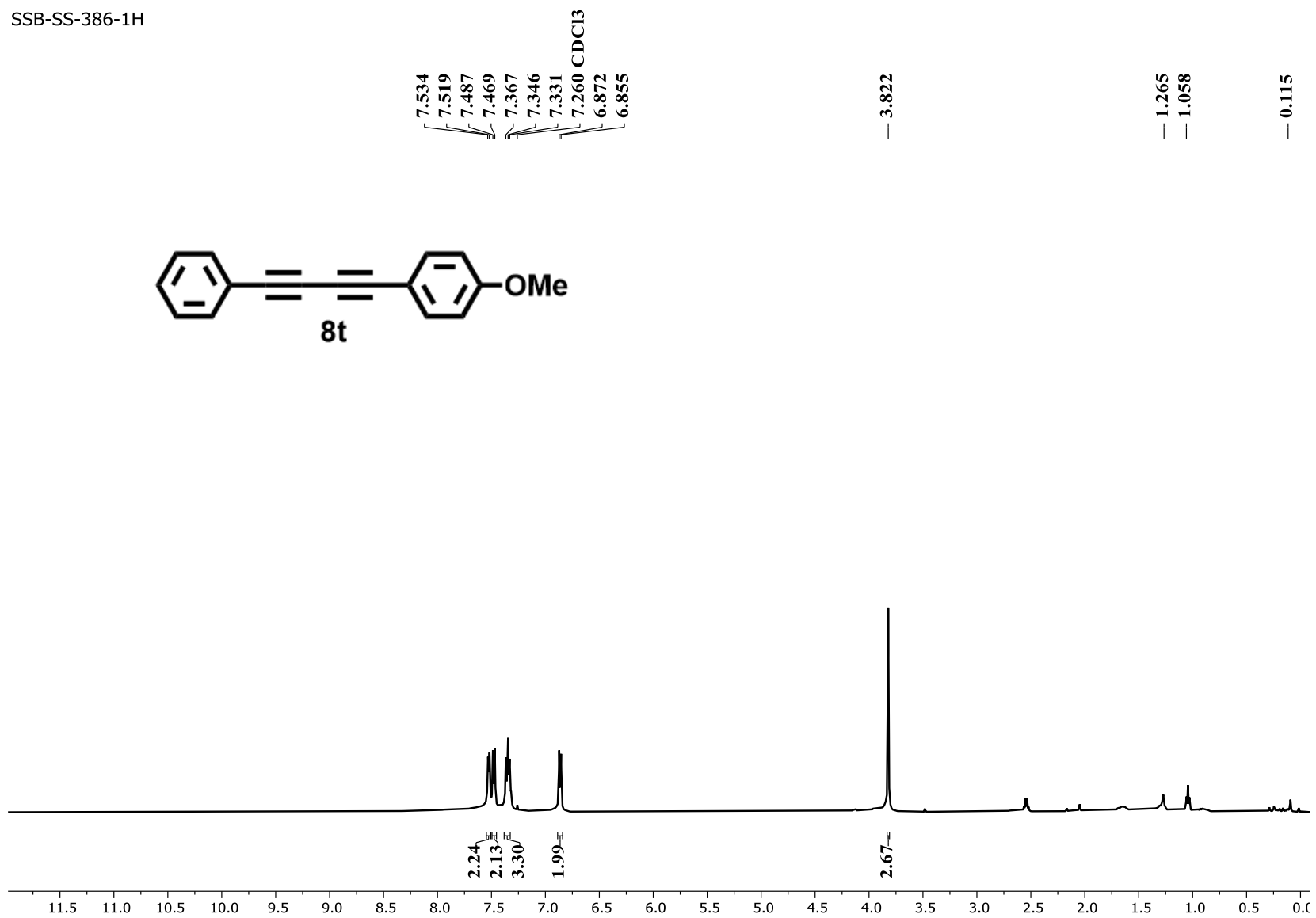


Figure S64. ¹H NMR spectrum of *1-methoxy-4-(phenylbuta-1,3-diyne-1-yl)benzene (8t)*.

SSB-SS-386-13C

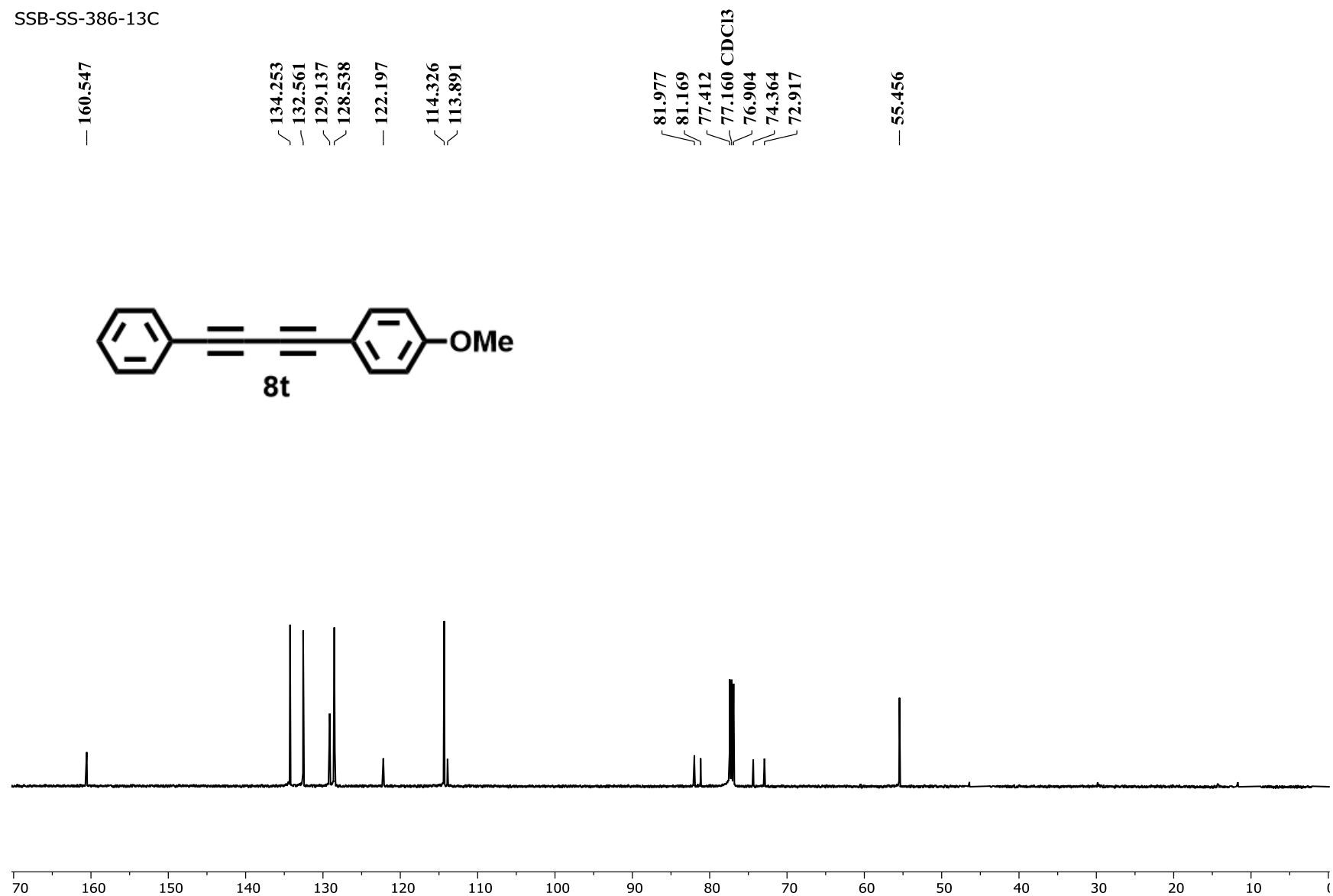


Figure S65. ¹³C NMR spectrum of *1-methoxy-4-(phenylbuta-1,3-diyne-1-yl)benzene (8t)*

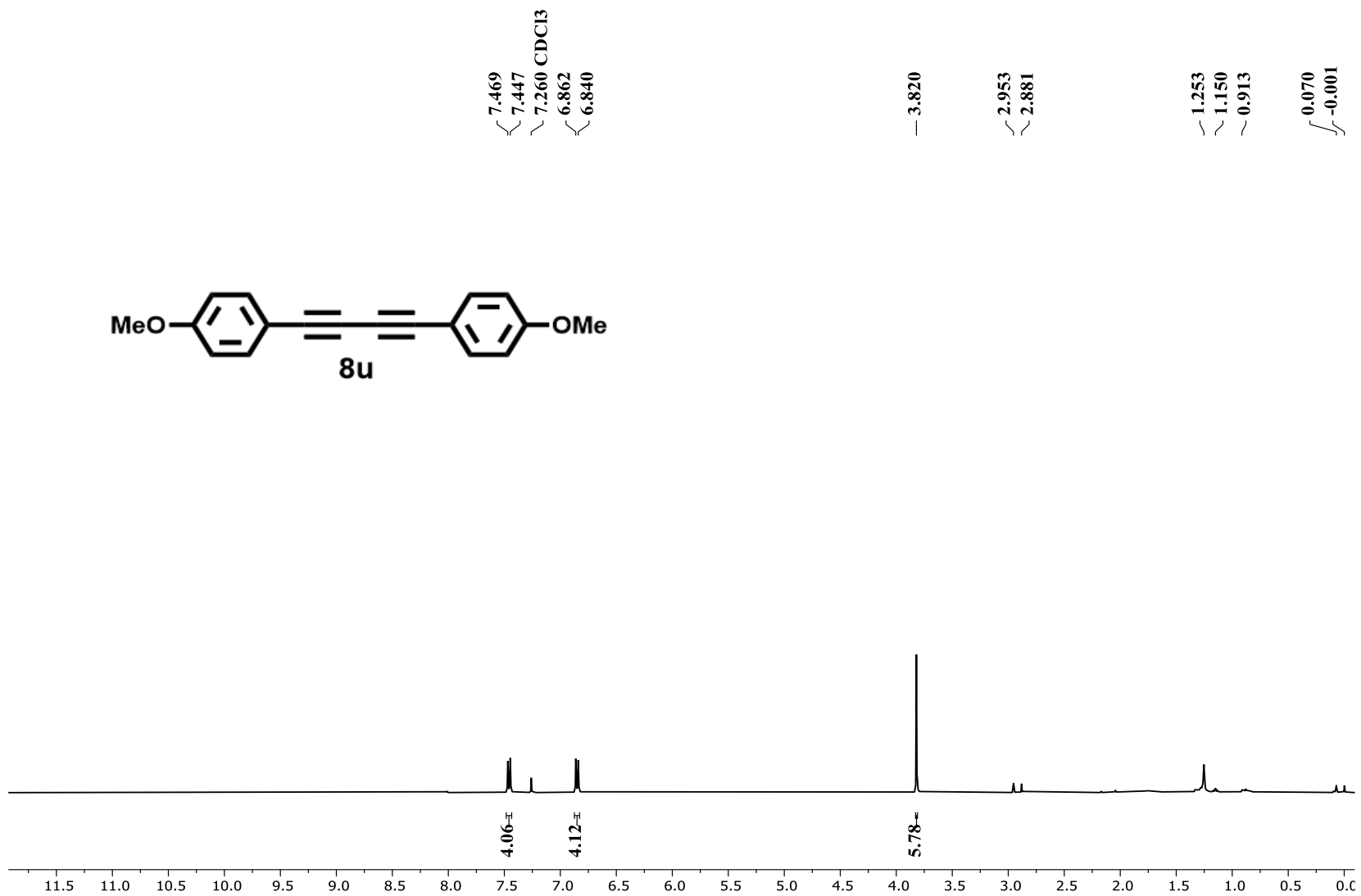


Figure S66. ¹H NMR spectrum of 1,4-bis(4-methoxyphenyl)buta-1,3-diyne (**8u**).

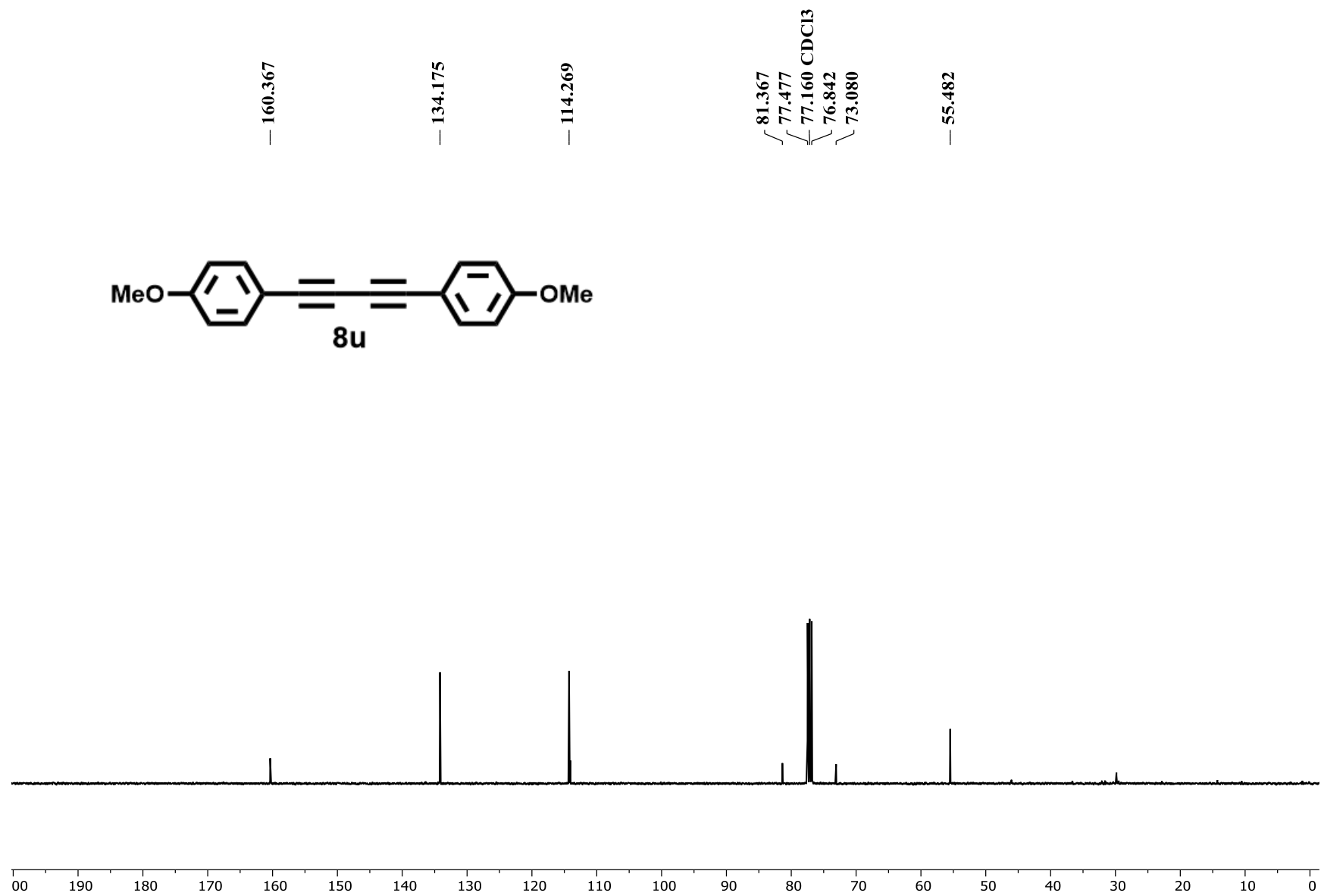


Figure S67. ¹³C NMR spectrum of *1,4-bis(4-methoxyphenyl)buta-1,3-diyne* (**8u**).